DISSERTATION

# THE NEUROINFLAMMATORY NEXUS: GLIAL DYSFUNCTION IN THE PATHOGENESIS AND THERAPEUTIC TARGETING OF NEURODEGENERATIVE AND NEURODEVELOPMENTAL DISORDERS

Submitted by

Sydney J. Risen

Department of Environmental Health and Radiological Sciences

In partial fulfillment of the requirements

For the Degree of Doctor of Philosophy

Colorado State University

Fort Collins, Colorado

Spring 2025

Doctoral Committee:

Advisor: Julie Moreno

Ronald Tjalkens
Tom LaRocca
Tara Nordgren

ABSTRACT

THE NEUROINFLAMMATORY NEXUS: GLIAL DYSFUNCTION IN THE PATHOGENESIS AND THERAPEUTIC TARGETING OF NEURODEGENERATIVE DISEASE AND NEURODEVELOPMENTAL DISORDERS

Chronic neuroinflammation is increasingly recognized as a fundamental driver of both neurodegenerative and neurodevelopmental disorders, linking immune dysregulation, glial dysfunction, and disease progression. In neurodegenerative protein misfolding disorders (NPMDs), including Alzheimer's disease, Parkinson's disease, and prion diseases, sustained microglial and astrocytic activation exacerbates protein aggregation, synaptic dysfunction, and neuronal loss, accelerating cognitive decline. Similarly, in neurodevelopment, aberrant inflammatory signaling during critical windows of brain maturation impairs synaptic formation, alters neurotransmitter systems, and predisposes individuals to long-term cognitive and behavioral deficits. Despite distinct manifestations, both disease categories share a pathological feature: a maladaptive neuroimmune response disrupting neural homeostasis. While neuroinflammation is widely implicated in these disorders, defining its molecular mechanisms, identifying therapeutic targets, and understanding environmental contributions remain critical research needs. This dissertation begins to address these gaps by investigating neuroinflammation as both a therapeutic target in NPMDs and a mechanistic link between environmental exposures and neurodevelopmental disruption.

The first investigation evaluates SB_NI_112, a novel brain-penetrant RNA-based therapeutic designed to selectively inhibit NF-κB and NLRP3 inflammasome pathways, key regulators of glial activation and chronic neuroinflammation. Pharmacokinetic and biodistribution studies in small- and large-animal models were first conducted to assess SB_NI_112's CNS

penetration and safety. These studies confirmed robust brain bioavailability (*~30%*) and a favorable safety profile, supporting its viability for therapeutic application. Following these findings, SB_NI_112 was tested in a murine prion disease model, where treatment significantly reduced microglial and astrocytic activation in disease-relevant brain regions, preserved hippocampal neurons, and mitigated neurodegeneration. These neuroprotective effects corresponded with improved cognitive performance in novel object recognition tasks, indicating functional preservation despite ongoing prion pathology. Notably, SB_NI_112 treatment extended survival, reinforcing inflammasome inhibition as a viable therapeutic strategy for NPMDs. These findings provide strong proof-of-concept for targeting neuroinflammatory pathways to slow disease progression and preserve cognitive function in neurodegenerative protein misfolding disorders.

The second investigation examines the role of environmental neurotoxicants in triggering neuroinflammation and impairing neurodevelopment. Using a juvenile mouse model, this study demonstrates that chronic low-dose manganese (Mn) exposure (50 mg/kg via drinking water) first alters gut microbiome composition, depleting the relative abundance of beneficial *Lactobacillaceae,* and increasing the relative abundance of pro-inflammatory *Erysipelotrichaceae*, contributing to gut-brain axis dysfunction. These microbial shifts coincide with significant gliosis in the enteric nervous system, suggesting early neuroimmune activation at the gut interface. This inflammatory response extends to the brain, where widespread microglial and astrocytic activation is observed alongside disruptions in neurotransmitter production and metabolism, including altered dopamine and serotonin homeostasis. Functionally, these neuroimmune and neurochemical disruptions correspond with changes in behavior, indicating impaired neural processing. The presence of inflammatory lesions in the intestinal lining further implicates gut inflammation as a mediator of Mn-induced neurodevelopmental deficits. These findings highlight the systemic impact of Mn exposure,

reinforcing the link between environmental toxins, neuroinflammation, and behavioral dysregulation.

Together, these studies further support the growing body of evidence that neuroinflammation is a primary driver of neurological disease rather than a secondary consequence, reinforcing the need for targeted neuroimmune interventions. By examining shared inflammatory features across NPMDs and environmentally induced neurodevelopmental disruptions, this work provides additional insight into how glial dysfunction contributes to neurological pathology. These findings support the continued development of neuroimmune-modulating therapeutics, emphasize early intervention, and highlight the importance of environmental risk mitigation. By bridging molecular, pharmacological, and environmental perspectives, this dissertation contributes to the broader understanding of neuroinflammation in disease progression, challenging traditional distinctions between neurological disorders and providing a foundation for future studies. The implications extend beyond basic science, offering translational potential for clinical intervention, public health strategies, and regulatory policies to reduce the burden of neuroinflammatory disease.

# ACKNOWLEDGMENTS

I extend my deepest gratitude to my advisor, Dr. Julie Moreno, whose guidance and support have been instrumental in my growth as both a scientist and an individual. Her unwavering encouragement, even in the face of her own challenges, has left a profound impact on me and everyone in our lab. In moments of doubt, when the data seemed insignificant or progress felt slow, her wisdom and insight provided the clarity to recognize the value in every step forward. Beyond her role as an exceptional scientist and mentor, she has been a model of dedication and ethical leadership. Her steadfast commitment to upholding the rigor and honesty of scientific inquiry has been especially meaningful as we navigated challenges that required us to advocate for the integrity of our work. She has shown through example, that being a scientist is not only about producing results but about ensuring that those results are pursued with responsibility, transparency, and respect for the scientific process. Her dedication to supporting women and underrepresented minorities in STEM, while balancing the immense demands of academia, reflects a deep and selfless devotion to shaping not only the next generation of scientists but also a more inclusive and principled scientific community. Her mentorship has shaped my development as both a researcher and an individual, and I am profoundly grateful for the opportunity to have learned from her.

My sincere appreciation goes to my committee members, Dr. Tom LaRocca, Dr. Ronald Tjalkens, and Dr. Tara Nordgren, whose expertise and thoughtful guidance have greatly enriched my research. Their willingness to challenge my ideas, offer new perspectives, and engage in meaningful discussions has strengthened not only the quality of this dissertation but developed my ability to think critically and approach scientific questions with greater depth. Having the opportunity to learn from such accomplished scientists has been both an honor and a privilege, and their collective insights have shaped my understanding of the field in ways that

extend beyond this project. I am especially grateful to Dr. LaRocca for the opportunity to collaborate on projects and publications that broadened my research and reinforced the interconnected nature of our work. Dr. Tjalkens and Dr. Nordgren have also provided invaluable feedback, helping me refine my approach and develop a more rigorous scientific perspective. Their mentorship has not only guided me through this dissertation but has also given me the confidence to tackle complex questions with curiosity and precision. I am truly grateful for the time and effort they have dedicated to my development and for the lasting impact their support has had on my growth as a scientist.

To my parents, Anne and Randy, I am profoundly grateful for your unwavering support, patience, and belief in me. From an early age, my stubbornness was a defining trait—unyielding, persistent, and often challenging—but you never saw it as something to change. Instead, you recognized its potential and taught me that determination, when guided with purpose, could be a source of growth rather than mere resistance. You nurtured my intellectual curiosity, encouraged my ambitions, and instilled in me a deep respect for education, not simply as a means of personal achievement but as a privilege that carries the responsibility to engage with the world thoughtfully and contribute meaningfully to the lives of others. Your guidance has shaped my perseverance, your encouragement has given me the confidence to push forward in moments of doubt, and your example has shown me that strength is built not only on persistence but also on purpose. Every step of this journey has been possible because of the foundation you built through your unwavering love, your sacrifices, and the values you instilled in me. For that, and for so much more, I dedicate this achievement to you. I am also grateful for my brother, Jack, who has shaped my ability to communicate and think critically in ways I could never have learned in a classroom. Through countless discussions—sometimes debates, sometimes outright arguments—he challenged my beliefs, forced me to articulate my thoughts more clearly, and taught me the importance of engaging with perspectives different from my

own. His ability to question, to push boundaries, and to approach ideas with both curiosity and conviction has influenced me more than he likely realizes.

To my partner, Meg, I am profoundly grateful for your unwavering support and the many ways you have grounded me throughout this journey. Your patience, understanding, and quiet strength have been a constant, even in the most difficult moments. Whether helping me troubleshoot software issues, expanding my coding abilities, or simply offering a steady presence when frustration left me at a loss for words, you have been an anchor in times of uncertainty. But beyond the practical support, you have given me something even more valuable, perspective. When stress clouded my judgment and frustration consumed me, you knew how to bring me back to center, reminding me to step back and see the bigger picture. I know that being the partner of someone pursuing a PhD is not without its challenges. The long hours, the unpredictable demands, and the inevitable emotional toll of this process have asked more of you than I can ever fully acknowledge. Yet, through it all, you have been constant. Even in my most stubborn moments, when exhaustion and self-doubt left me overwhelmed, when frustration turned into tears, you never faltered. You met my distress with patience, my tears with quiet reassurance, and my relentless drive with understanding. I cannot fully express how much your love and partnership have meant to me, but I am endlessly grateful. Thank you for standing by my side every step of the way and for making this journey not only possible but infinitely more meaningful. Through it all, our chosen family members—Bear, Coors, and Ozzy—have brought an immeasurable amount of comfort, laughter, and lightness into our lives. Whether it was their unwavering companionship during long nights of writing, their antics providing a much-needed distraction, or simply their quiet presence reminding me to pause and breathe, they have been a source of joy and perspective in their own right.

Finally, I am grateful for the refuge and wisdom I have found through yoga, a practice that has been essential in navigating the intensity and uncertainty of this chapter in my life. As

both a student and an instructor, I have come to understand the interplay between discipline and surrender, effort and rest—principles that extend far beyond the mat and into the fabric of research, teaching, and daily life. Yoga has given me the capacity to step back, quiet my mind, and approach setbacks with patience rather than frustration, fostering a steadiness that has carried me through the most demanding moments of this journey. Teaching has deepened this experience, strengthened my confidence, and reminded me of the power of presence, connection, and shared growth. Guiding others has taught me how to hold space with intention, to embrace imperfection, and to recognize learning as an ever-evolving process. The clarity and composure I have gained through this practice have shaped not only how I move through my own challenges but also how I engage with the world. For the strength, stillness, and community that yoga has given me, I am forever grateful.

# DEDICATION

To my grandfather, Donald, a compassionate veterinarian whose commitment to all creatures, great and small, knew no bounds. His belief in my education and research shaped my path, but it was his resilience in the face of adversity that left the deepest mark on me. The moment that altered his life, leaving him paralyzed, did not define him. Instead, he confronted this unimaginable challenge with optimism and fortitude, refusing to let it diminish his spirit. His legacy of perseverance and kindness continues to inspire me every day, reminding me that the greatest obstacles can be overcome with determination and grace.

To my grandmother, Barbara, whose strength was tested by the ruthless progression of Alzheimer's disease. Her tenacity in the face of this battle was not an act of defiance but a testament to her resilience. Witnessing the impact of her illness on her and those who loved her has fueled my commitment to understanding and combating neurodegenerative diseases. Her unwavering spirit, even in the most challenging moments, taught me that strength lies not in the absence of struggle, but in the refusal to surrender to it.

To my grandmother, Stella, who played a crucial role in my upbringing and whose generosity was limitless. Despite having little, she gave endlessly—her love, kindness, and support made everyone around her feel cherished. Even as Lewy body dementia took its toll, it never diminished the light she brought to the lives she touched. Her selflessness and compassion continue to guide me in both my personal and professional life, reminding me that the most profound impact we can have is through the love we show others.

I dedicate this dissertation to the memory of these three extraordinary individuals—their strength, love, and the profound influence they had on my life. Their experiences shaped my path and ignited a passion within me to contribute to the understanding of neurodegenerative diseases. Through my work, I aspire to honor their legacies and make a difference in the lives of

those affected. Their stories are forever intertwined with the fabric of this dissertation and my life's work, driving me to pursue answers, to offer hope, and to embody the values they exemplified. This work stands as a testament to the mark they left on my life and the lives of countless others.

TABLE OF CONTENTS

# CHAPTER 1 – NEUROINFLAMMTION ACROSS THE LIFESPAN: LINKING PATHOLOGY OF NEURODEGENERATIVE AND NERUODEVELOPMENTAL DISORDERS

## The Emerging Role of Neuroinflammation in Neurological Disease

Neurological disorders affect millions globally, with devastating impacts on individuals, families, and healthcare systems[1]. Among these conditions, neurodegenerative protein misfolding disorders (NPMDs) and neurodevelopmental disorders represent particularly challenging therapeutic targets, despite their distinct manifestations[2, 3]. This dissertation advances a central hypothesis: chronic neuroinflammation, driven by sustained glial activation and dysregulated immune signaling, represents a fundamental pathological mechanism that shapes neurological dysfunction across the lifespan. While these conditions manifest at distinct stages of life and present with different neurological impairments, they share common pathological mechanisms rooted in chronic glial dysfunction and aberrant immune responses[4, 5].

Microglia and astrocytes, as the principal supporting cells and immune regulators of the central nervous system (CNS), play essential roles in maintaining neural homeostasis, modulating synaptic function, and responding to injury[6, 7]. Under physiological conditions, these cells orchestrate a highly dynamic interplay, facilitating neuronal support and immune surveillance[8]. In neurodegenerative disorders, these cells respond to protein aggregation and cellular stress[9, 10], while in neurodevelopmental contexts, they guide critical processes of circuit formation and refinement[11, 12]. However, when inflammatory responses become excessive or persist beyond their intended resolution, a maladaptive cycle emerges that exacerbates neuronal dysfunction and disease progression, regardless of the initial trigger[13-15].

Chronic neuroinflammation has emerged as one of the most important, yet historically underappreciated, factors in the pathogenesis of neurological disorders[16, 17]. While the role of

acute inflammatory responses in immune defense and tissue repair is well established, the consequences of prolonged, low-grade inflammation within the CNS have only recently become a major focus of research[18, 19]. This persistent inflammatory state represents a critical intersection between environmental factors, genetic susceptibility, and cellular stress responses[20]. Increasing evidence suggests that systemic inflammation—originating from peripheral immune activation, metabolic dysfunction, or environmental exposures—can penetrate the CNS and further drive neuroinflammatory cascades, compounding the pathological effects of resident glial dysfunction[21-23].

The temporal dynamics of neuroinflammation also play a crucial role in determining its impact on neural function and development[5, 15, 24]. In the context of neurodegenerative disorders, chronic inflammation appears to both initiate and perpetuate pathological processes, creating a self-reinforcing cycle of cellular damage and immune activation[25, 26]. Similarly, in neurodevelopmental disorders, early-life inflammatory events can disrupt critical periods of brain development, leading to lasting alterations in neural circuit formation and function[27, 28]. Understanding these temporal relationships is essential for developing targeted therapeutic interventions that can effectively modulate inflammatory responses at different stages of disease progression.

**Inflammatory Mechanisms in Neurodegenerative Protein Misfolding Disorders (NPMDs)**

In neurodegenerative protein misfolding disorders, the intersection of protein aggregation and chronic inflammation creates a particularly challenging therapeutic landscape[29, 30]. While traditionally studied through the lens of protein accumulation, mounting evidence identifies chronic neuroinflammation as a primary driver of disease progression[31, 32]. Alzheimer's disease (AD), the most prevalent NPMD, exemplifies this complex pathology through the accumulation of amyloid-beta (Aβ) plaques and tau neurofibrillary tangles, accompanied by

persistent glial activation[33]. Central to this inflammatory response is the activation of microglia and astrocytes, which influence disease progression through both neuroprotective and neurotoxic mechanisms[6, 34, 35].

The inflammatory cascade in NPMDs is largely mediated by the NF-κB signaling pathway, which functions as a master regulator of inflammation[36]. Beyond its direct transcriptional activation of pro-inflammatory cytokines, NF-κB primes the NLRP3 inflammasome, a cytosolic multiprotein complex that amplifies neuroinflammatory responses by facilitating the maturation and release of IL-1β and IL-18[37]. This activation leads to a cascade of events including pyroptotic cell death in microglia, impaired autophagic clearance of misfolded proteins, and sustained inflammatory signaling[37]. The combined activity of NF-κB and NLRP3 creates a self-perpetuating cycle of neuroinflammation that accelerates disease progression[38, 39].

Microglia in NPMDs transition from a homeostatic surveillance state to an activated phenotype characterized by altered morphology and function[40, 41]. In their surveillance state, microglia exhibit a ramified morphology with numerous fine processes that continuously monitor the extracellular environment[42]. Upon activation, these cells retract their processes and adopt an amoeboid morphology suited for phagocytosis and cytokine secretion[42]. While this response initially serves a protective function by attempting to clear pathological protein aggregates, chronic activation leads to a dysregulated state that contributes to disease progression[2, 38, 39, 43, 44]. The sustained release of pro-inflammatory mediators such as TNF-α, IL-1β, and IL-6 creates an oxidative environment that compromises neuronal function and survival, while simultaneously impairing the ability of microglia to effectively clear protein aggregates[45].

Astrocytes undergo parallel changes in NPMDs, shifting from their normal supportive functions to a reactive state that further contributes to disease pathology[26]. Under physiological conditions, astrocytes maintain ion homeostasis, regulate neurotransmitter clearance, and

provide metabolic support to neurons[26]. However, in the context of chronic inflammation, reactive astrocytes exhibit impaired glutamate uptake, disrupted metabolic support for neurons, and increased production of pro-inflammatory factors. This transformation not only compromises their ability to maintain neuronal health but also reinforces the inflammatory environment created by activated microglia[6, 46]. The interaction between reactive astrocytes and activated microglia creates a feed-forward loop of inflammation that becomes increasingly difficult to resolve as disease progresses[46].

The central role of NF-κB and NLRP3 signaling in driving NPMD progression highlights these pathways as promising therapeutic targets[36, 47]. This dissertation will investigate a novel approach to interrupting this inflammatory cascade while preserving essential neuroimmune functions through the development of SB_NI_112, a brain-penetrant RNA-based therapeutic designed to selectively inhibit both NF-κB and NLRP3 signaling pathways[48-50]. By targeting these two critical nodes in the inflammatory cascade, we will examine whether this dual-targeting strategy can effectively modulate the self-perpetuating cycle of inflammation that characterizes NPMDs[48-50].

Prior to investigating the therapeutic potential of SB_NI_112, we conducted a biodistribution and toxicity study to ensure the safety of the drug in mice and to confirm its ability to cross the blood-brain barrier (BBB). Following these critical safety and pharmacokinetic assessments, we utilized a mouse model of prion disease, selected for its distinct advantages in studying neuroinflammatory mechanisms in protein misfolding disorders[51]. Unlike the protracted progression of AD and Parkinson's disease, prion diseases exhibit an accelerated disease course due to the self-replicating nature of misfolded prion proteins ($PrP^{Sc}$)[52]. This compressed timeline enables systematic evaluation of therapeutic interventions across all stages of neurodegeneration, from initial protein aggregation through terminal disease. In our study, we examined the effects of SB_NI_112 on glial activation states, inflammatory signaling cascades,

and disease progression, with particular emphasis on early intervention timing. The rapid and predictable progression of prion pathology, coupled with robust glial activation and inflammatory responses, provides an optimal experimental system for evaluating how modulation of the NF-κB/NLRP3 axis might influence disease progression.

Beyond direct effects on glial activation, this research investigates how modulation of the NF-κB/NLRP3 axis influences broader aspects of neurodegeneration, including protein aggregation, synaptic function, and neuronal survival. The complex interplay between inflammatory signaling and protein misfolding suggests that successful therapeutic strategies must address multiple aspects of disease pathology. Through detailed examination of these pathways in the prion disease model, this work aims to provide insights that may be applicable to other protein misfolding disorders where similar inflammatory mechanisms contribute to disease progression[50].

**Early-Life Inflammation and Neurodevelopmental Trajectories**

While glial dysfunction in neurodegeneration contributes to the breakdown of an already mature nervous system, similar inflammatory mechanisms during early brain development can profoundly alter neurodevelopmental trajectories[53-55]. During critical developmental windows, perturbations in glial signaling can have lasting neurological consequences[5, 56]. Persistent microglial activation can result in excessive synaptic pruning and impaired neuronal connectivity, while reactive astrocytes disrupt neurotransmitter balance, weaken blood-brain barrier integrity, and amplify inflammatory cascades[57, 58]. This sustained neuroimmune imbalance creates a pathological environment characterized by heightened excitotoxicity and oxidative stress, increasing the likelihood of cognitive and behavioral impairments that persist into adulthood[59].

The second major investigation of this dissertation will examine how environmental factors, particularly manganese (Mn) exposure, influence neurodevelopment through inflammatory mechanisms[60, 61]. This work will focus on understanding how early-life exposure to Mn might trigger and sustain inflammatory responses that alter developmental trajectories. Given that early-life Mn exposure occurs primarily through drinking water and infant formula, this research will place particular emphasis on understanding how the gastrointestinal tract and enteric nervous system may mediate neurodevelopmental impacts before direct central nervous system effects occur[62].

Using a juvenile mouse model, this work will investigate how chronic low-dose Mn exposure via drinking water potentially affects both the enteric and central nervous systems. The research examines several key aspects of Mn-induced inflammatory responses: alterations in the gut microbiome composition, changes in enteric nervous system signaling, and activation of inflammatory pathways that may impact neural circuit development[63, 64]. Of particular interest will be the potential role of glial cells—both enteric glia and central nervous system microglia and astrocytes—in mediating these effects.

This investigation will build upon emerging epidemiological evidence suggesting links between Mn exposure and neurodevelopmental disorders, particularly ADHD and ASD[65, 66]. While large-scale cohort studies have identified correlations between elevated Mn concentrations in drinking water and increased ADHD risk, the mechanisms underlying these associations remain poorly understood[67]. Through controlled experimental studies, this work will seek to elucidate the inflammatory pathways that might mediate these effects, with particular attention to how early-life exposure may influence long-term neurological outcomes.

A critical component of this research involves understanding the role of the enteric nervous system (ENS) in mediating Mn-induced neurotoxicity. The ENS, frequently described as the "second brain," comprises an extensive network of neurons and glial cells within the

gastrointestinal tract that maintain gut motility, immune function, and microbial homeostasis[68]. This intricate neural network contains as many neurons as the spinal cord and utilizes many of the same neurotransmitters and signaling molecules found in the central nervous system[68]. The ENS maintains bidirectional communication with the CNS through multiple pathways, including the vagus nerve, systemic immune signaling, and neuroendocrine mechanisms, enabling peripheral inflammatory signals to influence central neuroinflammation[69].

In a broader context, presence of Mn in drinking water and infant formula raises significant public health concerns, particularly in regions where groundwater contamination is prevalent[70]. Formula-fed infants face an especially high risk of excessive Mn exposure, as powdered formula mixed with contaminated water can substantially elevate Mn intake beyond levels encountered through breast feeding[62]. This vulnerability is compounded by the developmental timing of exposure, occurring during critical periods of brain development when inflammatory disruption can have maximal impact on long-term neurological outcomes[71].

**Bridging Pathways: A Framework for Understanding Neurological Disease**

The following research explores neuroinflammation across neurological disorders, investigating how inflammatory mechanisms fundamentally shape neurological dysfunction throughout the lifespan. By bridging insights from neurodegenerative protein misfolding disorders (NPMDs) and neurodevelopmental disorders, this research challenges traditional boundaries between these conditions. Current approaches typically segment neurological disorders based on age of onset or primary pathological mechanisms, but emerging evidence suggests inflammatory responses represent a critical biological process that transcends conventional categorizations[72, 73].

Specifically, this dissertation investigates neuroinflammatory mechanisms in NPMDs and the neurological consequences of developmental exposure to manganese (Mn). The research

aims to elucidate how chronic neuroinflammation, driven by sustained glial activation and dysregulated immune signaling, operates as a fundamental pathological mechanism, potentially influencing outcomes across life stages. The framework explores the relationship of early-life immune challenges creating enduring alterations in neuroimmune signaling, potentially predisposing individuals to later dysfunction[74, 75]. This concept of inflammatory priming suggests a dynamic, interconnected view of neurological health[76].

Methodologically, animal modeling and molecular techniques probe the complex interactions between inflammatory pathways, environmental exposures, and neurological outcomes. By examining cellular mechanisms and systemic responses, this dissertation develops a comprehensive understanding of how inflammatory processes contribute to neurological dysfunction. The scientific significance lies in its potential to reframe our understanding of neurological disorders. By demonstrating the interconnected nature of inflammatory mechanisms, this research opens new avenues for therapeutic strategies addressing a spectrum of conditions. The insights generated support continued holistic approaches to understanding neurological pathology.

The following chapters will delve into these interconnected research domains, presenting a comprehensive investigation of neuroinflammatory mechanisms across the lifespan. Chapter 2 examines the biodistribution and safety profile of SB_NI_112, providing critical insights into the pharmacokinetics, toxicity, and initial characterization of this novel therapeutic agent targeting the NF-κB and NLRP3 inflammatory pathways. Chapter 3 focuses on the preclinical testing of SB_NI_112 in a prion disease model, offering a detailed examination of the drug's efficacy in modulating glial activation, reducing neuroinflammation, and potentially slowing disease progression, with behavioral and histological assessments demonstrating improved cognitive functions and reduced neuronal loss. Chapter 4 shifts focus to the neurodevelopmental consequences of manganese exposure, exploring the intricate

relationships between environmental toxicants, glial dysfunction, and neuroinflammation. This chapter investigates the impact of chronic manganese exposure on the central and enteric nervous systems, examining microglial activation, alterations in dopaminergic signaling, and disruptions to the gut-brain axis.

To conclude this dissertation, Chapter 5 synthesizes the presented research domains, integrating insights from the preceding chapters to discuss the broader implications for understanding neuroinflammation as a cross-disease pathogenic mechanism. This comprehensive discussion explores how environmental factors, glial cell dynamics, and inflammatory pathways contribute to both neurodevelopmental and neurodegenerative disorders, ultimately proposing potential therapeutic strategies and future research direction. The concluding chapter emphasizes the significance of this work in advancing our understanding of neurological health, highlighting the critical role of neuroinflammation in shaping disease progression across the lifespan.

# CHAPTER 2 – LARGE- AND SMALL-ANIMAL STUDIES OF SAFETY, PHARMACOKINETICS, AND BIODISTRIBUTION OF INFLAMMASOME-TARGETING NANOLIGOMER IN THE BRAIN AND OTHER TARGET ORGANS[1]

## Overview

Immune malfunction or misrecognition of healthy cells and tissue, termed autoimmune disease, is implicated in more than 80 disease conditions and multiple other secondary pathologies. While pan-immunosuppressive therapies like steroids can offer limited relief for systemic inflammation for some organs, many patients never achieve remission, and such drugs do not cross the blood–brain barrier, making them ineffective for tackling neuroinflammation. Especially in the brain, unintended activation of microglia and astrocytes is hypothesized to be directly or indirectly responsible for multiple sclerosis, amyotrophic lateral sclerosis, Parkinson's disease, and Alzheimer's disease. Recent studies have also shown that targeting inflammasomes and specific immune targets can be beneficial for these diseases. Furthermore, our previous studies have shown targeting NF-κB and NLRP3 through brain penetrant Nanoligomer cocktail SB_NI_112 (abbreviated as NI112) can be therapeutic for several neurodegenerative diseases. Here, we show safety-toxicity studies, followed by pharmacokinetics and biodistribution in small- (mice) and large-animal (dog)studies of this inflammasome-targeting Nanoligomer cocktail NI112. We conducted studies using four different routes of administration: intravenous, subcutaneous, intraperitoneal, and intranasal, and identified the drug concentration over time using inductively coupled plasma mass spectrometry in the blood serum, the brain (including different brain regions), and other target organs such as

[1] This chapter appears in its entirety as: Risen, S., Sharma, S., Gilberto, V. S., Brindley, S., Aguilar, M., Brown, J. M., Chatterjee, A., Moreno, J. A., & Nagpal, P. (2024). Large- and Small-Animal Studies of Safety, Pharmacokinetics, and Biodistribution of Inflammasome-Targeting Nanoligomer in the Brain and Other Target Organs. *ACS Pharmacology & Translational Science*, *7*(11), 3439–3451. https://doi.org/10.1021/acsptsci.4c00068

liver, kidney, and colon. Our results indicate that the Nanoligomer cocktail has a strong safety profile and shows high biodistribution (F ~ 0.98) and delivery across multiple routes of administration. Further analysis showed high brain bioavailability with a ratio of NI112 in brain tissue to blood serum of ~30%. Our model accurately shows dose scaling, translation between different routes of administration, and interspecies scaling. These results provide an excellent platform for human clinical translation and prediction of therapeutic dosage between different routes of administration.

**Introduction**

The human immune system is the key line of defense in the body against infections and disease and is critical for our survival. Misrecognition of healthy cells, tissue, and organs by the immune system causes more than 80 chronic conditions, and these autoimmune diseases affect more than 24 million people in the US alone, with rising prevalence[77]. These diseases disproportionality affect women and are among the leading causes of death among young- and middle-aged women[78]. Besides being directly implicated in neurological diseases related to motor function like multiple sclerosis (MS) and amyotrophic lateral sclerosis (ALS), several other neurodegenerative diseases like Parkinson's disease (PD) and Alzheimer's disease (AD) are now hypothesized to be linked to nonspecific microglial activation[38, 79-81], the resident immune cells in the brain. While there are no available cures for these autoimmune diseases and more specifically for neuroinflammation, pan-immunosuppressive steroids, and other nonspecific therapies are utilized for managing symptoms and prolonging disease progression or symptom manifestation for systemic diseases. However, such nonspecific immune suppressive methods have significant side effects, especially systemic effects while treating long-term chronic conditions[82]. Therefore, more targeted immune modulation[83, 84] as well as detailed

pharmacokinetic (PK) and route of administration studies are necessary for corticosteroids and pan-immunosuppressive therapies to manage adverse effects and contraindications[82].

*Specific Immune Targeting Can Minimize Side-Effects*

Selective inhibition of key inflammatory nodes/targets such as TNF, IL-17, IL-23, and IL-6 has improved the remission rates and replaced standard-of-care for a growing number of autoimmune diseases[83, 84]. While recent advances in even more target-specific therapies such as tyrosine kinase 2 instead of Janus kinase inhibitors offer further hope in reducing side-effects (e.g., abnormal changes in blood cell, cholesterol, triglyceride levels, etc.)[85], use of more traditional pharmaceutical modalities such as small-molecule-based targeting is slow and low-throughput with mixed safety profile. On the other hand, high-throughput approaches such as design-based antisense oligonucleotides[86] can potentially improve translation rates, but suffer from delivery challenges, especially for neurological diseases[87, 88] and accumulation in first-pass organs[89, 90]. The emergence of new RNA-targeting antisense modalities such as Nanoligomers can have the combined advantage of high delivery and biodistribution profile of small molecules, extremely high target-binding affinity (KD ~ 3--5 nM) like antibodies, with the specificity and ease of design using nucleic acid-targeting[50, 91-95]. Nanoligomers are peptide nucleic-acid-based RNA therapeutic modality that have shown targeted up- and downregulation of proteins, with extremely high specificity, minimal off-targets, and a high safety profile[50, 91-95]. However, more detailed safety-toxicity and biodistribution studies need to be conducted across small- and large-animal models for these new modalities to gain greater acceptance toward human clinical translation and pharma adoption.

*Small- and Large-Animal Studies for Safety and Biodistribution and Intraspecies Scaling*

While rodents are acceptable small-animal models for autoimmune and neurological disease modeling and induction, dogs are the preferred large-animal model for clinical drug translation to further assess the safety profile, central nervous system (CNS),

PK/pharmacodynamic (PD), and biodistribution parameters[96]. We conducted extensive small- and large-animal studies for our targeted inflammasome inhibitor, an NF-κB and NLRP3 inhibitor combination (herein described as SB_NI_112 or NI112 in short) as the active pharmaceutical ingredient (API)[91-95], to assess safety-toxicity, develop a PK and biodistribution model to obtain relevant pharmacological parameters, and obtain insights for interspecies scaling for further translation. We observed extremely high biodistribution parameters across different routes of administration (biodistribution parameter $F > 0.98$), excellent drug delivery across the blood--brain barrier (BBB) (brain tissue concentration ≥25--30% of blood serum bound concentration), rapid absorption across different brain sections, lack of accumulation in first-pass organs, as well as renal clearance of unbound/excess drug (or missense molecules)[92, 95]. These pharmacological results prove the potential for further translation and the need for the adoption of new therapeutic modalities for the benefit of millions of patients across multiple autoimmune and CNS diseases.

**Results and Discussion**

We utilized four different routes of administration: intravenous (IV), subcutaneous (SQ), intraperitoneal (IP), and intranasal (IN) for a comprehensive assessment of safety-toxicity and biodistribution profiles in both small-animal (C57BL/6 mice) and large-animal (beagle dog) models. We explored dose-scaling in different routes, biodistribution parameters, and interspecies scaling reported in this work.

*Safety-Toxicity Assessment: Long-Term Repeat Dosing, 14 Day Acute (5× MTD) Dosing in Small- and Large-Animals for CNS*

We first started with a maximum tolerable dose (MTD) assessment of the NF-κB and NLRP3 inhibitor combination NI112_mouse [nfkb1 (Sequence: AGTGGTACCGTCTGCTA) and nlrp3 (Sequence: CTTCTACTGCTCACAGG)]. Prior studies have shown assessment of NI112

in relevant disease models (MS, AD, Prion/Creutzfeldt-Jacob disease, neuroinflammation, and autoimmune diseases) [48, 50, 91-95], and Nanoligomer selectivity and high-binding affinity[92, 95] (KD 3.17 nM, other PNA/RNA and PNA/DNA binding studies showed KD 5--8 nM[97]) along with rapid biodistribution and clearance. We observed a strong safety-toxicity profile in both animal models for longer-term repeat dosing (IP, 150 mg/kg, 3× a week for 12 weeks, Figures 2.1A-B, as well as single-dose acute toxicity (5× MTD for IV), followed by 14-day toxicity assessment and clinical monitoring (Figure 2.1C-F).

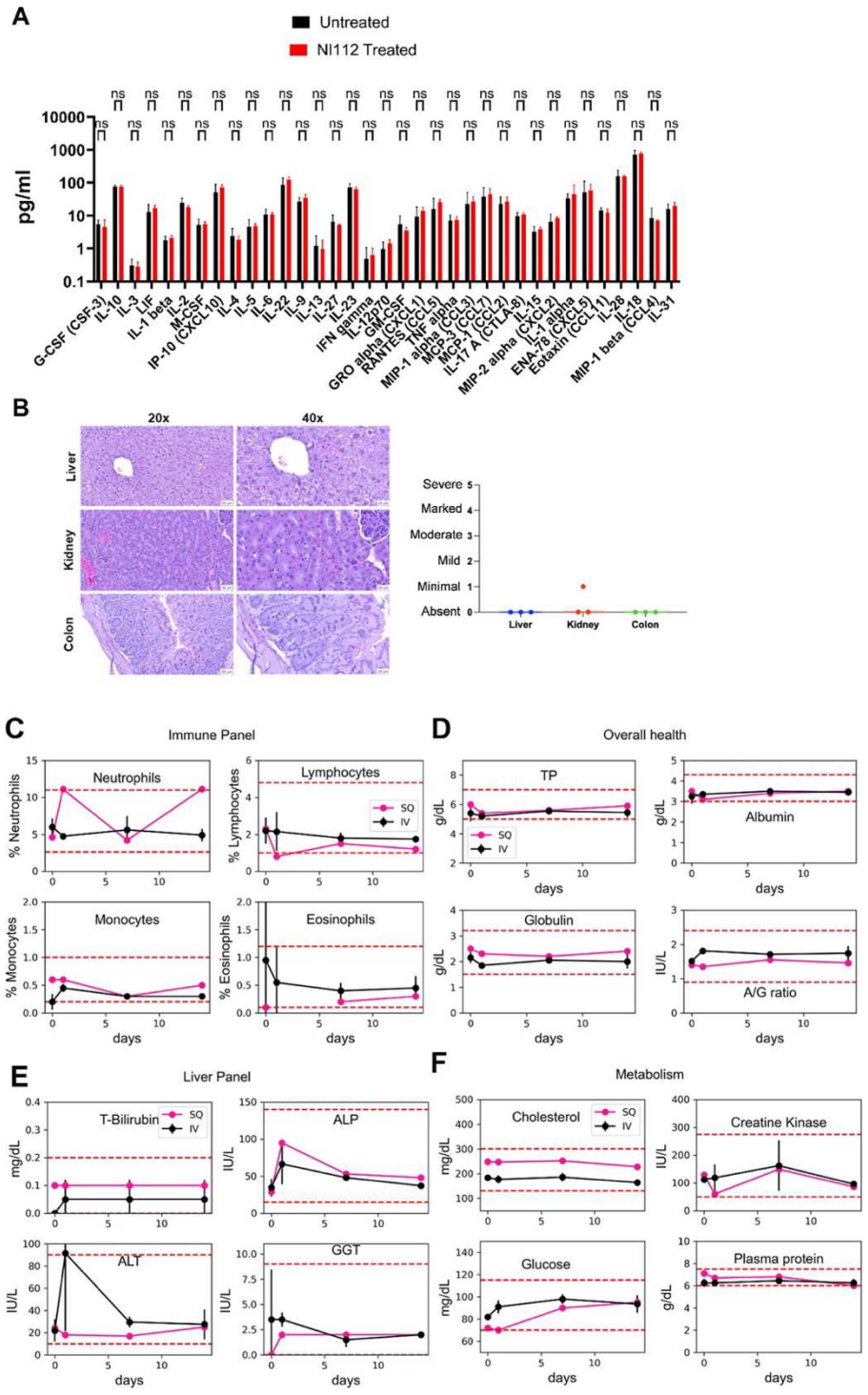


**Figure 2.1. Long-term safety-toxicity and acute single-dose studies reveal the high safety profile of NI112 Nanoligomer.** (A) 12-week dosing of NI112 3× a week shows no change in the immune profile of mice blood serum, as shown using 36-plex cytokine and chemokine markers, measured for treated and untreated animals ($n$ = 4/group), ns = nonsignificant using unpaired $t$-test for each cytokine. (B) H&E-stained histology of kidney, liver, and colon samples from mice

after high-dose (150 mg/kg 3× a week) long-term (12 weeks) treatment shows no immune cell infiltration or any immunogenic response. Histologic findings in each tissue were diagnosed and graded for severity on a 0–5 scale based on inflammation and hemorrhage; 0 = absent, 1 = minimal (10% of tissue affected), 2 = mild (10–25% of tissue affected), 3 = moderate (26–50% of tissue affected), 4 = marked (51–75% of tissue affected), and 5 = severe (75% of tissue affected). There were no significant histologic findings/differences in the liver, kidney, or colons of mice treated with NI112. Kidney nephrons displayed no evidence of inflammation within the glomeruli, supporting the renal clearance shown previously for Nanoligomer molecules. (19,20) (C) Immune panel studies of dogs treated with 75 mg/kg NI112_dog which corresponds to 500 mg/kg dosing in mice, and is well above the MTD. Dogs were monitored for 2 weeks post administration. The results show a lack of any immunogenic response, and no change in neutrophils, lymphocytes, monocytes, or eosinophils in blood. (D) Similar assessment of overall health using total protein (TP), albumin (A), globulin (G), and A/G ratio. (E) Assessment of the liver panel of these animals, and (F) metabolism. The red dashed lines show upper and lower normal limits for each measurement. The curves show mean values and bars show standard deviation (mean ± standard deviation, SD). These extensive studies show minimal side effects and a lack of long-term health concerns even at such high acute doses.

An important finding was that a single route (IV) showed a measurable MTD (100 mg/kg in mice, between 15 and 65 mg/kg in dogs), while other routes showed values well over 450–500 mg/kg, beyond the limit of testing parameters due to solubility limits. As shown in MTD Table 2.1 below, the use of missense Nanoligomers (dog NI112 in mice) also showed no tolerability issues for 450–500 mg/kg IV.

| *Admin Route* | *Molecule* | *Species* | *MTD (mg/kg)* |
|---|---|---|---|
| *IV* | NI112_Mouse | Mouse | 100 |
| *SQ* | | | >450 |
| *IV* | NI112_Dog (Missense) | Mouse | >450 |
| *SQ* | | | >450 |
| *IV* | NI112_Dog | Dog | 15 |
| *SQ* | | | >67.5 |

**Table 2.1. MTD Measurements for Mice and Dog Studies Using IV and SQ Route of Administration.** *n* = 4 for mice studies, *n* = 1–3 for dog studies. 1-test subject each in mice and dog studies showed side-effect/tolerability limit with the IV route, the mouse had experienced seizure-like behavior, and the dog exhibited excess salivation and vomiting.

IV route demonstrates extremely rapid delivery and uptake of Nanoligomers in the brain and other organs (~minutes), and some test subjects showed some adverse events (AEs) at high concentrations (75 mg/kg in dogs). However, the PK and biodistribution of other routes are slightly slower, leading to better tolerance for high drug-dosing. This along with lack of such MTD for missense administration suggests that the AEs are related to the speed/rapid uptake and target inhibition in the brain and other organs, rather than potential side-effects of the API/drug. The lack of such threshold for missense Nanoligomer also suggests the specificity of target engagement by the drug. We note during dog studies, one subject animal showed acute injection site pain, swelling, and discomfort at 75 mg/kg SQ dosing, which was traced back to the high pH of SQ injection due to the use of unbuffered saline media to dissolve dried NI112 powder. However, all subsequent dosing used phosphate-buffered saline, and no animal showed any issues with site injection pain or swelling.

Using these MTD values, we conducted two types of repeat-dosing (using IP) and acute-dosing tests (using IV and SQ). Due to rapid aging in mice, we used 13 to 15-week-old mice for longer-term (12 week) repeat dosing (3× a week, for chronic diseases) with IP injections to assess any biochemical or histological changes compared to sham-treated control animals. As shown in Figure 2.1A, we conducted a detailed blood serum evaluation using 36-cytokine and chemokine biomarkers in blood for any potential immunological or adverse outcomes (through clinical/health monitoring). We did not observe any statistical change any biomarker. Furthermore, we conducted a detailed histological evaluation and scoring for the first pass and clearance organs (liver, kidney, and colon, Figure 2.1B) for chronic-dosed animals, essential for drug metabolism and excretion. We did not observe any evidence of accumulation, organ damage, toxicity, or any immune cell infiltration, as shown using H&E staining. Also, in long-term studies, there was no evidence of accumulation or resulting inflammation in the medulla or nephrons (within glomeruli, Figure 2.1B), supporting renal clearance for Nanoligomer

molecules[92, 95]. These results again demonstrate the high safety profile of the drug for repeated dosing over longer periods.

Next, we conducted acute dose toxicity monitoring in large-animal models (dogs) using 75 mg/kg dose IV administration (5× MTD for IV route). Using the body surface area (BSA) scaling factor [canine equivalent dose (CED) (mg/kg) = mouse dose (mg/kg) × (mouse Km/canine Km)], where Km is the BSA scaling factor to estimate the canine equivalent dose from mouse studies[98]. This dose factor for safety-toxicity and PK analysis was 0.15[98]. We assessed the impact of extremely high doses (e.g., 5× MTD using IV administration) or potential acute drug toxicity in a large-animal model (dogs). We monitored these animals over the recommended 14-day period, with extensive clinical sign monitoring and health checkups, and detailed biomarker assessment, as shown in Figure 1C--F. We dosed dogs using IV and SQ at 75 mg/kg dose. While few test subjects showed some short-term AEs, and 75 mg/kg dose was marked as above MTD in our studies, we sought to further evaluate any adverse health impact. Using a battery of complete blood count (CBC)/chemistry tests for potential immunogenic response (by monitoring neutrophils, lymphocytes, monocytes, or eosinophils in blood, Figure 2.1C), overall health (total protein TP, albumin A, globulin G, and A/G ratio, Figure 2.1D), liver enzymes [T-bilirubin, alkaline phosphatase (ALP), alanine transaminase (ALT), gamma-glutamyl transferase (GGT), Figure 2.1E], and metabolic markers (like cholesterol, creatine kinase, glucose, and plasma protein, Figure 2.1F), we did not observe any pathogenic change in any test subject. We also monitored red blood cells, electrolytes, and kidney function for the acute-dosed beagle dogs to assess any adverse health impact through these biochemical markers. We did not observe any lasting health effects throughout the biomarker assays and the 14-day clinical monitoring. We also repeated these studies at the estimated MTD values for different routes, but again did not observe any abnormal values or clinical concern in any test subject.

This showed a well-tolerated, nontoxic, and nonpathogenic safety profile of API Nanoligomer NI112 treatment using extremely high (acute) dosing in large animals.

*Modeling Biodistribution of the API in Blood Serum and Target Organs*

We measured API NI112 concentration [using inductively coupled plasma mass spectrometry (ICP--MS), see Methods] in blood for 4-different administration routes (IV, IP, IN, and SQ) in mice, with time, and used the multiexponential decay to estimate the time-dependent bound and unbound API concentration (Figure 2.2A).

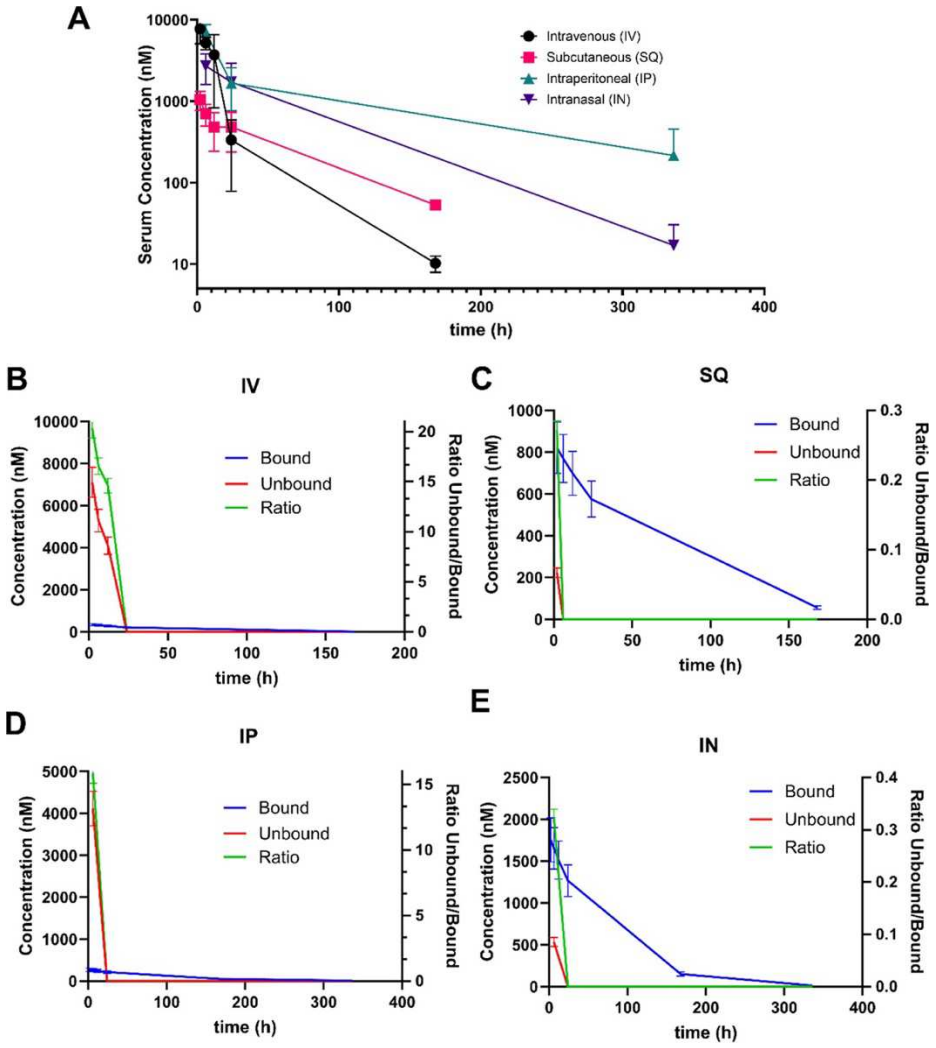


**Figure 2.2. Bound and Unbound API NI112 with time using different routes of administration.** (A) Mice studies showing NI112 concentration in blood serum with time using four different routes of administration at MTD IV (100 mg/kg), IP (500 mg/kg), SQ (450 mg/kg), and IN (500 mg/kg). The multiexponential decay with time was used to derive bound and unbound API (NI112) concentration with time using (B) IV; (C) SQ; (D) IP; and (E) IN route. Right *Y* axis shows the ratio of unbound/bound API in blood serum. The curves show mean values, with the bars showing standard deviation (mean ± SD). Number of animals $n = 4$/group for IV and SQ, $n = 6$/group for IN and IP route of administration.

Briefly, the longtime-decay exponential of blood serum API (bound serum) was assessed as a fraction of the unbound API (Figure 2.2B-E), and observed the unbound API decays with time, almost to zero, within 24 h of drug administration in mice. Another important observation was that while IV and IP routes exhibited an appreciable unbound/bound API ratio (Figure 2.2B, D), SQ and IN routes had a very low ratio of unbound API measured in the blood (Figure 2.2C, E). Eventually (~24 h post administration) all the measured API is bound. These results are consistent with our prior studies, which tracked any unbound API (and all missense sequences) cleared through urine by the animals[92, 95]. We also used PK solver[99] to derive PK parameters for the API in blood serum and measurement of biodistribution coefficient ($F = AUC_{Test\ Route}/AUC_{I.V.}$ $AUC_{max}$: area under the curve), as shown in Figures S10 and S11. While IV and SQ routes showed rapid uptake in the blood (T 2 h) compared to IP and IN, the target organ brain tissue concentration showed higher variance. The half-life in blood (~1--2 days) was also significantly lower than in the brain (~1--2 weeks), showing the rapid uptake of API in different organs and drug clearance from the bloodstream through urine[92, 95].

Further measurements of API NI112 were done in the target organ (the brain, Figures 2.3 and 2.4) and other potential target and/or first pass and clearance organs (liver, kidney, and colon, Figure 2.5).

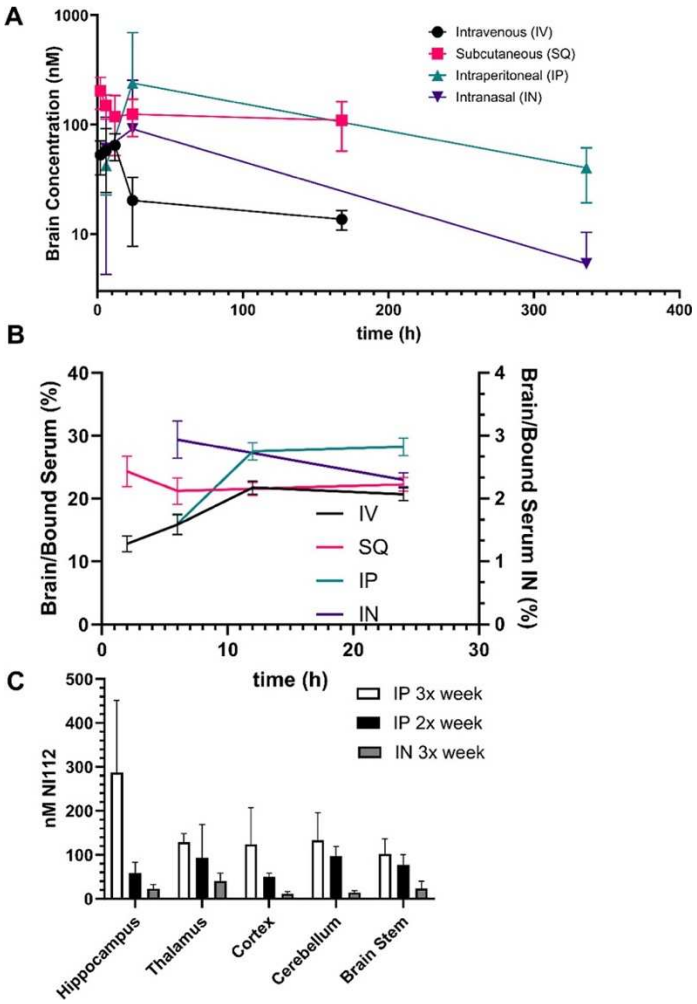


**Figure 2.3. High drug bioavailability and BBB-crossover for neurological disease application.** (A) Mice studies showing NI112 concentration in brain tissue with time using four different routes of administration at MTD IV (100 mg/kg), IP (500 mg/kg), SQ (450 mg/kg), and IN (500 mg/kg). (B) Ratio of brain tissue to bound API concentration in blood serum shows a fairly consistent value (~25–30%) for three routes of administration IV, IP, and SQ. Right *Y* axis shows the ratio of brain tissue/bound API in blood serum for IN administration which is 1 order of magnitude lower (~3%). (C) High bioavailability of API (NI112) in different brain regions with different dosing regimens (3× a week and 2× a week) using IP and IN route at 150 mg/kg dose. The curves show mean values, with the bars showing standard deviation (mean ± SD). Number of animals $n = 4$/group for IV and SQ, $n = 6$/group for IN and IP routes of administration.

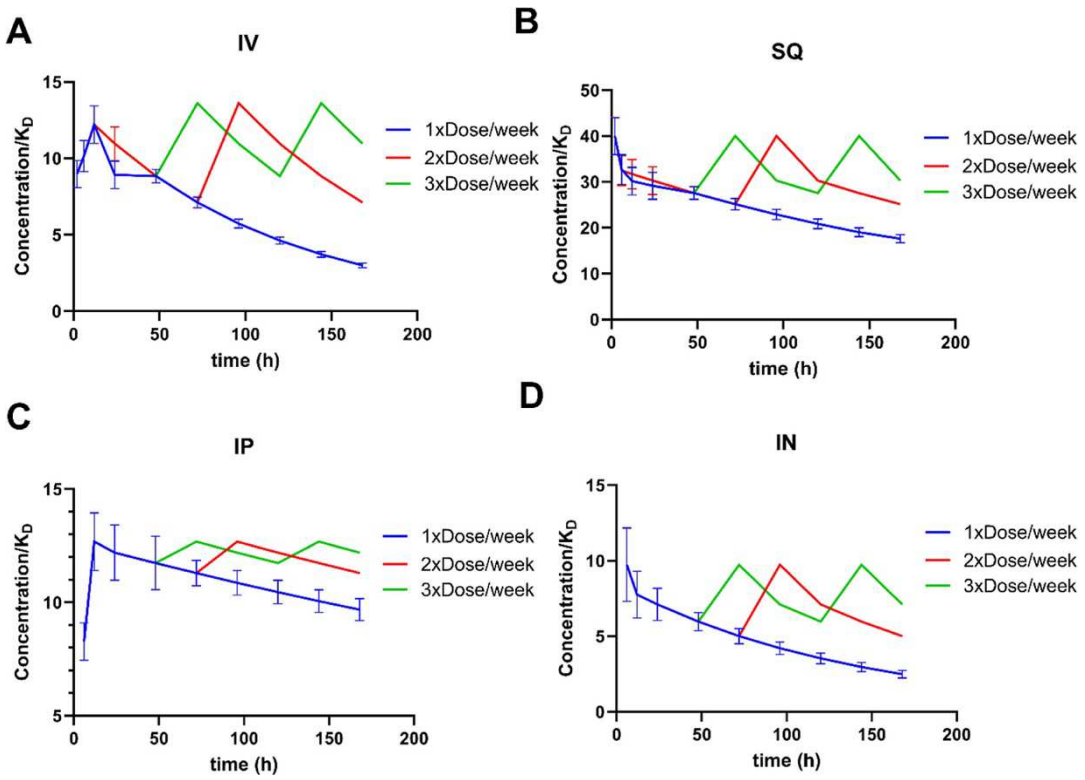


**Figure 2.4. Dosing and repeat dose modeling data for small-animal studies in the target organ (the brain).** (A) IP administration of API NI112 concentration in brain tissue normalized with drug $K_D$ (5 nM, Nanoligomer measured $K_D$ of 3.37 nM, (19,20) other PNA studies show values 5–8 nM (27)) with time using IV (100 mg/kg dosing). The blue curve with standard deviation shows the measured values after a single dose at MTD, whereas red (2× a week) and green (3× a week) are modeled values, shown without SE for clarity. (B) SQ dosing (450 mg/kg) showing single and repeat dosing effects on target organ (the brain) concentration normalized by $K_D$. (C) IP (500 mg/kg) and (D) IN (500 mg/kg) show high drug bioavailability of API (NI112) in brain regions with different dosing regimens (3× a week and 2× a week). The curves show mean values, with the bars showing standard deviation (mean ± SD). Number of animals $n$ = 4/group for IV and SQ, $n$ = 6/group for IN and IP routes of administration.

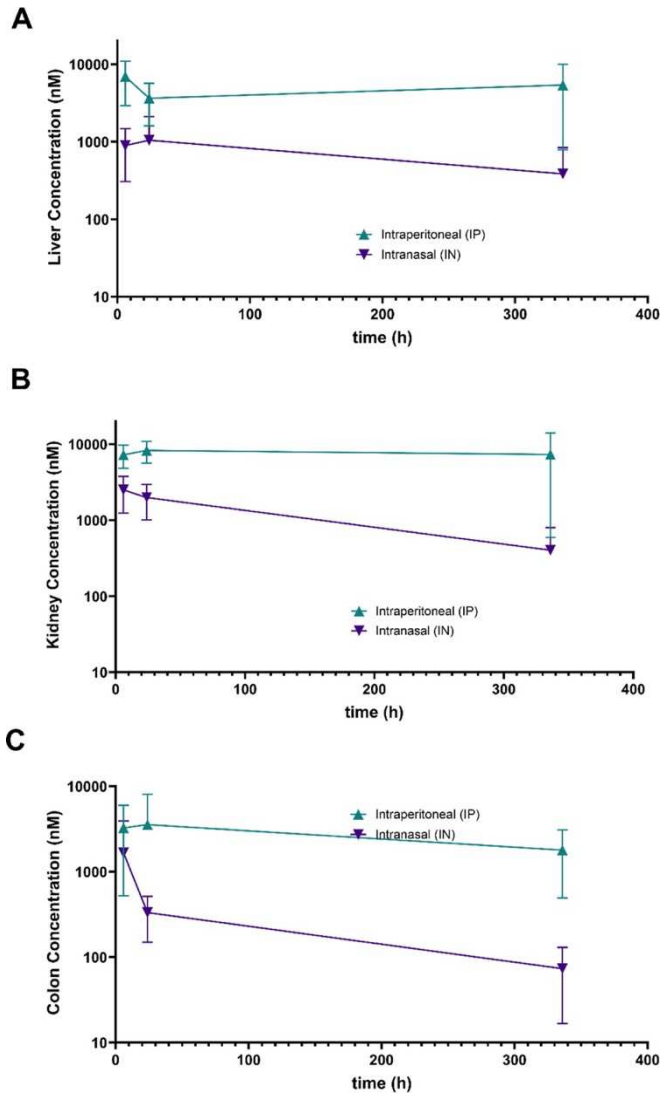


**Figure 2.5. NI112 tissue concentration in the first pass and clearance organs.** Mice studies showing NI112 concentration in different first pass and clearance organ tissues with time using IP and IN routes of administration (A) liver, (B) kidney, and (C) colon. The curves show mean values, with the bars showing standard deviation (mean ± SD). Number of animals $n$ = 6/group for IN and IP routes of administration.

We found high drug bioavailability (~30% of the drug) in the brain across the BBB, compared to API concentration in the blood, and much higher values in liver, kidney, and colon. We even observed excellent biodistribution among different brain regions (hippocampus, thalamus, cortex, cerebellum, and brainstem, Figure 2.3C), providing good confidence for drug delivery and using other Nanoligomer target sequences for different neuronal disease applications. We also developed a model for predicting the target organ concentration and precise dosing concentration and dose frequency (Figure 2.4). The predictive nature of such PK/PD biodistribution profile, combined with detailed disease model studies in small-animals could provide an excellent platform using dose scaling and similar interspecies translation parameters for large-animal model.

*Biodistribution in the Large-Animal Model (Dogs)*

We measured NI112 concentration with time in blood serum for IV, and SQ dosing in dogs (Figures 2.6–8).

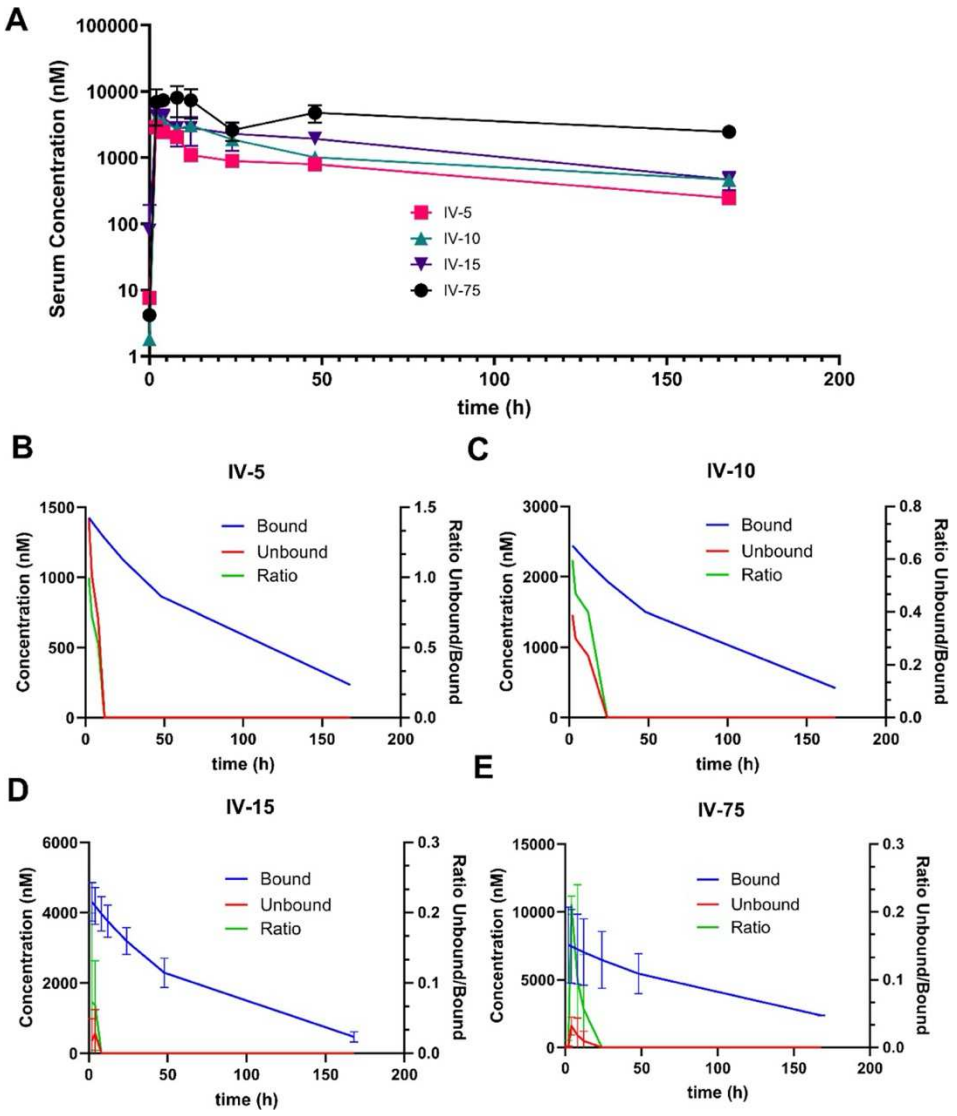


**Figure 2.6. Large-animal dog studies using IV administration of API NI112 at different concentrations.** (A) Blood serum concentration of the API with 5, 10, 15, and 75 mg/kg dosing in beagle dogs. Multiexponential decay of API concentration was used to determine bound and unbound serum concentrations for (B) 5 mg/kg; (C) 10 mg/kg; (D) 15 mg/kg (MTD, *n* = 3/group); and (E) 75 mg/kg (5× MTD) IV dose. The blue curve (bound) and red curve (unbound) show API in blood, along with the Ratio of unbound/bound API (green curve, shown on Right *Y*-axis). The curves show mean values, with the bars showing standard deviation (mean ± SD).

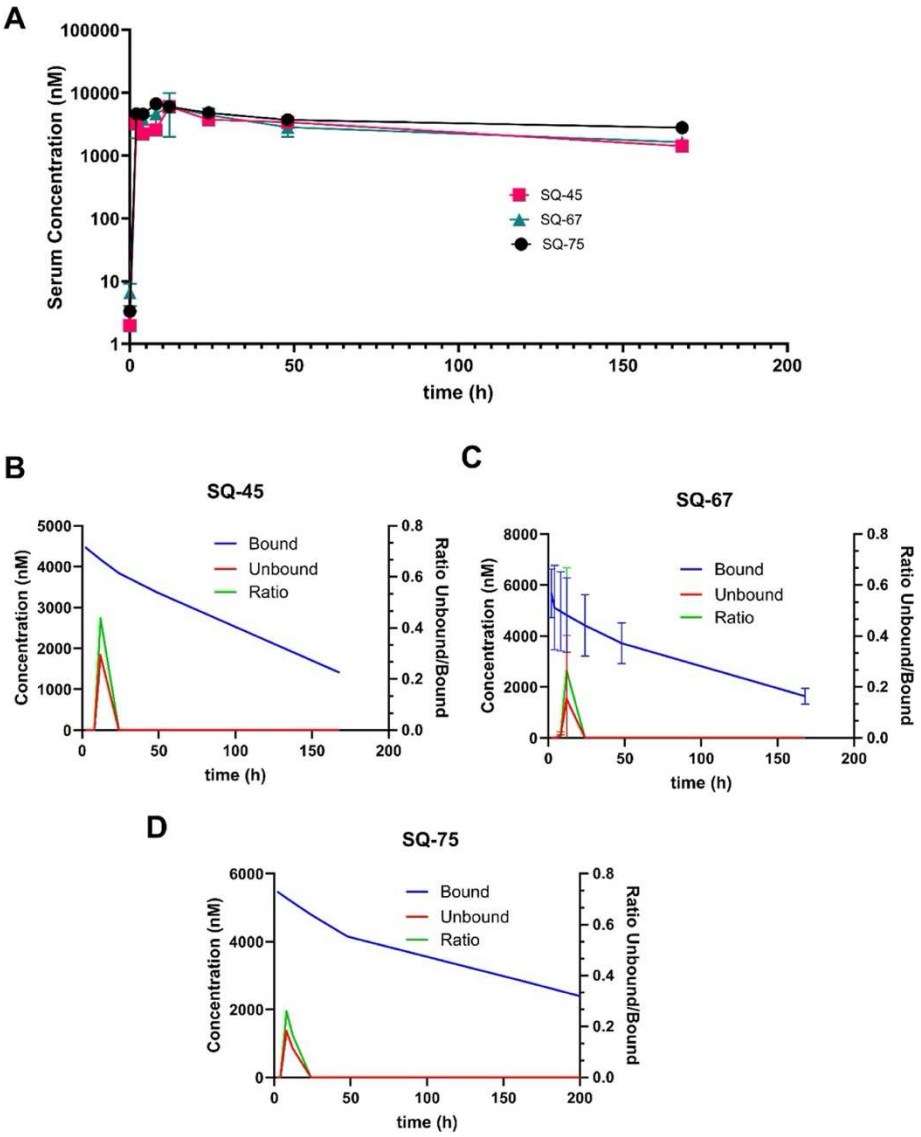


**Figure 2.7. Large-animal dog studies using SQ administration of API NI112 at different concentrations.** (A) Blood serum concentration of the API with 45, 67, and 75 mg/kg dosing in beagle dogs. Multiexponential decay of API concentration was used to determine bound and unbound serum concentrations for (B) 45; (C) 67; and (D) 75 mg/kg SQ dose. The blue curve (bound) and red curve (unbound) show API in blood, along with the Ratio of unbound/bound API (green curve, shown on Right *Y*-axis). The curves show mean values, with the bars showing standard deviation (mean ± SD).

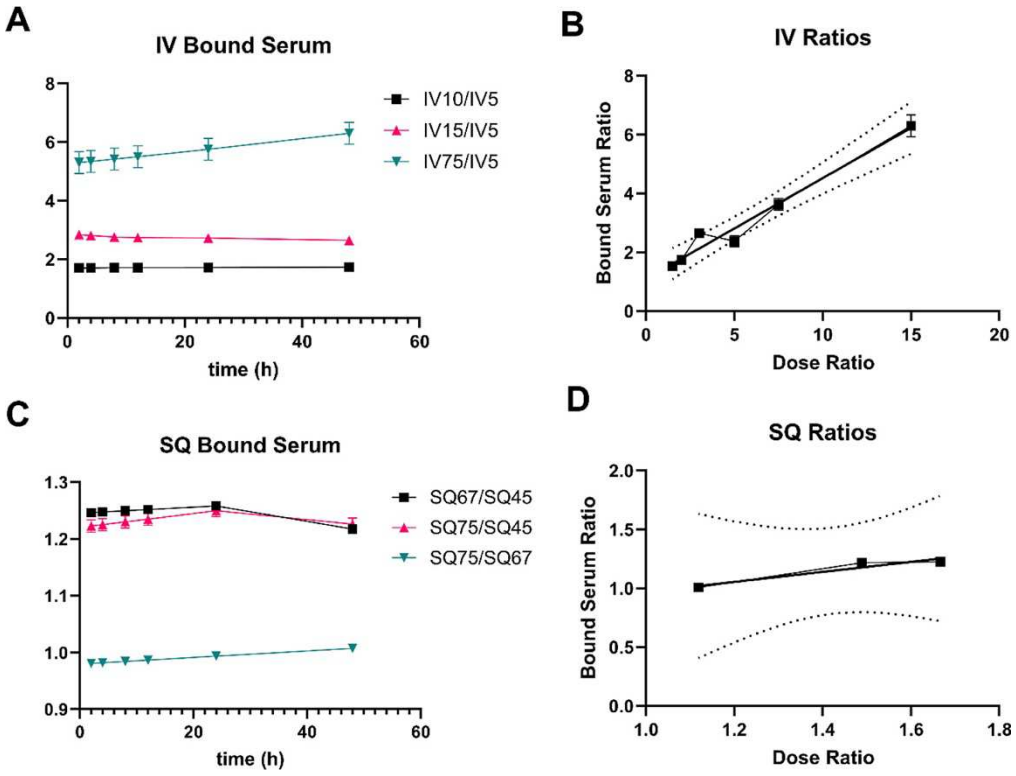


**Figure 2.8. Dose scaling in dog studies using IV and SQ administration of API NI112 at different concentrations.** (A) IV concentration of bound serum shows a nearly constant ratio with the lowest concentration (5 mg/kg). The ratio of 75/5 mg/kg (inverted triangle), 15/5 mg/kg (upward triangle), and 10/5 mg/kg (square) shows flatline values. (B) Linear regression between the bound serum ratio and the dose ratio, with dashed curves showing the 5 and 95% confidence intervals. (C) Bound serum ratio between respective SQ doses. (D) Linear regression between bound serum ratio and dose ratio, showing easily predictable dose scaling that can be used to determine dosing and target organ concentrations in large-animals (beagle dogs). The curves show bound API from mean values, and the bars show standard deviation (mean ± SD).

We obtained PK parameters for different routes and concentrations used. The PK parameters showed similar peak API concentration as rodents but significantly higher bound API concentrations with time and much higher AUC values due to higher target mRNA and protein concentration (NF-κB and NLRP3) in dogs than mice, well beyond BSA scaling used. These AUC ratios also correspond to interspecies scaling and are better predictors than BSA estimation (Km ratios) used for dose scaling between mice and dog studies. We also modeled multiexponential decay to estimate the bound and unbound API concentration with different IV (Figure 2.6) and SQ (Figure 2.7) doses. Our model showed a strong predictive, linear relationship (ratios/slope slightly lower than 1) between the bound serum API concentration with time and dose ratios (Figure 2.8). Therefore, our PK parameters and the model showed an excellent biodistribution profile for API NI112, and very predictive dose scaling for both small- and large-animal models. Therefore, we proceeded to combine our model results (small- and large-animal) to develop interspecies scaling and translation parameters for API NI112.

Using the detailed PK, biodistribution, and scaling models for large and small mammals, we attempted to develop interspecies scaling and translation parameters. While the proposed BSA scaling utilized the Km ratio as a simplistic model, several studies have highlighted the inadequateness of such simple model scaling and the need for more concrete (AUC) and other PK and biodistribution-based modeling parameters to scale. We observed that even though the doses were BSA-scaled between large-animal (dog) and small-animal (mice) studies for both IV and SQ administration of API based on Km (the Km dose factor for dog/mice was 0.15), the value we observed for two routes was not one (Figure 2.9).

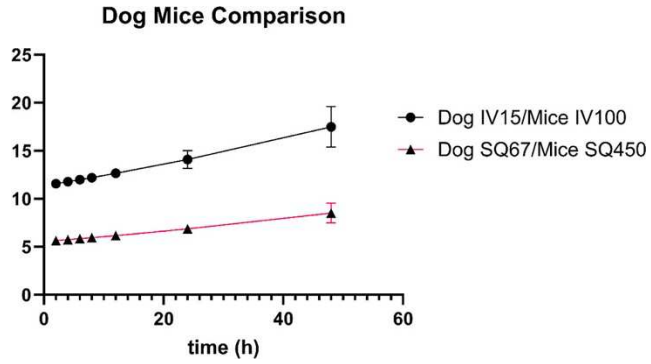


**Figure 2.9. Scaling between large-animal (dog) and small-animal (mice) studies using IV and SQ administration of API NI112 at different concentrations.** The doses chosen were based on the $K_m$ scaling described above [CED (mg/kg) = mouse dose (mg/kg) × (mouse $K_m$/canine $K_m$)] to estimate the canine equivalent dose from mouse studies. The dose factor for dogs/mice was 0.15. (29) The curves show bound API from mean values, and the bars show standard deviation (mean ± SD)

Using the ratio of these scaled doses between species, we observed a clear ratio of 5--6.5 for SQ, and between 12 and 15 for IV administration, presumably based on accessible target ratio (NF-κB and NLRP3 protein amount between species) and AUC ratios (Figure 2.9). Our previous studies showed that 150 mg/kg NI112 IP dosing in mice was therapeutic in several neurological diseases[49, 50, 93]. Based on dose scaling for different routes in mice shown here (Figure 2.4), it corresponds to 50 mg/kg SQ and 30 mg/kg IV dosing in mice. For interspecies scaling, using both BSA (factor 0.15) and SQ and IV factors shown in Figure 2.9, CED corresponds to 1.5 mg/kg SQ and 0.35 mg/kg IV dosing in dogs and using BSA scaling from dog to human, an estimated human equivalent dose (HED) of 0.5--0.75 mg/kg SQ and 0.175 mg/kg IV. For a 70 kg human, this roughly translates to therapeutic dosing of 35--52 mg of API through SQ and 12.5 mg dosing through IV. We continue to develop a predictive model for further scaling for human translation but can use these models and scaling/translation ratios to provide a better estimate for HED. Together, the developed model and pharmacological biodistribution parameters obtained provide a good foundation for further translation and assessment of the API.

**Conclusions**

In conclusion, we conducted a detailed safety-toxicity assessment (long-term repeat dosing and extremely high 5× MTD acute dosing) in small- (C57BL/6 mice) and large-animal (beagle dogs) models for the assessment of neurotherapeutic API NI112. We assessed histological, detailed biochemical (through multiplexed ELISA), and extensive CBC/chemistry biomarker monitoring of immune, metabolic, liver, kidney, and cardiac function. Not a single test subject showed any lasting health impact of the drug administration, and no evidence of any immunogenic response, drug accumulation, tissue damage, or immune cell infiltration was observed. Overall, the animals showed that the new Nanoligomer modality has a strong safety

profile. We also conducted detailed PK and biodistribution studies using different routes of administration (IV, SQ, IP, and IN) at different doses, and obtained relevant PK parameters. We observed high biodistribution across the target organ, the brain (~30% of API in the brain across BBB, compared to that bound in blood serum), and across the different brain regions (the hippocampus, thalamus, cortex, cerebellum, and the brain stem) and high therapeutic bioavailability (>15--40 *KD*) for low/moderate dosing and effective target engagement. We found good agreement between administered dose ratios and measured API across the blood serum, the brain, and other first-pass and clearance organs as well as good agreement between interspecies parameters obtained. While the simple BSA scaling did not provide directly translatable doses (BSA-scaled doses across species do not result in ratios of 1), the values obtained here can provide an excellent starting point/platform for further testing and clinical translation of the API for inflammatory and CNS diseases.

**Methods**

*Nanoligomer Synthesis*

NFκB and NLRP3 antisense Nanoligomers were synthesized at Sachi Bio following established methods detailed elsewhere[91, 93, 94]. Briefly, the 17-base-long peptide nucleic acid (PNA)[91, 93, 94, 100] sequence was selected to optimize solubility and specificity, targeting the start codon regions of *nfkb1* (Sequence: AGTGGTACCGTCTGCTA) and *nlrp3* (Sequence: CTTCTACTGCTCACAGG), within the Mouse genome (GCF_000001635.27), identified using our bioinformatics toolbox[94]. The PNA was synthesized on a Vantage peptide synthesizer (AAPPTec, LLC) by using solid-phase Fmoc chemistry. Fmoc-PNA monomers, wherein A, C, and G monomers were shielded with Bhoc groups, were obtained from PolyOrg Inc. Post synthesis, the peptides were attached to gold nanoparticles and subsequently purified using size-exclusion filtration. The conjugation process and the concentration of the purified

Nanoligomer was measured using absorbance at 260 nm (for PNA detection) and 400 nm (for nanoparticle quantification).

*In Vivo Mice Studies*

Adult female and male C57Bl6/J mice purchased from Jackson Laboratories were housed throughout all experiments at ~18–23 °C on a 12-light/12-dark cycle. Fresh water and *ad libitum* food (Tekland 2918; 18% protein) were routinely provided to all cages. Animals were consistently health checked by the veterinary staff at Colorado State University (CSU). This protocol was approved by the CSU Institutional Animal Care and Use Committee (IACUC) and Laboratory Animal Resources staff.

*Tissue Collection*

Mice were culled after deep anesthetizing with isoflurane, and ~1 mL of blood was removed via cardiac puncture followed by cervical dislocation. The brain was sliced sagittally, the right side of the brain was fixed in 10% normal buffered formalin (NBF) and the left hippocampus, thalamus, brainstem, and a piece of the left cortex and cerebellum tissue were removed, flash-frozen, and stored at –80 °C until further processing. The liver, kidney, and colon were also removed, fixed in 10% NBF, and processed (paraffin-embedded) for immunostaining (details below).

*Large-Animal Dog Studies*

All aspects of the study were approved by the CSU IACUC (protocol ID 4320, approved April 18, 2023). Fifteen healthy, purpose-bred, mixed-sex (14 female, 1 male) beagles between 2 and 3 years of age were enrolled. Dogs weighed a mean of 8 kg with a range of 6.7 to 10.6 kg. All animals were housed in an on-site research facility and were fed, cleaned, socialized, and examined daily by Laboratory Animal Resource staff or veterinarians. Due to animal temperament and intergroup aggression, dogs were housed in 1 group of 5 dogs, 2 groups of 3 dogs, and 2 groups of 2 dogs. Each dog was identified by a distinct ear tattoo. Dogs were

offered water continuously and were fed Exclusive Adult Dog Chicken & Brown Rice Formula dry food in the mornings. Blood samples were collected at time $t$ = 0, 2, 4, 8, 12, 24, 48 h, 7, and 14 days. VCOG Grading Scale was used. 1 being mild; asymptomatic or mild symptoms, clinical signs, or diagnostic observations only; interventions not indicated. 2 being moderate; outpatient or noninvasive intervention indicated; moderate limitation of activities of daily living (ADL). 3 being severe or medically significant but not immediately life-threatening; hospitalization or prolonged hospitalization indicated; disabling, significantly limiting ADL. 4 being life-threatening consequences; urgent interventions indicated. 5 being death related to AE.

*Multiplexed ELISAs*

Blood serum and tissue homogenates from mice were subjected to analysis using the ThermoFisher 36-plex Procartaplex cytokine/chemokine panel[91, 93]. The process involved homogenizing 25 µL of 10 mg/mL brain tissues with ProcartaPlex Cell Lysis Buffer (ThermoFisher) and 5 mm stainless steel beads (Qiagen) at 25 Hz for 1.5--3 min, utilizing a Qiagen/Retsch Bead Beater. After homogenization, samples underwent centrifugation at 16 000*g* for 10 min at 4 °C. Following centrifugation, homogenized samples were evaluated for protein concentration using the DC Protein Assay (Bio-Rad) kit protocol. Protein measurements were acquired with a Tecan GENios microplate reader.

The homogenate was then processed in accordance with the manufacturer's provided protocol and analyzed using a Luminex MAGPIX xMAP instrument. Standards for each cytokine/chemokine were utilized at 1:4 dilutions (8-fold dilutions), alongside background and controls. Subsequently, sample concentrations were determined from a standard curve using the Five Parameter Logistic (5PL) curve fit/quantification method.

*Inductively Coupled Plasma Mass Spectrometry*

ICP-MS quantification was conducted following established protocols as outlined in prior publications[92, 95]. Briefly, tissue samples underwent homogenization in a TissueLyser II bead mill (Qiagen, Germantown, MD) at 30 Hz for 3 min, with the addition of 1 µL of deionized water per 1 mg of organ tissue. Homogenates were subsequently digested in 500 µL of aqua regia (3:1 hydrochloric acid to nitric acid) for 4 h at 100 °C. Pellets resulting from the digestion process were resuspended in water and subjected to analysis using a NexION 2000B single quadrupole ICP--MS system (PerkinElmer, Waltham, MA). The sample introduction utilized a Meinhard nebulizer with a cyclonic glass spray chamber, and a nickel sample and skimmer cone were employed in conjunction with an aluminum hyperskimmer cone. A seven-point linear standard curve was generated within a concentration range of 0--250 ppb Au, and linearity was defined at an R^2^ value of greater than 0.995. The 1000 ppm gold standard solution (Ricca Chemical Company, Arlington, TX), and TraceMetal grade 70% HNO3 (ThermoFisher Scientific, Waltham, MA) were used as obtained. All water used was sourced from a Milli-Q system (Millipore, Burlington, MA). Subsequent data analysis was carried out using Microsoft Excel.

*Hematoxylin and Eosin Staining for Tissue Morphology*

Brains and visceral organs were fixed in 10% NBF at room temperature for at least 48 h. Tissues were processed using a Leica TP1020 Automatic Benchtop Tissue Processor and embedded in paraffin wax (Cancer Diagnostics, Cat #: EEPAR56). Tissues were sectioned on a ThermoFisher Scientific HM 325-2 Manual Microtome at 5 µm thickness and mounted on positively charged glass slides (Superfrost Plus, Cancer 232 Diagnostics, Cat #: 4951) for staining and analysis. One section per animal was deparaffinized and stained with hematoxylin

(Cancer Diagnostics, Cat#: #HTV-4) and eosin (Cancer Diagnostics, Cat#: #ETV) (H&E) for the determination of histopathological changes. Whole tissue images were taken for analysis using an Olympus DP70 camera using an Olympus UPlanSApo 20× objective (N.A. = 0.75).

*Statistics*

Statistical tests, numbers of mice, and *p*-values are indicated in the figure legends. GraphPad Prism and Microsoft Excel were used for the statistical analysis.

*Ethics Approval*

Mice were euthanized by deeply anesthetizing with isoflurane, followed by decapitation. All mice were bred and maintained at Lab Animal Resources, accredited by the Association for Assessment and Accreditation of Lab Animal Care International, in accordance with protocols approved by the Institutional Animal Care and Use Committee at Colorado State University. All dog experiments were also approved by the Clinical Review Board and the Institutional Animal Care and Use Committee at Colorado State University.

# CHAPTER 3 – TARGETING NEUROINFLAMMATION BY PHARMACOLOGIC DOWN-REGULATION OF INFLAMMATORY PATHWAYS IS NEUROPROTECTIVE IN PROTEIN MISFOLDING DISORDERS[2]

## Overview

Neuroinflammation plays a crucial role in the development of neurodegenerative protein misfolding disorders (NPMDs). This category of progressive diseases includes, but is not limited to, Alzheimer's disease, Parkinson's disease, and prion diseases. Shared pathogenesis involves the accumulation of misfolded proteins, chronic neuroinflammation, and synaptic dysfunction, ultimately leading to irreversible neuronal loss, measurable cognitive deficits, and death. Presently, there are little to no effective treatments to halt the advancement of NPMDs. We hypothesized directly targeting neuroinflammation by downregulating the transcription factor, NF-κB and the inflammasome protein, NLRP3, with the brain-penetrant, non-toxic, SB_NI_112, would be neuroprotective. To achieve this, we used a cocktail of RNA targeting therapeutics (SB_NI_112) shown to be brain-penetrant, non-toxic, and targeting both NF-κB and NLRP3. We utilized a mouse-adapted prion strain as a model for NPMDs to assess aggregation of misfolded proteins, glial inflammation, neuronal loss, cognitive deficits, and lifespan. Prion-diseased mice were treated either intraperitoneally or intranasally with SB_NI_112. Behavioral and cognitive deficits were significantly protected by this combination of NF-κB and NLRP3 down-regulators. Treatment reduced glial inflammation, protected against neuronal loss, prevented spongiotic change, rescued cognitive deficits, and significantly lengthened lifespan of prion-diseased mice. We have identified a non-toxic, systemic pharmacologic that down-regulates NF-κB and

[2] This chapter appears in its entirety as: Risen, S. J., Boland, S. W., Sharma, S., Weisman, G. M., Shirley, P. M., Latham, A. S., Hay, A. J. D., Gilberto, V. S., Hines, A. D., Brindley, S., Brown, J. M., McGrath, S., Chatterjee, A., Nagpal, P., & Moreno, J. A. (2024). Targeting Neuroinflammation by Pharmacologic Downregulation of Inflammatory Pathways Is Neuroprotective in Protein Misfolding Disorders. *ACS Chemical Neuroscience*, *15*(7), 1533–1547. https://doi.org/10.1021/acschemneuro.3c00846

NLRP3, prevents neuronal death and slows the progression of neurodegenerative disease. Though mouse models do not always predict human patient success, and the study was limited due to sample size and number of dosing methods utilized, the findings here serve as a proof of principle for continued translation of therapeutic SB_NI_112 for prion disease and other misfolded protein diseases. Based on success in a murine prion model, we look forward to continued testing in a variety of neurodegenerative disease models, including Alzheimer's Disease and Parkinson's Disease.

**Introduction**

Chronic inflammation in the brain has emerged as a significant contributor to neurodegenerative disease pathogenesis and progression. Alzheimer's disease (AD), Parkinson's disease (PD), and prion diseases share many common characteristics; accumulation and aggregation of misfolded proteins, glial activation, chronic neuroinflammation, neuronal loss, cognitive deficits, and death[101-105]. These diseases can be placed under the broader category of neurodegenerative protein misfolding disorders (NPMDs) and are associated with the presence and aggregation of misfolded amyloid-β (Aβ) in AD, alpha synuclein (α-Syn) in PD, or the prion protein (PrPSc) in the brain, which lead to behavioral deficits and subsequent progressive neuronal death[106]. Many disease modifying treatments have been directly targeted toward the aggregated proteins associated with such disease, though none have been successful in stopping disease progression[107-109]. Innate immune activation of microglia and astrocytes appears to be particularly important in the context of NPMDs[110-112]. Furthermore, new evidence suggests that the compounded effect of misfolded proteins leads to further glial and astrocyte activation[51, 106, 113, 114]. Therefore, chronic neuroinflammation has been identified as a promising therapeutic target for NPMDs. However,

the only current interventions include anti-inflammatory steroids, but their effectiveness as neurotherapeutic countermeasures has not yet been established physiologically[115, 116].

During NPMD-induced neuroinflammation, there is significant crosstalk between microglia, astrocytes, and neurons via critical inflammatory cell signaling events involving initiation of the nuclear factor kappa B (NF-κB) pathway and subsequent NOD (nucleotide-binding oligomerization domain), LRR (leucine rich repeat), and pyrin-containing 3 (NLRP3) inflammasome formation[117-119]. NF-κB, when translocated into the nucleus, promotes transcription of several inflammatory cytokines and chemokines, including NLRP3, pro-interleukin-1β (pro-IL-1β), and pro-interleukin-18 (pro-IL-18), triggering a cascade of microglial and astrocytic inflammation[120]. These reactive astrocytes are directly toxic to neurons and endothelial cells during prion disease[121, 122]. Many recent studies, including human patient, in vitro, and in vivo animal models, have pointed to the assembly of the NLRP3 inflammasome in microglia and astrocytes as a significant contributor to inflammatory-related amplification of misfolded proteins in NPMDs[38, 123-127]. Formation of the NLRP3 inflammasome is a critical step for activation of pro-inflammatory cytokines and perpetuation of the immune response through microglial pyroptosis[128, 129]. Pro-caspase-1 is activated by proximity-induced autocatalytic activation upon recruitment to the NLRP3 inflammasome. Active caspase-1 cleaves pro-IL-1β and pro-IL-18 into their mature and biologically active forms, cytokines IL-1β and IL-18[128, 130]. In mouse models of APP/PS1 mutation and a tauopathy, NLRP3 inflammasome assembly has been identified as a significant contributor to inflammatory-related amplification of Aβ plaques and neurofibrillary tangles[38, 123]. Similarly, the NLRP3 inflammasome promotes α-Syn production in mouse models of PD[126, 127]. Activation of NF-kB in prion disease augments neuronal death by increasing the expression of pro-apoptotic genes and triggering the release of cytochrome C, resulting in mitochondrial dysfunction and endoplasmic reticulum stress[131]. Additionally, the upregulation of inflammatory cytokines IL-1β and tumor necrosis factor (TNF), formerly known

as tumor necrosis factor alpha (TNFα), at sites of synaptic damage trigger the production of reactive oxygen species including hydrogen peroxide and nitric oxide, leading to excitotoxicity and neuronal death[132-134].

Based on the extensive evidence supporting central involvement of NLRP3 inflammasome formation following NF-κB activation in the progression of NPMD's, it is important to develop potential therapeutics to inhibit NF-κB and NLRP3. Therapeutic intervention to target and inhibit NLRP3 inflammasome formation arises as a potential three-hit treatment against NPMDs by: 1) reducing inflammatory signaling amongst microglia and astrocytes[117-119], 2) preventing propagation of misfolded proteins[114, 123], and 3) upregulating microglia autophagy to accelerate removal of misfolded proteins[135-137]. No studies to date have explored combined NF-κB and NLRP3 inhibition as a therapeutic intervention for NPMD's.

In the present study, we utilized non-toxic, brain-penetrant Nanoligomers designed to downregulate NF-κB and NLRP3[93]. Nanoligomers are stable, non-toxic, and bioavailable, with the capability to cross the blood brain barrier (BBB) through various routes of administration[91]. A previous study displayed effective gene regulation in vivo with a similar Nanoligomer therapeutic aimed at down-regulation of NF-κB and tumor necrosis factor receptor 1 (TNFR1) in an LPS-induced murine model of neuroinflammation[93]. The combined NF-κB and NLRP3 down-regulator, SB_NI_112, displays high target specificity and minimal off-targeting (Sharma et al., 2022). To study the impact of targeting NLRP3 inflammasome formation as a therapeutic for NPMDs, we utilized a mouse model of infectious prion disease in wild-type (C57BL/6) mice. A prion model allows for study of a naturally occurring NMPD without the need for transgenic mice. Prion diseases are rare neurodegenerative diseases that result from the native conformation of the cellular prion protein ($PrP^{C}$) misfolding to the infectious form, $PrP^{Sc}$[138, 139]. All prion diseases display the common characteristics of NPMDs, including the accumulation and aggregation of a misfolded protein (PrPSc), glial activation, chronic inflammation, neuronal loss,

cognitive deficits, and death[91, 93]. Previous literature has shown that therapeutics developed for prion disease mice can be translated into other NPMDs, though the few compounds shown to reduce signs of prion disease in mouse models are associated with several negative side effects[132]. In this study, we found that treatment with SB_NI_112 to down-regulate NF-κB and NLRP3 reduced glial inflammation, protected against neuronal loss, prevented spongiotic change, rescued cognitive deficits, and significantly lengthened lifespan of prion-diseased mice. These findings, if validated clinically, have important implications for improving the quality of life for patients suffering with NPMDs.

**Results & Discussion**

Attempts to slow the progression of NPMDs have proven to be difficult. Many promising treatments are toxic or must be delivered directly to the brain, making translation to human patients difficult[107, 132, 140, 141]. NPMDs have highly complex etiology, making the root cause, or multiple causes, difficult to identify and target. Neuroinflammation has arisen as a promising target, as chronic stimulation of the brain's immune system leads to increased protein misfolding and neuronal death[51, 106, 111]. The NF-κB pathway and subsequent NLRP3 inflammasome formation have been identified as key contributors to chronic neuroinflammation present in NPMDs[124, 125, 131, 133]. Here, we employed a mouse prion model to test the efficacy of a combined NF-κB and NLRP3 down-regulator for NPMD treatment.

Wild-type, C57Bl6/J, (Jackson Laboratories) mice were infected intracerebrally with 0.1% prion brain homogenates from Rocky Mountain Laboratories (RML) or normal brain homogenates (NBH) derived from C57Bl6/J mice as the controls. SB_NI_112 treatment began at 10 weeks post-inoculation (wpi) or approximately 40% of prion disease progression and continued until the mice succumbed to the disease (Figure 3.1). As the disease progressed and treatment continued, behavioral assessments including novel object recognition, burrowing, and

nesting, were performed at 12 wpi to train and establish a baseline for each experimental cohort, then continued throughout the study. All three behavioral assessments measure hippocampal integrity, the brain region known to show the first clinical pathology including glial inflammation and spongiotic change[142, 143].

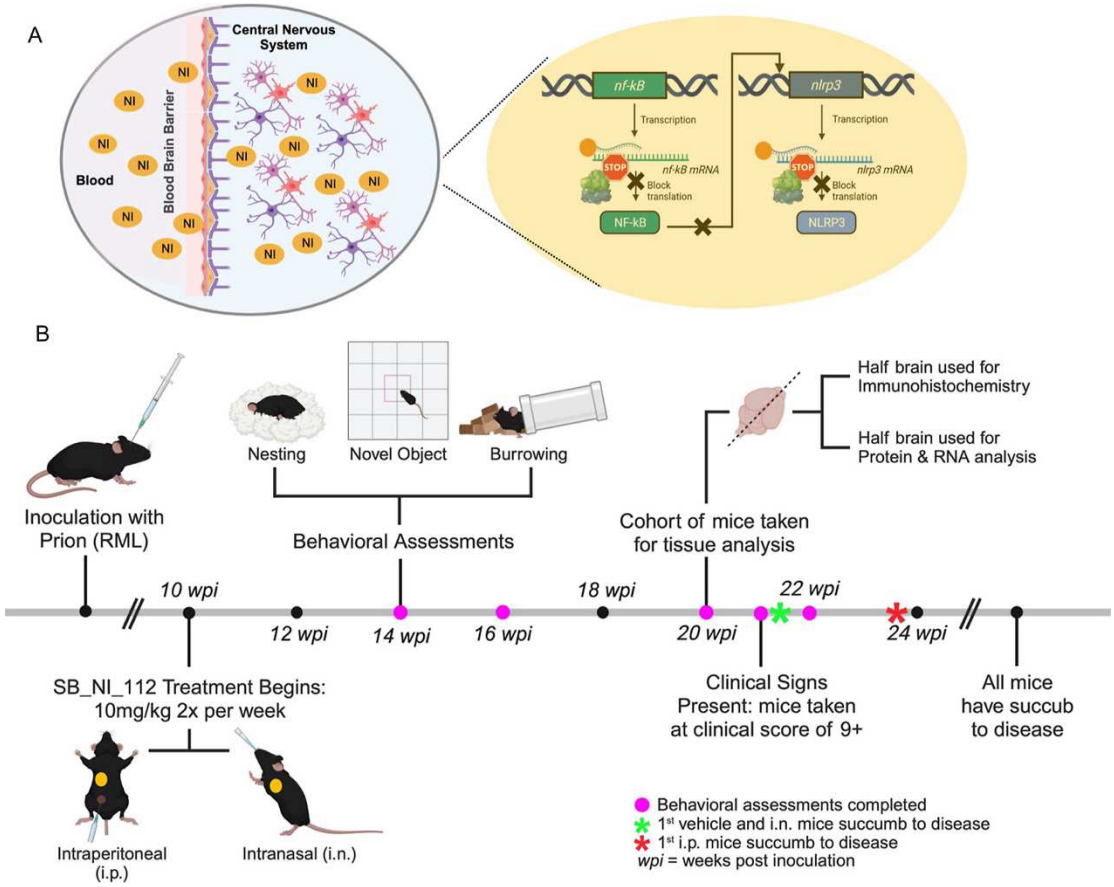


**Figure 3.1. Experimental Design.** Wild-type C57BL/6 mice were inoculated with RML mouse-adapted prion or normal brain homogenate (NBH). Incubation period is 10 weeks. Prion diseased mice were treated with NF-κB and NLRP3 down-regulator SB_NI_112 or vehicle via intraperitoneal (i.p.) or intranasal (i.n.) routes of exposure, twice a week at 10 mg/kg starting at 10 weeks post inoculation (wpi). Mice were monitored for changes in cognition and behavior throughout the disease progression. At 20 wpi brain tissue was dissected for analysis of disease progression including glial inflammation, spongiotic change, and neuronal loss. Created with BioRender.com

*SB_NI_112 penetrates the blood-brain barrier and is systemically non-toxic.*

With a focus on reducing inflammation in the brain, it was important to assess whether SB_NI_112 effectively crosses the blood brain barrier (BBB). Biodistribution and toxicity testing was completed in naïve C57BL/6 female and mice. Penetration of SB_NI_112 across the blood-brain barrier was confirmed with ICP-MS and detected in the hippocampus (76.1 nM +/- 44.3), cortex (49.9 nM +/- 11.4), cerebellum, (96.9 nM +/- 45.0) and brainstem (96.6 nM +/- 32.4) (Figure 3.2A), which is significantly higher than the dissociation constant of SB_NI_112[95].

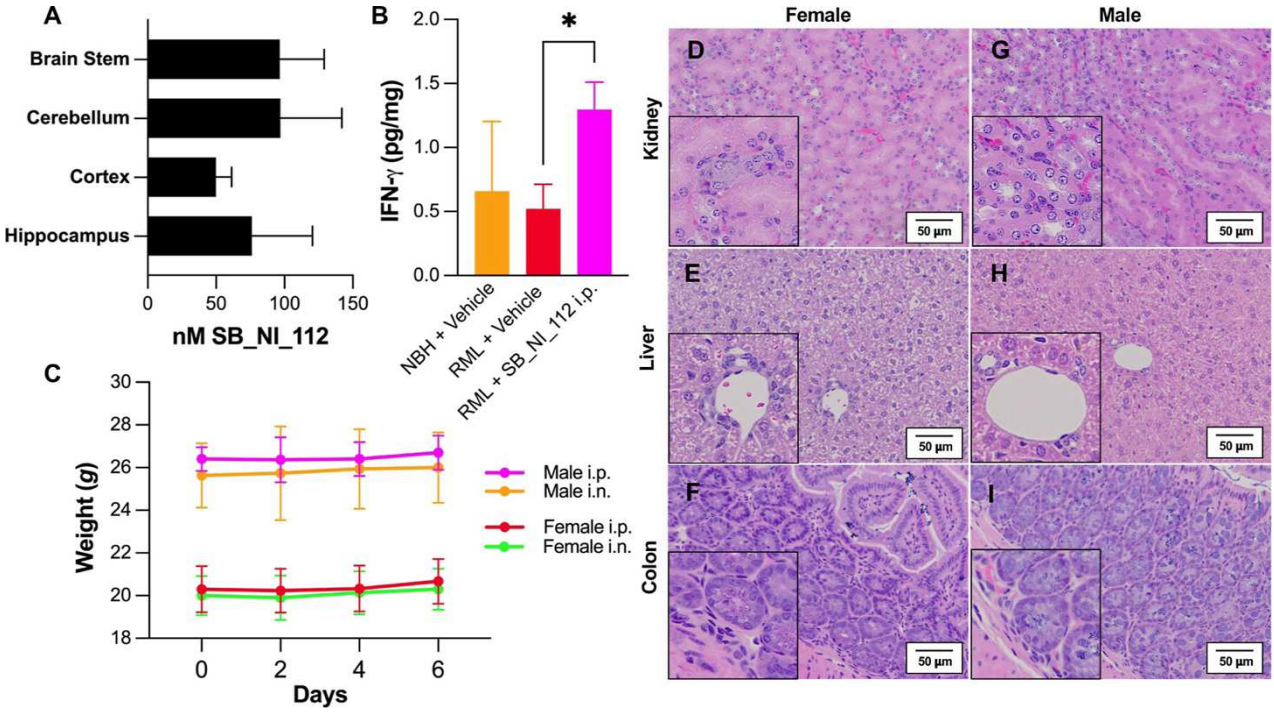


**Figure 3.2. NF-κB and NLRP3 down-regulator SB_NI_112 penetrates the brain and is systemically non-toxic.** Levels of SB_NI_112 in brain regions following dosing at 150 mg/kg i.p. three times per week for two weeks (A). Expression of IFN-γ measured with ELISA (B). N=2 for NBH + Vehicle, N=4 for RML + Vehicle and RML + SB_NI_112 i.p. 10 mg/kg. One-way ANOVA, error bars = SEM, *$p < 0.05$. Weights of mice following a single dose of 500 mg/kg SB_NI_112 i.p. (C). Representative images at 20x of colon, kidney, and liver for female (D-F) and male (G-I) C57BL/6 mice one week after 500 mg/kg dose.

Down-regulation of NF-κB and NLRP3 with SB_NI_112 leads to dampening of chronic inflammation while preserving key immune pathways needed to respond to infectious pathogens (Nuvolone et al., 2015). Despite down-regulation of NF-κB and NLRP3, interferon gamma (IFN-γ) expression was significantly higher in prion infected mice treated with SB_NI_112 ($p = 0.048$ (2-way t-test, Excel) or 0.0468 (One-way ANOVA, Graphpad Prism)), and not significantly different from control NBH mice (Figure 3.2B). This displays the use of SB_NI_112 specifically interferes with the NF-κB and NLRP3 pathway but does not alter expression of immune signaling molecules essential for response to infections.

Both female and male naïve C57BL/6 mice treated with a single dose of SB_NI_112 at 500 mg/kg intraperitoneally (i.p.) had no weight loss 1 week after dosing (Figure 3.2C) and displayed no morphologic toxicity in the colon (Figure 3.2C, F), kidney (Figure 3.2D, G), or liver (Figure 3.2E, H) via hematoxylin and eosin staining. No immune cell infiltration was identified in these organs and the parenchymal cells were intact. Based on previous studies completed with similar therapeutics[91, 93], we chose to dose mice conservatively at 10 mg/kg two times per week. Prion-diseased mice were split into 3 treatment groups: vehicle i.p., SB_NI_112, intranasal (i.n.), and SB_NI_112 i.p.

To confirm therapeutic SB_NI_112 successfully inhibits both NF-κB and NLRP3, we performed western blots to analyze the ratio of active NF-κB (phosphorylated p65; p-p65) compared to inactive form (p65) and NLRP3 protein expression. Interestingly, we identified a higher success of inhibition with intraperitoneal delivery than intranasal. SB_NI_112 provided significant reduction of p-p65 in prion disease mice compared to untreated counterparts (Figure 3.3A, B, and D: p-value = 0.0333).

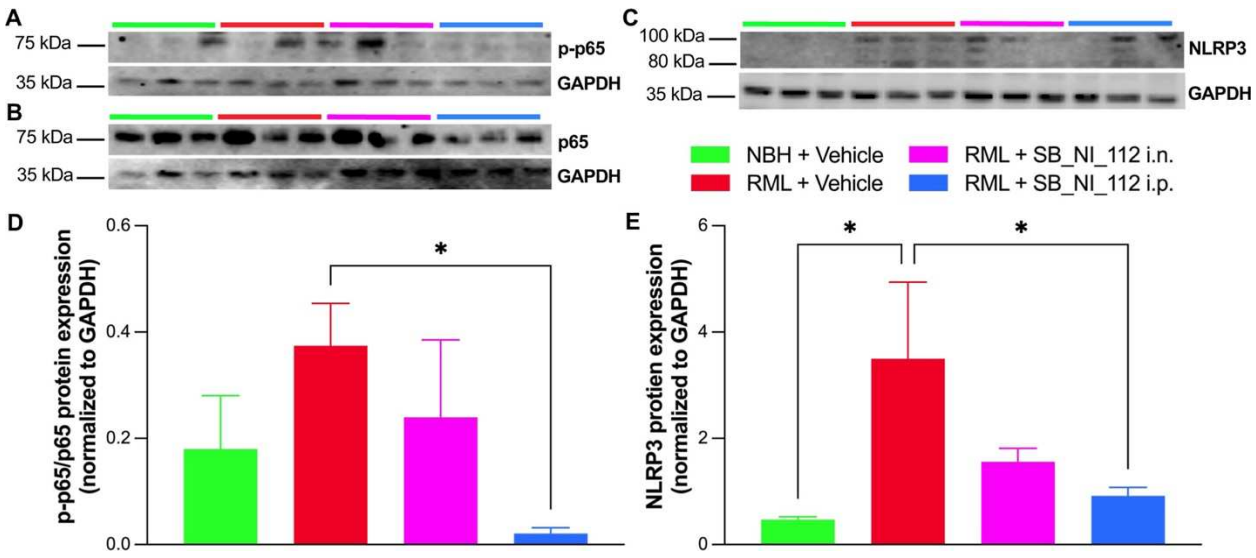


**Figure 3.3. Intraperitoneally delivered SB_NI_112 significantly reduces phosphorylated p65 and NLRP3 protein expression in prion-diseased mice.** Western blot images for phosphorylated-p65 (p-p65;A), p65 (B), and NLRP3 (C). Quantification of p-p65/p65 protein expression normalized to GAPDH (D). Quantification of NLRP3 protein expression normalized to GAPDH (E). N=3 for all groups. One-way ANOVA, error bars = SEM, * $p < 0.05$.

Intraperitoneal treatment also significantly reduced NLRP3 expression in prion-diseased mice compared to untreated counterparts (Figure 3.3C, E; p-value = 0.0380). This difference in effectiveness is likely due to inconsistency of intranasal delivery compared to and intraperitoneal method. The higher success of SB_NI_112 dosed intraperitoneally to inhibit NF-κB and NLRP3 is supported by the following behavioral and histological results obtained.

*Prion-induced behavioral and cognitive deficits occur significantly later in mice treated with NF-κB and NLRP3 down-regulator.*

Down-regulation of NF-κB and NLRP3 significantly protects against behavioral and cognitive changes associated with RML treated prion disease. RML mouse-adapted prion strain preferentially seeds and accumulates in the hippocampus[142, 143]. Two common hippocampal behaviors affected by RML prion disease include nesting and burrowing activity[144, 145]. To assess nesting, mice were given napkins to nest in overnight and scored between one (no nest formed) and five (fluffy built nest) weekly starting at 16 wpi. Monitoring of nest formation was found to be significantly higher among i.p. treated mice at 20 wpi (average score 4.5, p = 0.0001), 21 wpi (average score 3.2, p = 0.0007), and 22 wpi (average score, 2.5, p = 0.0216) (Figure 3.4A) compared to vehicle-treated prion-infected (average score 1 at 20 wpi, and 0.5 at 21 and 22 wpi) nest formation, while i.n. treated mice show a trend though no significant change in nesting throughout the disease.

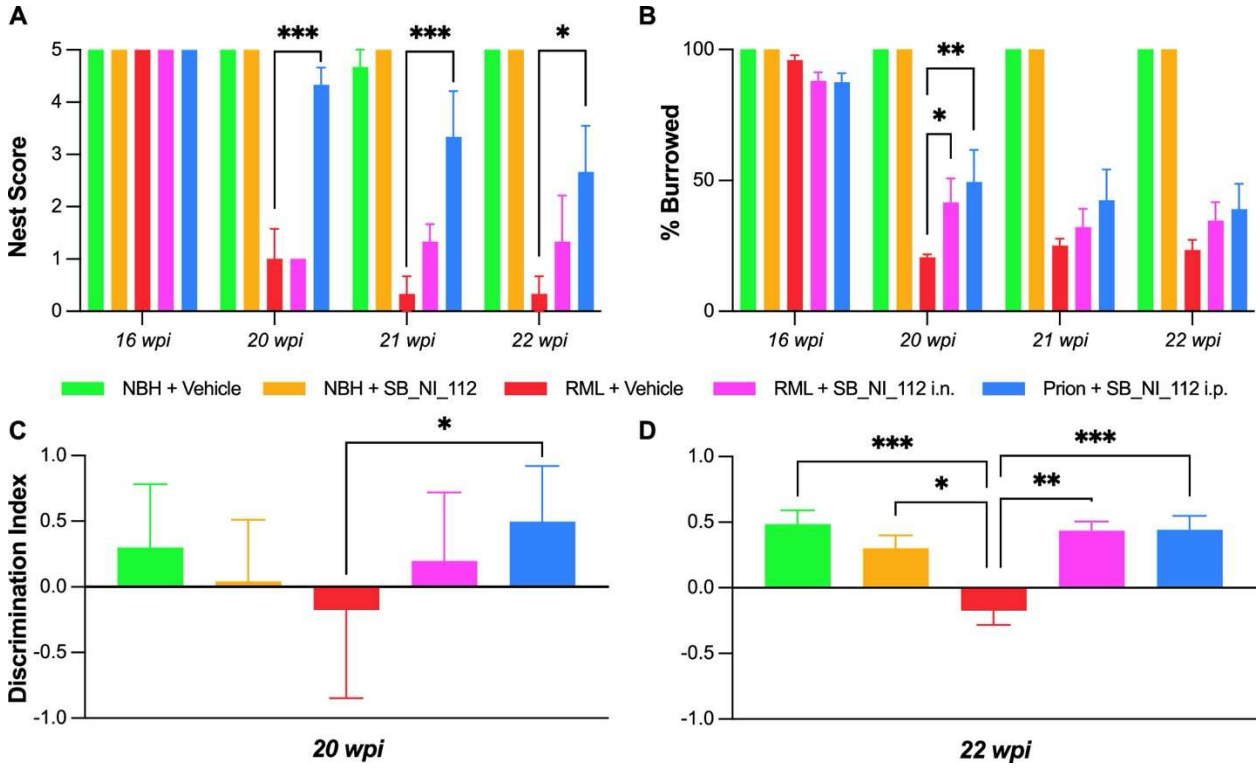


**Figure 3.4. Behavioral and cognitive deficits are protected by NF-κB and NLRP3 down-regulation with SB_NI_112 in prion diseased mice.** A significant increase in the ability of the mice to build proper nests at 20, 21, and 22 wpi with SB_NI_112 i.p. compared to vehicle treatments. Two-way ANOVA, error bars = SEM, * $p < 0.05$, ** $p < 0.01$, *** $p < 0.001$, **** $p < 0.0001$. In the hippocampal burrowing assay, i.p. and i.n. SB_NI_112 treated mice showed significantly better ability to burrow, along with high dose SB_NI_112 i.p. at 16 weeks, compared to untreated counterparts (B). Two-way ANOVA, error bars = SEM, * $p< 0.05$, ** $p< 0.01$. Only i.p. SB_NI_112 showed a significant difference in discrimination index at 20 wpi, higher discrimination index trends with i.n. SB_NI_112 (C). Both i.p. and i.n. SB_NI_112 treated mice had significantly higher scores in spatial novel object recognition at 22 wpi (D). N=9-12. One-way ANOVA with pos-hoc analysis, error bars = SEM, * $p< 0.05$, ** $p< 0.01$, *** $p< 0.001$, **** $p< 0.0001$

Similarly, a significant increase in the ability of the mice to build proper nests at 19 wpi (average score 4.5, $p = 0.0039$) and 21 wpi (average score 3.2, $p = 0.0005$) was shown with high dose i.p. treatment with SB_NI_112 compared to vehicle treatments (average score 2.5 at 19 wpi and 1 at 20 wpi).

Mice were given a plastic tube filled with food pellets within their home cages for 30 min to burrow freely. Following this time, the food pellets left in the tubes were weighed and the percent burrowed calculated. Prion-diseased mice are known to stop burrowing as the disease progresses[144-146], but at 20 wpi, 21 wpi, and 22wpi, prion-diseased mice given therapeutic SB_NI_112 (i.n. and i.p.) had a later onset of deficits in burrowing activity (Figure 3.4B), showing a significance of protection at 20 wpi (average percent burrowed 47, $p = 0.0475$ for i.n.; average percent burrowed 42, $p = 0.0032$ for i.p.), trending through 22 wpi. (Figure 3.4B) A significant difference in the hippocampal burrowing assay was only indicated at 16 wpi (average percent burrowed 75, $p > 0.0365$) when mice were treated with the high dose SB_NI_112 compared to the vehicle (average percent burrowed 51).

Cognitively, mice with RML-induced prion disease have a significant decrease in the ability to recognize a familiar object as the RML prion strain begins to aggregate within the hippocampus, the brain region essential for memory and learning[143-145]. Both i.n. and i.p. SB_NI_112 treatment protected prion-induced deficit in novel object recognition when compared to vehicle-treated diseased mice (Figure 3.4C, D). The ratio of time the mouse spent with the novel object to the familiar object (seen 24 hours beforehand) was calculated and noted by the discrimination index. The closer the discrimination index (DI) is to a value of one the more intact the hippocampal memory is, implying lower disease progression in the animal. At 20 wpi, only SB_NI_112 i.p. showed a significantly higher discrimination index compared to untreated counterparts (mean discrimination index score 0.253, $p > 0.05$), with a trend of improvement with low dose i.n. SB_NI_112 (mean discrimination index -0.152) (Figure 3.4C). At 22 wpi, both

i.p. (mean discrimination index score 0.449, $p < 0.0005$) and i.n. treated mice (mean discrimination index score 0.434, $p < 0.005$) had a significant increase when compared to vehicle-treated diseased mice with a discrimination index of -0.174 (i.e., preferring the familiar object) (Figure 3.4D). There was also a trend towards improved novel object recognition in high dose treated mice compared to untreated counterparts at 22 wpi.

*Down- regulation of NF-κB and NLRP3 with SB_NI_112 treatment reduces glial inflammation.*

Brain tissues were collected at 20 wpi and 24 wpi from low dose treatment groups. Formalin-fixed tissues were processed and embedded into paraffin wax and sectioned at 5μm. Brains were stained for both microglial and astrocytic inflammation (Figure 3.5-6).

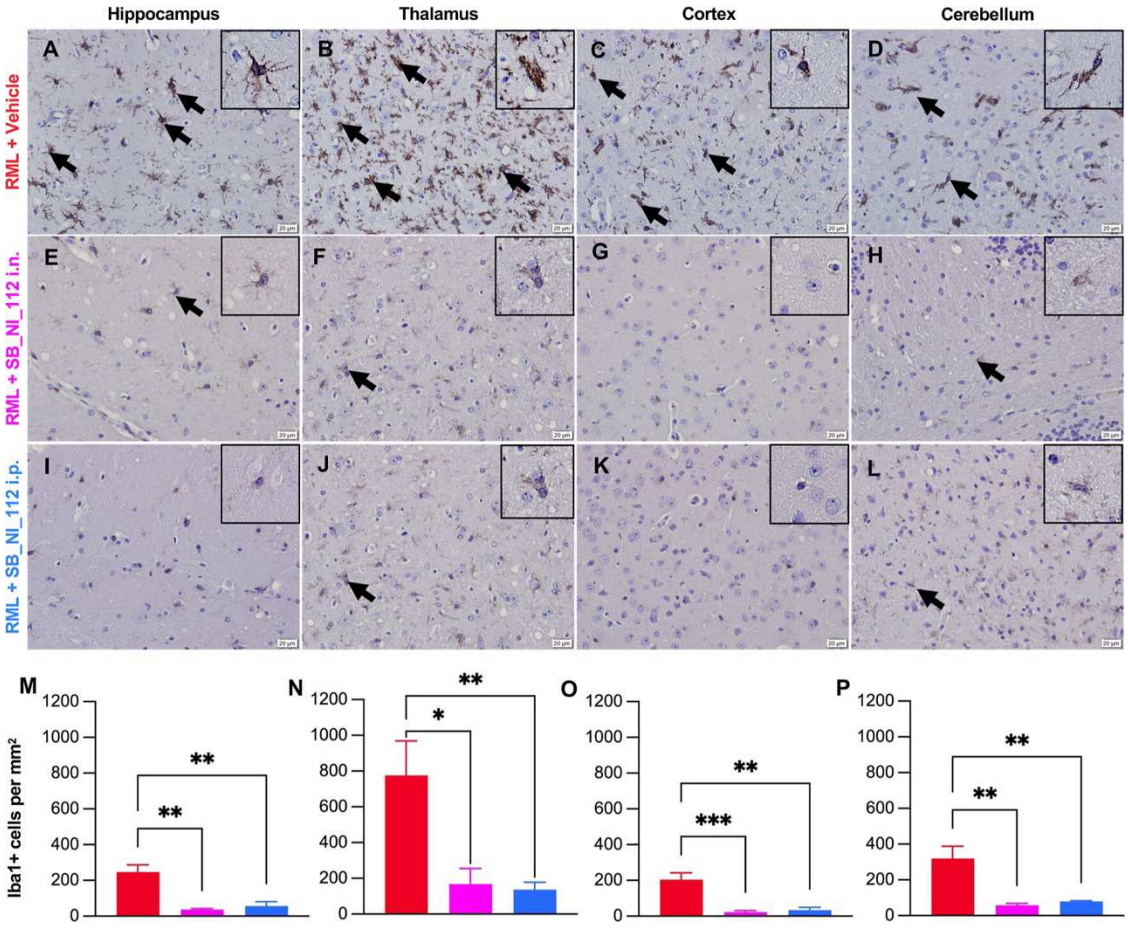


**Figure 3.5. Microglial inflammation is significantly decreased by NF-kB and NLRP3 down-regulation with SB_NI_112 in prion diseased mice at 20 wpi.** Representative images of the hippocampus, thalamus, cortex, and cerebellum with Iba1+ cells, a marker of activated microglia, with vehicle (A-D), SB_NI_112 i.n. (E-H), and SB_NI_112 i.p. (I-L) treatment. Quantitative analysis of each brain region identifies a significantly lower number of Iba1+ cells in the hippocampus (M), thalamus (N) cortex (O), and cerebellum (P) with both i.n. and i.p. treatment. Arrows represent examples of positive cells. Arrows represent examples of positive cells. Scale bar = 20$\mu$m, N=3-4. One-way ANOVA, error bars = SEM, *p > 0.05, **p> 0.001, ***p > 0.0001.

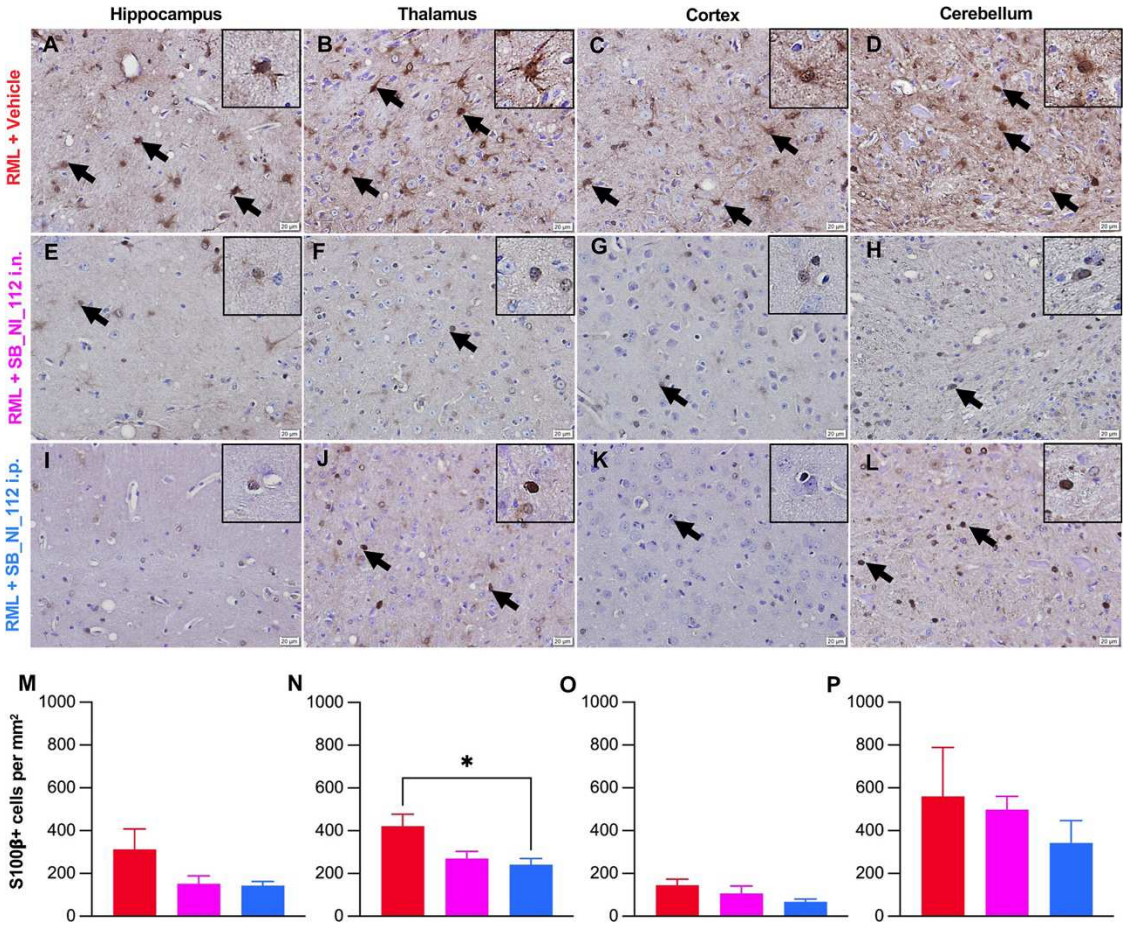


**Figure 3.6. Astrocytic inflammation is significantly decreased by NF-κB and NLRP3 down-regulation with SB_NI_112 in prion disease mice at 20wpi.** Representative images of the hippocampus, thalamus, cortex, and cerebellum with S100β+ cells, a marker of activated microglia, with vehicle (A-D), SB_NI_112 i.n. (E-H), and SB_NI_112 i.p. (I-L) treatment. Quantitative analysis of each brain region identifies a significantly lower number of S100β+ cells in the thalamus (N) and a trend of a decrease of inflamed astrocytes in the hippocampus (M) and cortex (O), and cerebellum (P) with treatment. Arrows represent examples of positive cells. Arrows represent examples of positive cells. Scale bar = 20$\mu$m, N=3-4. One-way ANOVA, error bars = SEM, * $p < 0.05$.

Microglia inflammation was identified as Iba1+ cells (Figure 3.5), and S100β+ cells denote inflamed astrocytes (Figure 3.6). Four main brain regions known to be affected in RML prion infection were analyzed: the hippocampus, cortex, thalamus, and cerebellum. Representative images of each brain region for all treatment groups are displayed for both microglial (Figure 3.5A-L) and astrocytic gliosis (Figure 3.6A-L), and arrows point out examples of positively stained cells.

In the thalamic region, both microglial and astrocytic inflammation were significantly suppressed by down-regulation of NF-κB and NLRP3 with SB_NI_112, both i.n. and i.p. (Figure 3.5N and 3.6N respectively) at 20 wpi. Within the thalamic region, vehicle treated samples had a mean of 775.4 Iba1+ microglia per mm2, followed by SB_NI_112 i.p. treatment with a mean of 168.6 Iba1+ microglia per mm2 ($p = 0.0115$ compared to vehicle), and SB_NI_112 i.n. treatment with a mean of 168.6 Iba1+ microglia per mm2 ($p = 0.0087$ compared to vehicle). In regards to astrogliosis in the thalamus, vehicle treated samples had a mean of 421 S100β+ astrocytes per mm2, followed by SB_NI_112 i.p. treatment with a mean of 270 S100β+ astrocytes per mm2, ($p = 0.0613$ compared to vehicle), and SB_NI_112 i.n. treatment with a mean of 240.8 S100β+ astrocytes per mm2, ($p = 0.0282$ compared to vehicle). Within the hippocampal region, vehicle treated samples had a mean of 246 Iba1+ microglia per mm2, followed by SB_NI_112 i.n. treatment with a mean of 56.31 ba1+ microglia per mm2 ($p = 0.0019$ compared to vehicle), and SB_NI_112 i.p. treatment with a mean of 36.75 Iba1+ microglia per mm2 ($p = 0.0010$ compared to vehicle). In the cortex, vehicle-treated samples had a mean of 203 Iba1+ microglia per mm2, followed by SB_NI_112 i.n. treatment with a mean of 33.22 Iba1+ microglia per mm2 ($p = 0.0014$ compared to vehicle), and SB_NI_112 i.p. treatment with a mean of 22.32 Iba1+ microglia per mm2 ($p = 0.0010$ compared to vehicle). Lastly, in the cerebellum vehicle-treated samples had a mean of 319.6 Iba1+ microglia per mm2, followed by SB_NI_112 i.n. treatment with a mean of 80.05 Iba1+ microglia per mm2 ($p = 0.0023$ compared to vehicle), and

SB_NI_112 i.p. treatment with a mean of 57.71 Iba1+ microglia per mm2 ($p = 0.0013$ compared to vehicle). There was a trend towards astrocyte reduction for both i.p. and i.n. treatment groups in the hippocampus (Figure 6M), Cortex (Figure 6O), and cerebellum (Figure 3.5P).

Microglia are closely associated with plaques in multiple forms of human prion disease including Creutzfeldt-Jakob disease, Gerstmann-Straussler-Scheinker, and kuru and it has been shown that microglia play a role in neuronal cell death during prion disease[147, 148]. Microglial activation appears before the manifestation of clinical signs of prion disease, indicating microglial inflammation plays a role in the progression of prion disease. Furthermore, the deposition of prion proteins alone does not directly predict regions of neurodegeneration[148]. In addition to microglial activation, astrogliosis is found early in prion disease pathology, and reactive or inflamed astrocytes are known to be synaptotoxic in the pathogenesis of prion disease[121, 122, 149]. Further, NF-κB and NLRP3 activation are implicated in the induction of neurotoxic astrocytes by microglia. Global microglial ablation of NLRP3 ameliorates A1-like astrocytes in vitro and in vivo, decreasing neuronal dysfunction. Our research supports this claim by displaying decreased microglial and astrocytic inflammation down-regulating NLRP3 and NF-κB with brain-penetrant SB_NI_112 (Figure 3.5-6). Though a less significant difference was seen in inflamed astrocytes (S100β+ cells) between treated and untreated groups, this may be due to temporal differences in microglial and astrocyte activation throughout chronic inflammation or a proposed cell-type specific activation of NLRP3 in microglia compared to astrocytes[150, 151].

*SB_NI_112 protects against prion-induced spongiosis and neuronal loss.*

Morphologic spongiosis or vacuoles within the brain tissue is a hallmark of prion disease that increases as the disease progresses[138, 139]. To assess and quantify this change, we used pathological scoring of the hippocampus, thalamus, cortex, and cerebellum following H&E staining. Scores were given ranging from + (mild spongiosis) to +++ (high spongiosis) by three

blinded researchers Figure 3.6E-P. This revealed protection against spongiform change in both i.p. and i.n. SB_NI_112 treatment of prion diseased mice when compared to vehicle-treated prion diseased mice at 20 wpi. Representative images from each brain region with corresponding average spongiosis score are displayed for RML + Vehicle, RML + SB_NI_112 i.n., and RML + SB_NI_112 i.p. Overall, down regulation of NF-κB and NLRP3 with SB_NI_112 protects against hallmark spongiosis in prion disease. Beyond spongiosis, the loss of neurons within the hippocampus following RML prion infection is well established[142]. Therefore, we quantified neuronal loss in SB_NI_112 treatment groups to untreated counterparts. Neuronal numbers within the CA1 region of the hippocampus (Figure 3.7A-C) were significantly higher with down-regulation of NF-κB and NLRP3 by low dose i.n. and i.p. delivered SB_NI_112 compared to the vehicle (Figure 7D, $p>0.05$).

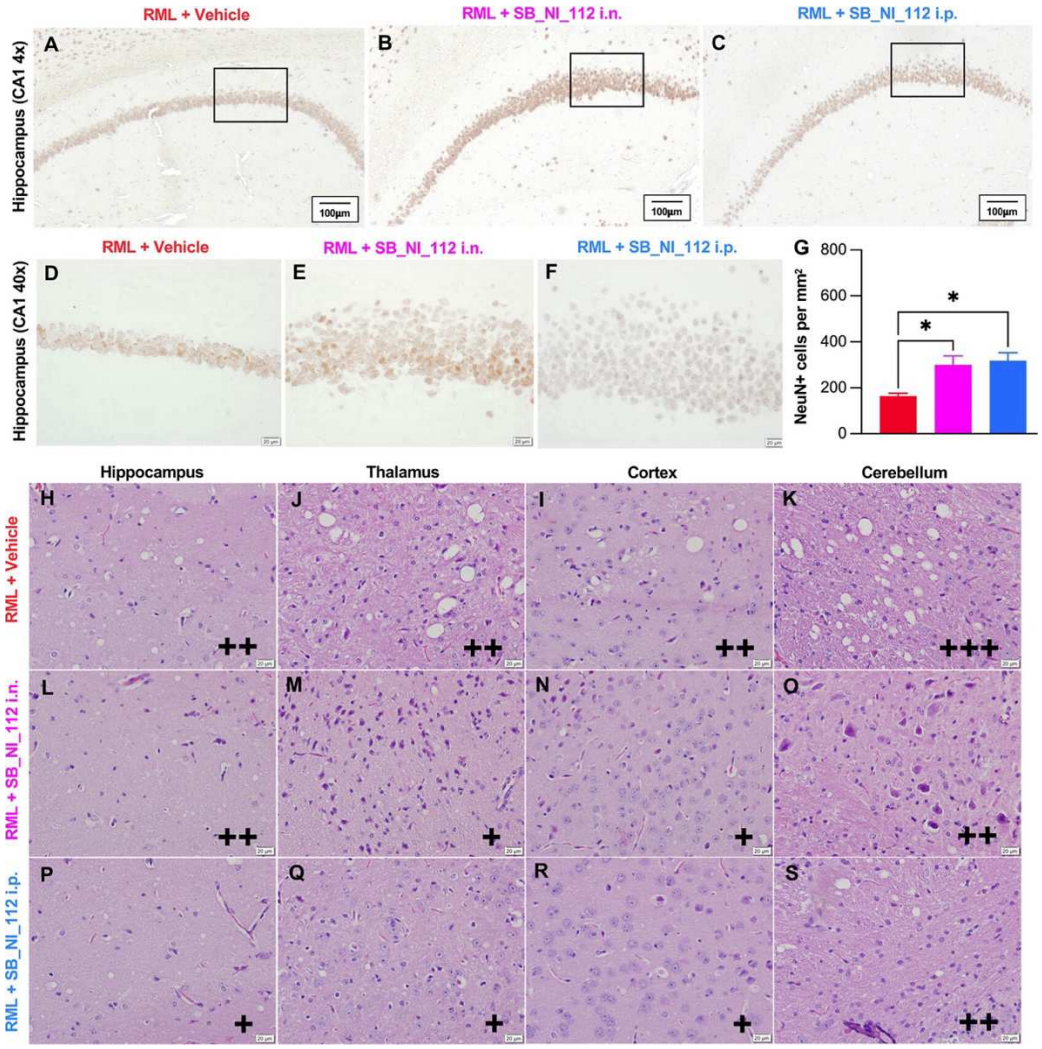


**Figure 3.7. Prion induced neuronal loss and spongiotic change is significantly decreased by NF-κB and NLRP3 down-regulation with SB_NI_112 in prion diseased mice.** Representative images of the NeuN + cells (neuronal cell bodies) in the CA1 region of the hippocampus (A-C) Significant decrease in the number of neurons lost at 20 wpi with treatment via i.p. and i.n. SB_NI_112 (D). Scale bar = 20mm, N=3-4. One-way ANOVA *p > 0.05. Representative images of the spongiotic change in hippocampus, thalamus, cortex, and cerebellum with vehicle (E-H)), low dose SB_NI_112 i.n. (I-L), and low dose SB_NI_112 i.p. (M-P). Pathological scoring of each brain region identifies a protection or decrease of pathological score at all brain regions analyzed; + = mild spongiosis, ++ = moderate spongiosis, +++ = severe spongiosis. N=3-4.

Critically, SB_NI_112 prevents the neuronal loss and spongiform change induced by RML prion infection. As neuronal loss is the direct cause of behavioral and cognitive deficits, and ultimate fatality due to prion disease, it is imperative potential therapeutics show success in this metric[142].

*Treatment with SB_NI_112 improved clinical scores and survival in mice despite accumulation of $PrP^{Sc}$*

At 22 wpi, vehicle-treated mice begin to show a significant increase in clinical signs of prion disease (Figure 3.8A).

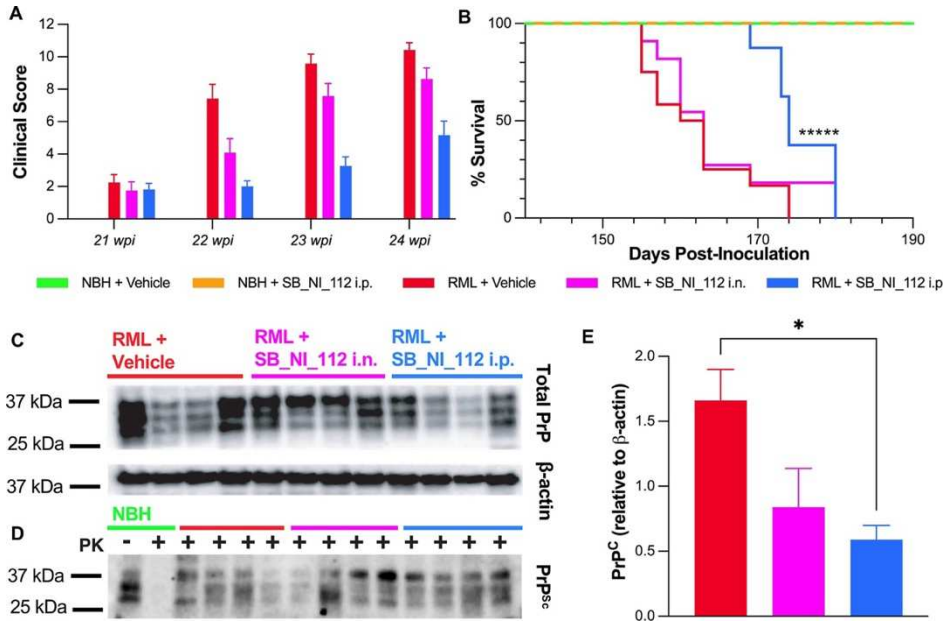


**Figure 3.8. Prion diseased mice treated with NF-κB and NLRP3 down-regulator had significantly lower clinical scores and increased lifespan, independent of $PrP^{Sc}$ accumulation.** Clinical scores of mice treated with i.n. or i.p. SB_NI_112 at 22 and 23 wpi were significantly lower than vehicle treated counterparts, continued significance at 24 wpi with i.p. SB_NI_112 (A). N=9 for prion positive i.p. and i.n. groups, N=9-12 for all other groups. One-way ANOVA, error bars = SEM, * $p < 0.05$, ** $p < 0.01$, *** $p < 0.001$, **** $p < 0.0001$. Mice treated with low dose SB_NI_112 i.p. lived significantly longer than untreated counterparts (B) Survival curve, ***** ($p < 0.000001$). Total PrP and $PrP^{Sc}$ levels detected after proteinase K (PK) ( – indicates not added, + indicates added) digestion at 20 wpi measured by immunoblot (C). Total PrP relative to β-actin was significantly different among SB_NI_112 i.p. treated and untreated groups (D). N=4 for all groups. One-way ANOVA, error bars = SEM, * $p < 0.05$. No significant difference was seen in total $PrP^{Sc}$ relative to $PrP^{C}$ (E). Total $PrP^{Sc}$ relative to $PrP^{C}$ was equivalent in prion-infected mice treated with vehicle and SB_NI_112 i.n. and i.p. treatment (E). N=4 for all groups. One-way ANOVA, error bars = SEM. All immunoblots were performed on frontal cortex lysates.

At 22 wpi, vehicle-treated mice begin to show a significant increase in clinical signs of prion disease (Figure 8A). From 22 wpi to 24 wpi i.p. SB_NI_112 treated diseased mice have significantly ($p<0.0001$ for all weeks) lower clinical scores than vehicle-treated diseased mice, and SB_NI_112 i.n. treatments displayed significantly lower scores at 22 wpi ($p <0.0001$) and 23 wpi ($p = 0.0197$). Untreated Prion clinical signs included tail rigidity, hyperactivity, ataxia, extensor reflex (clasping), tremors, righting reflex, kyphosis, and poor grooming[142, 145, 146]. Each sign was rated on a scale from 0-5. All clinical sign scores were combined for a total score. SB_NI_112 i.p. treated mice had clinical scores with a mean lower than 2 at 22 wpi, 3 at 23 wpi, and 5 at 24 wpi, compared to clinical score mean of 6+ points higher in untreated counterparts (Fig 3.8A). Mice receiving i.n. treatments averaged scores of 3 at 22 wpi and 7 at 23 wpi (Fig 3.8A). Of note, clinical scores in high dose treated mice were significantly lower ($p = 0.0120$) at 22 wpi, with a trend towards lower scores at 23 and 24 wpi (Supplemental Figures 1E). See supporting videos for visual of clasping (supporting videos 1-3), righting reflex (supporting videos 4-6), and walking (supporting videos 7-9) in Control (NBH), RML + vehicle, and RML + Sb_NI_112 i.p. at 22 wpi. Mice were considered terminal and euthanized after reaching a total score of 9 or above. Additionally, mice with a weight loss greater than 10% were considered terminal and euthanized. The date of euthanasia was documented for survival analysis (Figure 8B).

The lifespan of prion disease mice was significantly increased with i.p. SB_NI_112 Nanoligomer treatment ($p <0.000001$) compared to vehicle-treated mice (Figure 3.8B). No change or protection of i.n. delivered SB_NI_112 was seen in survival of prion-diseased mice. Human sporadic Creutzfeldt-Jakob disease has a mean survival of 7-8 months after diagnosis (Salehi et al., 2022). On average, i.p treatment with SB_NI_112 significantly increased prion-diseased mouse lifespan. Untreated mice had a mean survival of 162 days, i.p. SB_NI_112 treated 174 days, and i.n. SB_NI_112 163 days. Of note, the first mouse without SB_NI_112

treatment reached a clinical score indicative of sacrifice 15 days before the first mouse receiving i.p. treatment. 15 mouse days equate to approximately 6 months in human years, a near doubling of expected survival time after diagnosis[152]. Importantly, there was no toxic pathology induced by the down regulation of NF-κB and NLRP3 by SB_NI_112 (Figure 2A).

To determine if SB_NI_112 modulates the accumulation of the misfolded prion protein, PrPSc, immunoblotting was performed on cortical brain homogenates for levels of the cellular PrPC and proteinase K-resistant PrPSc (Fig 3.8C). Total PrP relative to β-actin was significantly different among treated and untreated groups (Figure 3.8D). No significant difference was seen in total PrPSc relative to PrPC (Figure 3.8E). Similarly, other studies examining potential prion therapeutics have shown similar results in regard to total $PrP^{Sc}$ [142, 143]. This indicates dampening chronic inflammatory signaling protects against prion-associated neurodegeneration independent of PrPSc accumulation. SB_NI_112, down-regulator of NF-κB and NLRP3, shows efficacy in slowing the disease clinically, behaviorally, and pathologically while increasing predicted survival after diagnosis, and use as a combination therapy for individuals diagnosed with prion disease.

*NLRP3 inflammasome involvement in progression of prion disease.*

The level of influence the NLRP3 inflammasome has on prion disease progression is still debated within the literature. The NLRP3 inflammasome was found to be involved in lipopolysaccharide (LPS)-primed microglia after exposure to a synthetic neurotoxic prion fragment in vitro[124, 125]. Previous studies highlight the importance of the NLRP3 inflammasome in the production of IL-1β and IL-18 in systemic inflammation and neurodegenerative disease, including prion disease[38, 120, 123, 126, 127, 153]. An in vitro study in BV2 microglia and co-cultured glia reported that aggregated prion protein was involved in both priming and activation of the NLRP3 inflammasome[125].

Regarding cytokine production in our study, at 16wpi, IL-28 is significantly reduced in i.p. treated (average 30.1 pg/mg total protein, $p < 0.05$) mice compared to untreated counterparts (average 43.4 pg/mg total protein) (Figure S2). Interestingly, an in vivo study found levels of IL-1β at end-stage prion disease were not affected by the absence of NLRP3 and that NLRP3 knockout mice succumbed to RML prion in a similar time frame to wild-type counterparts[154]. Conversely, our in vivo research supports the involvement of the NLRP3 inflammation in prion disease progression, as downregulation of NLRP3 and upstream signaling molecule NF-κB decreased glial inflammation, protected against neuronal loss, prevented spongiotic change, rescued cognitive deficits, and significantly lengthened lifespan of prion-diseased mice. Additionally, inflammatory cytokines IL-2, IL-1α, and IL-1β, trended lower in prion-diseased mice treated with i.p. SB_NI_112, similar to NBH controls, when compared to untreated counterparts. Principal component analysis revealed trending differences between treated and untreated prion-diseased mice ($p = 0.094$) (Figure S2 E). Based on conflicting data, there are likely additional inflammatory pathways upregulated by PrPSc in conjunction with the known direct degenerative impact PrPSc aggregates have on neurons[155].

**Conclusions and Future Prospects**

Down-regulation of NF-κB and NLRP3 in a mouse-adapted RML prion model slows disease progression by reducing glial inflammation, delaying development of behavioral deficits and clinical signs, preventing loss of neurons, and extending lifespan. Because treatments successful in prion disease are anticipated to work in other NPMDs due to common pathogenesis, these findings, if validated clinically, have important implications for patients diagnosed with prion disease and those suffering from more widespread neurodegenerative diseases like AD and PD.

Though all mice eventually succumbed to disease in this study, PrPSc misfolding and accumulation in prion disease, in comparison to other misfolded proteins in NPMDs (Aβ in AD and α-Syn in PD), is substantially more rapid and aggressive[156]. Additionally, properly functioning microglia can phagocytose and degrade both Aβ and α-Syn. It is only when microglia lose the ability to degrade misfolded proteins and the load of Aβ or α-Syn becomes too high that aggregation and progression of disease state occurs in AD and PD respectively[38, 123, 126, 127]. Recent research supports chronic inflammation and NLRP3 inflammasome stimulation decreases microglial autophagy, leading to increased Aβ or α-Syn production and aggregation in the brain[135-137]. Furthermore, inflammation in other glial cells, namely astrocytes, leaves them unable to properly perform metabolic, structural, homeostatic, and neuroprotective tasks[156].

It is important to note that though many treatments for NPMDs have been promising in early research, many fail due to toxicity and low efficacy rates in animal models or human trials[106, 157, 158]. At this time, our research has identified no measurable toxicity or side effects associated with Nanoligomer SB_NI_112 at single high doses of 500 mg/kg or repeated dosing of 150 mg/kg. Additionally, the NF-κB and NLRP3 down-regulator is stable and bioavailable, has confirmed ability to cross the BBB, and displays high target specificity with minimal off-targeting. Our mechanism of action results (Figure 3.3) displaying superior inhibition of NF-κB and NLRP3 via i.p. route of delivery compared to i.n., combined with behavioral and histological data, support that an intraperitoneal dosing method is more successful at delivery therapeutic SB_NI_112 to the brain, thus providing better protection against neuroinflammation and prion disease progression.

A secondary study was completed at 150 mg/kg three times per week to explore the impact of a higher dose. However, we saw no difference in RML prion associated behavioral assessment scores and clinical signs of 10 mg/kg 2x per week and high dose 150 mg/kg 3x per

week treatment groups (Figure 3.3), indicating there may be a threshold at which the treatment against neuroinflammation, specifically NF-κB and NLRP3, is effective against RML prion disease. Because there is no indication to treat with a higher dose, as it does not increase the therapeutic effect, we did not continue with additional methods to assess disease progression in the high dose study.

Specifically in prion disease, there have been few small molecules, antibodies and other compounds that show promise in treatment of disease pathogenesis. Therapeutic oligonucleotides for the prion protein or PrP-lowering antisense oligonucleotides (ASO) have proven to lower the toxic load of the disease-causing misfolded prion protein increasing survival of infected mice. Critically this was irrespective of the strain or type of prion the mice were exposed to but, only successful with the highly invasive intracerebroventricular injection, a critical limitation of this treatment[159]. The use of antibodies as an immunotherapy and small molecules against the prion protein has been studied for years and in rodents the progression and acceleration of the toxic PrPSc is reduced, but unfortunately the protection of these do not translate well to patients[158, 160-164]. The development of human specific antibodies is showing some efficacy in patients however the need for the ability to give the immunotherapy to patients earlier, prior to severe disease states, seems to be essential[165].

Nanoligomers present significant benefits compared to other small-molecules, antibodies, and antisense oligonucleotide (ASO) platforms. First, their efficient biodistribution and facile delivery across the BBB and reaching various sections of the brain without using invasive administration methods such as Intracerebroventricular injection used in other ASO based treatments[159, 166]. Second, lack of any immunogenic response, any adverse systemic effect or accumulation makes these molecules preferable to other small molecules. This study focusing on a Prion infection model, showed that Nanoligomers directed at the inflammasome demonstrate neuroprotection, improved animal survival rates, and enhanced cognitive function.

This underscores the technology's safety and broader potential applications. Another significant advantage of the Nanoligomers discovery engine lies in its capability to selectively target specific gene(s) for either upregulation or downregulation of expression as needed. Notably, recent research demonstrated that a low dosage of 5 mg/kg of Nanoligomer significantly reduced inflammation in the mouse hippocampus during LPS-induced neuroinflammation[93].

Limitations of our study include a low sample size at each individual time point. Higher significance may have been achieved with a larger sample size, particularly regarding behavioral testing timepoints for the later more diseased timepoints. Moreover, adding more behavioral time points (weekly vs. biweekly) could display more detailed changes in behavior as prion disease progresses. Additionally, there may be other routes of dosing that provide stronger protection against prion disease progression, including intravenous, subcutaneous, or oral routes. Finally, because the therapeutic showed high safety efficacy, it would be beneficial to test a higher dose concentration and more often frequency in dosing.

In summary, targeting the NLRP3 inflammasome via down-regulation of NF-κB and NLRP3 with SB_NI_112 has promising therapeutic potential for NPMD's. SB_NI_112 reduces inflammatory signaling amongst microglia and astrocytes, which is highly neuroprotective. At the least, targeting chronic neuroinflammation in NPMDs is an essential component in the "cocktail" of multi-target therapeutic interventions that are likely necessary for successful modification and halting of disease. Next steps include studying SB_NI_112 therapeutic intervention in additional neurodegenerative murine models of Parkinson's Disease, Alzheimer's Disease, Multiple Sclerosis, and Amyotrophic Lateral Sclerosis. We also plan to examine other dosing routes including oral, intravenous, and subcutaneous. Additionally, we are beginning clinical trial research for use of SB_NI_112 in dogs displaying signs of canine cognitive dysfunction. The ultimate goal is to translate neurotherapeutic SB-NI_112 for human treatment of NPMDs.

## Methods

*Mice and Brain homogenates*

C57Bl/6 (Jackson Laboratory) mice were intracranially inoculated with 30$\mu$l of 0.1% 22L or Rocky Mountain Laboratories (RML) strains of mouse-adapted prions, or normal brain homogenate (NBH), in 1% Pen-Strep (1:1 penicillin-streptomycin**)**. Mice were monitored for weight loss and clinical signs of prion disease and euthanized after showing signs of terminal illness. 20% brain homogenates in phosphate-buffered saline (PBS) were made using beads and a tissue homogenizer (Benchmark Bead Blaster 24) and stored at -80C. Brain homogenates were aliquoted and treated with UV light for 30 minutes to sterilize before being used for cell culture.

*Nanoligomer Design and Synthesis*

The Nanoligomer design, sequences, and synthesis has been described in our previous work. Nanoligomers were designed and synthesized (Sachi Bioworks Inc.) according to published methods[91, 93, 94]. The Nanoligomer is composed of a nanobiohybrid molecule based on antisense peptide nucleic acid (PNA)[91, 93, 94, 167]. conjugated to nanoparticle for improved delivery. The PNA moiety was chosen to be 17 bases long (to optimize solubility and specificity) antisense to the start codon regions of nfkb1 (N terminus- -C terminus, sequence: AGTGGTACCGTCTGCTA) and nlrp3 (N terminus- -C terminus, sequence: CTTCTACTGCTCACAGG) within the Mouse genome (GCF_000001635.27). Potential PNA sequences were screened for solubility, self-complementing sequences, and off-targeting within the mouse genome (GCF_000001635.27). The PNA portion of the Nanoligomer was synthesized on Vantage peptide synthesizer (AAPPTec, LLC) with solid-phase Fmoc chemistry. Fmoc-PNA monomers were obtained from PolyOrg Inc., with A, C, and G monomers protected with Bhoc groups. Following synthesis, the peptides were conjugated with gold nanoparticles and purified via size-exclusion filtration. Conjugation and concentration of the purified solution

was monitored through UV-Vis (Thermo Scientific, NanoDrop) measurement of absorbance at 260 nm (for detection of PNA) and 400 nm (for quantification of nanoparticles). Nanoligomers were stored at 4°C until further use.

*Biodistribution and Toxicity*

Six female and six male C57Bl/6 (Jackson Laboratory) mice, 8-10 weeks of age, were injected with a single dose of 500 mg/kg intraperitoneal or intranasal SB_NI_112. Mice were monitored for 2 weeks for safety/tox study and dosing. Weight was monitored daily, along with any changes in behavior/well-being. At the end of the study, mice were euthanized, and tissues harvested for histopathological scoring, blood concentration of any inflammatory markers, albumin content in serum. Using three-fold lower concentration than the maximum tolerated dose (MTD) (150 mg/kg), eight female and eight male C57Bl/6 mice were dosed for 2 weeks with 2 doses/week. Mice were euthanized and harvested to measure distribution of Nanoligomer through different tissues using ICP-MS.

*Nanoligomer Administration*

At 10 weeks post RML prion or NBH inoculation, mice were treated two times per week either intraperitoneally (i.p.) or intranasally (i.n.) with 10 mg/kg of SB_NI_112 diluted in sterile phosphate buffered saline (PBS). For high dose study, mice were treated three times per week with 150 mg/kg of SB_NI_112 i.p. Mice receiving treatment i.n. were anesthetized prior to administration and laid in an intranasal apparatus that controlled isoflurane throughout the intranasal procedure.

*Cognitive assay: Novel Object Recognition*

Mice were tested in a rectangular arena (28cm x 43cm) and habituated by exploring the empty arena for ten minutes. During day one of testing, mice were placed in the arena with two identical objects (constructed with Legos) and video monitored for 5 minutes of exploration. On day two of testing, one of the known objects was replaced by a novel object, and the 5-minute

exploration was filmed using a 1080P FHD Mini Video Camera. All objects and the arena were cleansed thoroughly with 70% ethanol between trials to ensure the absence of olfactory cues. Time exploring both the known and novel object was calculated by blinded observers. Discrimination index (DI) calculated following Absolute vs Relative Analysis protocol[53]. All objects were tested prior to use to ensure the mice would explore them.

*Hippocampal Behavioral assays: Burrowing and Nesting*

Briefly, mice were placed in a large cage with a PVC tube (2.33" x 5.75") full of food pellets, as described[142, 144, 168]. The percentage of burrowing activity is calculated from the difference in the weight of pellets in the tube before and after 2 hours. To test nesting, we placed three fresh napkins in each cage. After 24 hours, cages were examined for nesting activity. Nests were scored on a scale of 0-5, where 0 represents no nesting activity, and 5 represents a high-quality nest.

*Clinical Scoring of mice*

Eight key clinical signs were monitored in mice daily beginning at 20 or 21 wpi. Clinical signs included tail rigidity, hyperactivity, ataxia, extensor reflex, tremors, righting reflex, kyphosis, and poor grooming. Each sign was rated on a scale from 0-5. All clinical sign scores were combined for a total score. Mice considered terminal and euthanized after reaching a total score of 9 or above. Additionally, mice with a weight loss greater than 10% were considered terminal and euthanized.

Immunohistochemistry

Paraffin-embedded brains were sectioned at 4 $\mu$m and stained with NeuN antibody (1:250; Cell Signaling) for CA1 neuronal counts. Astrogliosis was detected with S100$\beta$ antibody (1:400; Abcam ab41548) and Iba1 antibody (1:400; Abcam, ab5076) was used for microglial counts. Nonspecific binding was blocked before primary antibodies with 10% Horse Serum (Sigma Aldrich). A biotinylated secondary antibody (Vector Labs) was used, and stain was

visualized with diaminobenzidine reagent. All images were taken with CellSens Dimension Desktop 3.1 and counted with CellSens (Iba1 and S100β+) or manually (NeuN).

*Immunoblotting*

Cell lysates were isolated using the protein lysis buffer (50mM Tris, 150mM NaCl, 2mM EDTA, 1mM MgCl2, 100mM NaF, 10% glycerol, 1% Triton X-100, 1% Na deoxycholate, 0.1% SDS and 125mM sucrose) supplemented with Phos-STOP and protease inhibitors (Roche). A BCA Protein Assay kit (Thermo Scientific) was used to quantify protein concentration of lysates, and 250 mg or 500mg protein was digested with 20 $\mu$g/ml proteinase K (PK) (Roche) for $PrP^{Sc}$ blots for 1 hour at 37C. This digestion allows all other proteins to be digested so $PrP^{Sc}$ can be detected, therefore loading control antibodies cannot be used for these blots. Digestion was terminated with 2mM PMSF and lysates were spun at 40,000 x g for 1 hour at 4C before being loaded on a gel. For $PrP^{C}$ blots, 20 mg of samples was used. Samples were run using 4-20% acrylamide SDS page gels (BioRad) and then transferred onto 0.45$\mu$m PVDF blotting paper (MilliPore). Primary antibody Bar-224 (Cayman Chemical Company) was used at 1:1,000 dilution for $PrP^{Sc}$ blots and 1:5,000 dilution for $PrP^{C}$ blots. HRP-conjugated secondary antibodies were used at a concentration of 1:5,000 (Vector Laboratories). For $PrP^{C}$ blots, loading control GAPDH was ran at a 1:5,000 dilution (MilliPore), with HRP-conjugated anti-mouse secondary at 1:5,000 dilution (Southern Biotech). The protein antibody complex was visualized using SuperSignal West Pico PLUS Chemiluminescent Substrate (Thermo Scientific) and visualized with the BioRad ChemiDoc MP.

*Quantification of Cytokine & Chemokine in mouse tissues*

Briefly, dissected brain tissues were flash-frozen and homogenized using a mortar and pestle to form a homogenate solution in tissue cell lysis buffer (Thermo Fisher, EPX-99999-000). Samples were then centrifuged at 16,000xg for 10 min at 4°C and supernatant was transferred to a fresh tube. Bio-Rad's DC Protein Assay Kit was used to determine protein

content, and all samples were diluted to 10 mg protein/mL. Quantification of cytokines/ chemokine was performed with Cytokine & Chemokine 36-Plex Mouse ProcartaPlex Panel 1A (EPXR360-26092-901), analyzed on a Luminex MAGPIX xMAP instrument, and quantified using xPONENT software. For standard curves, eight four-fold dilutions of protein standards were used

*ICP-MS*

Briefly, tissue samples were homogenized in a TissueLyser bead mill (Qiagen, Germantown, MD) at 30 Hz for 3 min with the addition of 1 µl deionized water per 1 mg organ tissue. Volumes of homogenates ranging from 10 to 130 µl were then digested in 500 µl of aqua regia (3:1 hydrochloric acid to nitric acid) for 4 hours at 100 °C. Pellets were resuspended in water and analyzed with a NexION 2000B single quadropole ICP-MS (PerkinElmer, Waltham, MA). A Meinhard nebulizer was used with a cyclonic glass spray chamber for the introduction of the sample. A nickel sample and skimmer cone were used with an aluminum hyperskimmer cone. The ICP-MS was optimized daily with a calibration solution of 1 ppb In, Ce, Be, U, and Pb. Au was the analyte monitored. Data was collected using the sample acquisition module in Syngistix software (version 2.3). Data was analyzed using Microsoft Excel by converting measured Au concentrations to pg/mg organ via organ homogenate volume used. A seven-point linear curve with a 1000 ppm Au standard solution (Ricca Chemical Co, Arlington, TX) was generated at a concentration range of 0- 250 ppb. Indium was spiked into each sample at a concentration of 5 ppb. Linearity of the standard curve was defined at an $R^2$ value of greater than 0.995. TraceMetal grade 70% $HNO_{3-}$ was purchased from ThermoFisher Scientific (Waltham, MA). All $H_2O$ used was from a Milli-Q system (Millipore, Burlington, MA).

*Statistical Analysis*

All data is presented as mean +/- SEM unless otherwise specified. A ROUT (Q = 10%) outlier test was performed on all data to identify potential outliers, which were removed from the

data set. Differences between experimental groups were analyzed using a One-way ANOVA or Two-way ANOVA. Statistical analysis was completed using Prism. Significance is denoted throughout the manuscript as * = $p \leq .05$, ** = $p \leq 0.01$, *** = $p \leq 0.001$, and **** = $p \leq 0.0001$.

*Ethics Approval*

Mice were euthanized by deeply anaesthetizing with isoflurane followed by decapitation. All mice were bred and maintained at Lab Animal Resources, accredited by the Association for Assessment and Accreditation of Lab Animal Care International, in accordance with protocols approved by the Institutional Animal Care and Use Committee at Colorado State University.

# CHAPTER 4 – ENTERIC GLIAL INGLAMMATION AND NEURODEVELOPMENTAL PERTERBATIONS TRIGGERED BY CHRONIC LOW-DOSE EXPOSURE TO MANGANESE VIA DRINKING WATER[3]


**Summary**

Manganese (Mn) is an essential trace element critical for a range of physiological functions, including neurotransmitter synthesis and cellular metabolism. However, excessive Mn exposure can lead to neurotoxicity, which has been linked to neurodegenerative diseases such as Parkinson's disease (PD) and Alzheimer's disease (AD). It has been shown that Mn toxicity may also contribute to the risk of neurodevelopmental disorders, including attention-deficit hyperactivity disorder (ADHD) and other learning disorders. While much of the research on Mn toxicity has focused on the central nervous system (CNS), the enteric nervous system (ENS), which is often the primary site of Mn exposure, may also play a significant role in mediating neurodevelopmental changes. Despite growing recognition of Mn's potential role in neurodevelopmental disorders, the exact mechanisms underlying ADHD-like symptoms remain inadequately understood. This study examines the impact of low-dose Mn exposure on neurodevelopment in juvenile mice, focusing on behavioral and pathologic changes resembling ADHD-related deficits. Mice were exposed to manganese chloride (MnCl2) via drinking water at a low dose, and behavioral and pathologic outcomes were subsequently assessed. Notably, a significant increase in hyperactivity was observed during open field testing, consistent with ADHD-like symptoms. Fecal samples were collected for metabolomic profiling to identify


[3] Portions of this chapter are based on material to be submitted for publication as: Risen, S. J., Campos, C., Weisman, G., Madrid, N. Z., Lee, D., Streifel, K. M., & Moreno, J. A. (in preparation). Enteric glial inflammation and neurodevelopmental perturbations triggered by chronic low-dose exposure to manganese via drinking water in juvenile mice.

potential alterations in the gut microbiome that may contribute to these neurodevelopmental changes. Additionally, glial cell activation in both the ENS and CNS was evaluated through immunohistochemistry (IHC), revealing significant inflammatory responses in both compartments following Mn exposure. Results demonstrate marked alterations in the gut microbiome, coupled with enhanced glial inflammation and shifts in neurotransmitter profiles within both the gut and brain. Findings suggest that Mn exposure, even at low environmental concentrations, has the potential to disrupt normal neurodevelopmental processes and contribute to ADHD-like pathologies. By examining interactions between the gut microbiome, the ENS, and the CNS, new insights are gained into the neurodevelopmental consequences of Mn toxicity and its potential role in the pathogenesis of neurodevelopmental disorders such as ADHD.

**Introduction**

The increasing body of evidence linking environmental contaminants to adverse health outcomes has increasingly highlighted manganese (Mn), an essential trace element that poses significant neurotoxic risks, particularly during critical developmental periods in childhood. While manganese is vital for various physiological functions, including neurotransmitter synthesis and cellular metabolism, excessive exposure—especially through drinking water—can lead to neurodevelopmental disorders such as attention-deficit hyperactivity disorder (ADHD)[169]. Alarmingly, many drinking water supplies worldwide contain manganese concentrations that exceed recommended safety levels, thereby exposing millions of children to potential neurotoxic effects[169].

Recent research has illuminated the intricate relationship between manganese exposure and the gut microbiome, a complex ecosystem crucial for host health and neurodevelopment. Dysbiosis, characterized by an imbalance in the gut microbial community, has been implicated

in the development and progression of neurodevelopmental disorders, including ADHD[170]. The gut microbiome communicates with the central nervous system (CNS) through the gut-brain axis, influencing neurological function via mechanisms such as inflammation and neurotransmitter modulation[170]. Disruption of this microbial community due to manganese-induced oxidative stress may yield cascading effects on neurodevelopment, potentially exacerbating behavioral and cognitive deficits associated with ADHD.

Epidemiologic studies consistently link manganese exposure to cognitive impairments and behavioral abnormalities in children. For instance, in a large cohort study children exposed to manganese in drinking water exhibited neurobehavioral deficits, whereas another study displayed a correlation between manganese levels and diminished intellectual performance[169, 171]. Notably, recent animal studies have shown that low-dose manganese exposure can lead to behavioral changes resembling ADHD symptoms, including hyperactivity and alterations in neurotransmitter profiles[70]. These findings suggest that even low concentrations of manganese in drinking water can adversely affect cognitive functions, raising critical questions about the safety thresholds for manganese exposure in public health guidelines.

The neurotoxic mechanisms underlying these associations may involve direct effects on neurotransmitter systems and brain structures integral to cognitive function, particularly the dopaminergic system, which is known to be impaired in ADHD[70]. Manganese has been shown to accumulate in dopaminergic neurons, leading to decreased dopamine levels, a neurotransmitter crucial for attention and impulse control[172]. Furthermore, manganese exposure has been linked to disruptions in the glutamine-glutamate-GABAergic cycle, which is vital for maintaining proper brain function[173]. The interaction of manganese with other environmental neurotoxins, such as lead, may compound the neurodevelopmental risks, necessitating a comprehensive understanding of the multifaceted nature of these exposures[174].

A critical aspect of the gut-brain axis involves the vagus nerve, which serves as a primary conduit for communication between the enteric nervous system (ENS) and the CNS. Glial inflammation within the gut, triggered by manganese exposure, may propagate signals through the vagus nerve, potentially influencing neurodevelopmental outcomes. Recent studies indicate that gut inflammation can lead to the trans neuronal propagation of pathological proteins, such as amyloid-beta and tau, from the gut to the brain via the vagus nerve[175]. This suggests that inflammatory mediators released in the gut can travel along the vagus nerve, impacting brain function and contributing to neurodevelopmental disorders. Furthermore, research has shown that pathological α-synuclein, associated with Parkinson's disease, can spread from the ENS to the CNS through the vagus nerve, highlighting the potential for similar mechanisms in the context of manganese-induced neuroinflammation[176].

Considering these, this research article aims to explore the potential impact of juvenile low-dose manganese exposure via drinking water on the gut microbiome and its subsequent implications for neurodevelopmental disorders, particularly ADHD. Using a rodent model, juvenile mice were exposed to manganese chloride (MnCl2) at low doses (15 mg/kg or 50 mg/kg) via drinking water (Figure 4.1).

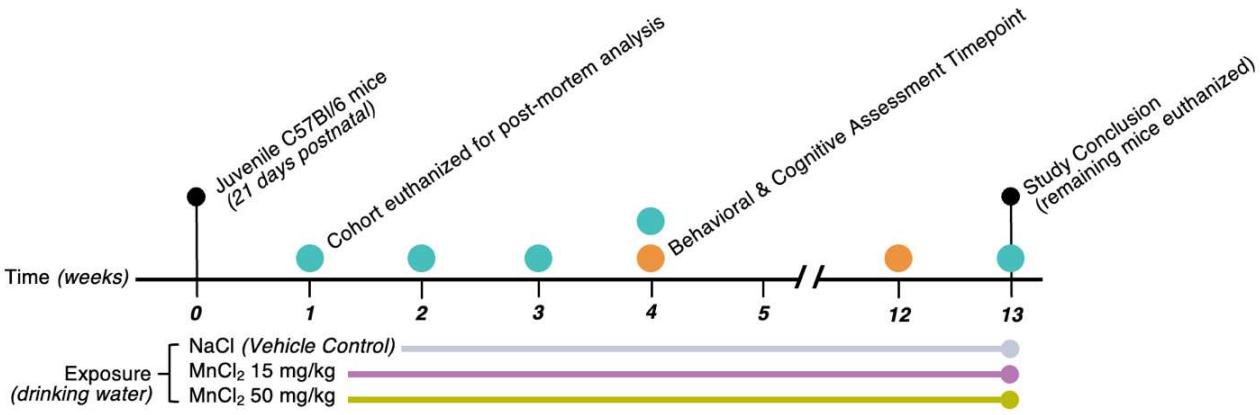


**Figure 4.1. Experimental Design.** C57Bl/6 mice were given either 15 mg/kg or 50 mg/kg $MnCl_2$ in water ad libitum posting weaning (Day 21) or NaCl (vehicle). At 1, 2, 3, and 4 weeks of exposure, a cohort of mice was sacrificed for post-mortem analysis. Behavioral (open-field) and cognitive (novel object recognition) assessments were performed on behavioral cohorts of mice at 4- and 12-weeks of exposure. After 13 total weeks of exposure all remaining mice were euthanized for post-mortem analysis.

Behavioral assessments were conducted using open field tests to evaluate hyperactivity and other ADHD-like symptoms. Additionally, fecal samples were collected for bacterial species profiling to identify potential alterations in the gut microbiome that may contribute to these neurodevelopmental changes. Preliminary results indicate marked alterations in the gut microbiome, coupled with enhanced glial inflammation and shifts in neurotransmitter profiles within both the gut and brain. Notably, at the 50 mg/kg dose, a significant increase in hyperactivity was observed during open field testing, consistent with ADHD-like symptoms. By elucidating the pathways through which manganese influences both microbial health and neurodevelopment, including the role of the vagus nerve in mediating gut-brain communication, this study seeks to contribute to the growing body of literature advocating for stringent regulatory measures regarding manganese levels in drinking water and to inform public health strategies aimed at safeguarding the neurodevelopmental integrity of vulnerable populations.

**Results & Discussion**

This study provides evidence that chronic manganese (Mn) exposure induces widespread neurobehavioral, metabolic, and inflammatory perturbations, highlighting a multi-systemic mechanism of Mn neurotoxicity. The observed behavioral alterations, gut microbiome shifts, neuroinflammatory activation, and disruptions in neurotransmitter metabolism suggest that Mn exposure not only affects the central nervous system (CNS) directly but also exerts its effects through gut-brain axis dysfunction. These findings reinforce the growing recognition that environmental toxicants such as Mn can have far-reaching consequences on neurodevelopment by disrupting interconnected physiological pathways[177].

*Manganese Exposure Alters Locomotor Activity, Stereotypic Behaviors, and Cognitive Performance in a Sex-Dependent Manner*

To assess the behavioral consequences of manganese ($MnCl_2$) exposure, we evaluated locomotor activity, stereotypic behaviors, and cognitive performance in male and female mice at weeks 4 and 12 following exposure to 50 mg/kg $MnCl_2$ or saline in drinking water. The results indicate significant sex-dependent and time-dependent effects of Mn exposure on movement patterns, perseverative behaviors, and cognitive processing. Locomotor activity, measured as total distance traveled (cm) in an open field test (Figure 4.2A), did not differ significantly between $MnCl_2$-exposed and control groups at Week 4.

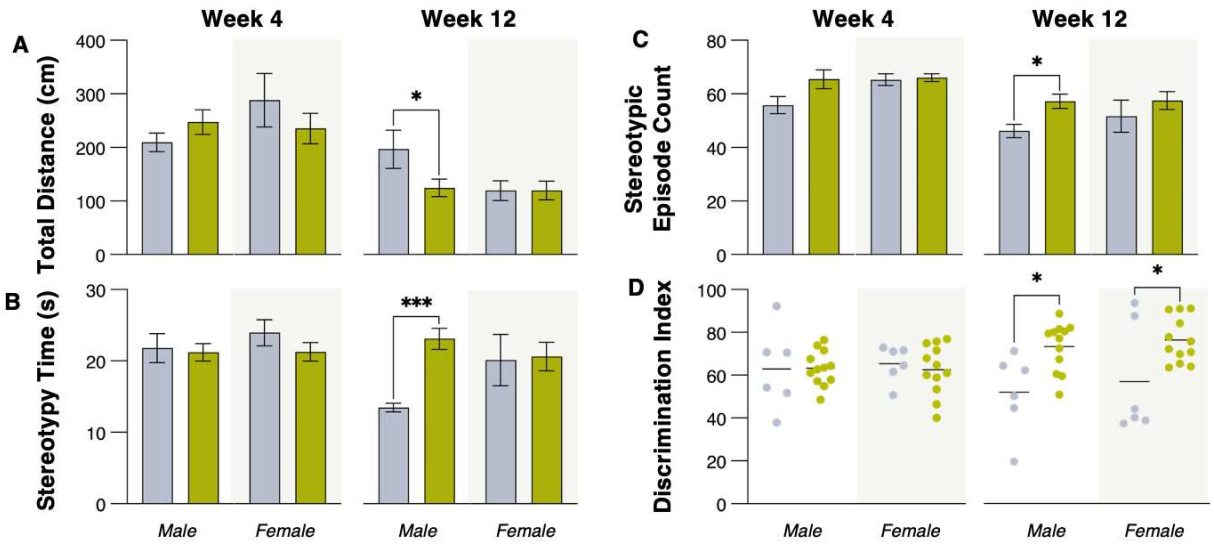


**Figure 4.2. Juvenile mice exposed to MnCl at 50mg/kg in drinking water exhibited significant sex-dependent behavioral changes consistent with ADHD-like signs.** Behavioral assessments were conducted at Week 4 and Week 12 to evaluate locomotor activity, repetitive behaviors, and cognitive performance in male and female mice exposed to 50 mg/kg $MnCl_2$ in drinking water. (A) Total distance traveled (cm) was not significantly different between groups at Week 4 but was significantly reduced in $MnCl_2$-exposed male mice at Week 12 ($p < 0.05$). (B) Stereotypy time (s) was significantly increased in $MnCl_2$-exposed male mice at Week 12 ($p < 0.0005$), with no significant differences observed in females. (C) Stereotypic episode count was unchanged across groups at Week 4 but was significantly increased in $MnCl_2$-exposed male mice at Week 12 ($p < 0.05$). (D) Discrimination index was significantly lower in $MnCl_2$-exposed male and female mice at Week 12 ($p < 0.05$), with no significant differences at Week 4. Statistical analysis was performed using a Two-way ANOVA with post-hoc Tukey test, error bars represent SEM, *$p < 0.05$, **$p < 0.005$, ***$p < 0.0005$, ****$p < 0.0001$.*

However, by Week 12, $MnCl_2$-exposed male mice exhibited a significant reduction in total distance traveled compared to controls ($p < 0.05$), while female mice showed no significant differences at either time point. This indicates that manganese exposure leads to a progressive decline in movement activity in males, while locomotor patterns in females remain unaffected.

Stereotypic behavior, a measure of repetitive movements, was assessed using stereotypy time (s) (Figure 4.2B) and stereotypic episode count (Figure 4.2C). At Week 4, no significant differences in stereotypic behaviors were observed between control and $MnCl_2$-exposed groups in either sex. However, by Week 12, $MnCl_2$-exposed male mice exhibited a significant increase in stereotypy time ($p < 0.0005$), while female mice did not show any significant differences. Similarly, stereotypic episode count remained unchanged at Week 4 but was significantly elevated in $MnCl_2$-exposed males at Week 12 ($p < 0.05$). These results suggest that chronic manganese exposure increases repetitive behaviors in a sex-specific manner, predominantly affecting males.

Cognitive function was assessed using the discrimination index in a novel object recognition test (Figure 4.2D) as a quantification of an animal's ability to differentiate between a familiar and a novel object based on exploratory behavior. At Week 4, no significant differences in discrimination index were observed between $MnCl_2$-exposed and control groups. However, by Week 12, $MnCl_2$-exposed male and female mice exhibited a significant increase in discrimination index ($p < 0.05$), indicating increased novelty-seeking behavior.

The progressive nature of Mn-induced behavioral effects, particularly the reduction in locomotor activity and the increase in stereotypic behaviors observed in males at Week 12, suggests that Mn accumulates over time, leading to progressive dysregulation of motor control pathways[172]. This aligns with previous reports linking Mn toxicity to basal ganglia dysfunction, a key region responsible for motor control and a primary site of Mn accumulation[178, 179]. The increased stereotypy further supports the hypothesis that Mn alters dopaminergic signaling in

the striatum, which was corroborated by the observed impairments in dopamine metabolism[180, 181].

Interestingly, rather than inducing cognitive deficits, Mn exposure resulted in an increase in the discrimination index in both sexes at Week 12, suggesting a transient enhancement of recognition memory and cognitive flexibility. While this pattern deviates from classical models of Mn neurotoxicity, it is possible that Mn-induced changes in dopamine and serotonin metabolism initially enhance cognitive function before later-stage neurotoxic effects emerge. Future studies should determine whether this cognitive enhancement persists or if it represents a compensatory response to early Mn exposure that ultimately declines with prolonged neurotoxic insult.

*Manganese Exposure Drives a Time-Dependent Shift in Gut Microbiome Composition Associated with Pro-Inflammatory Dysbiosis*

Taxonomic profiling revealed progressive and systematic alterations in gut microbiome composition in response to manganese (50 mg/kg $MnCl_2$) exposure, with the most pronounced deviations occurring over time (Figure 4.3A). At Week 1 (Figure 4.3B), microbiomes in both treatment cohorts exhibited similar community structures, with a predominance of *Lactobacillaceae* (Firmicutes) and *S24-7* (Bacteroidetes).

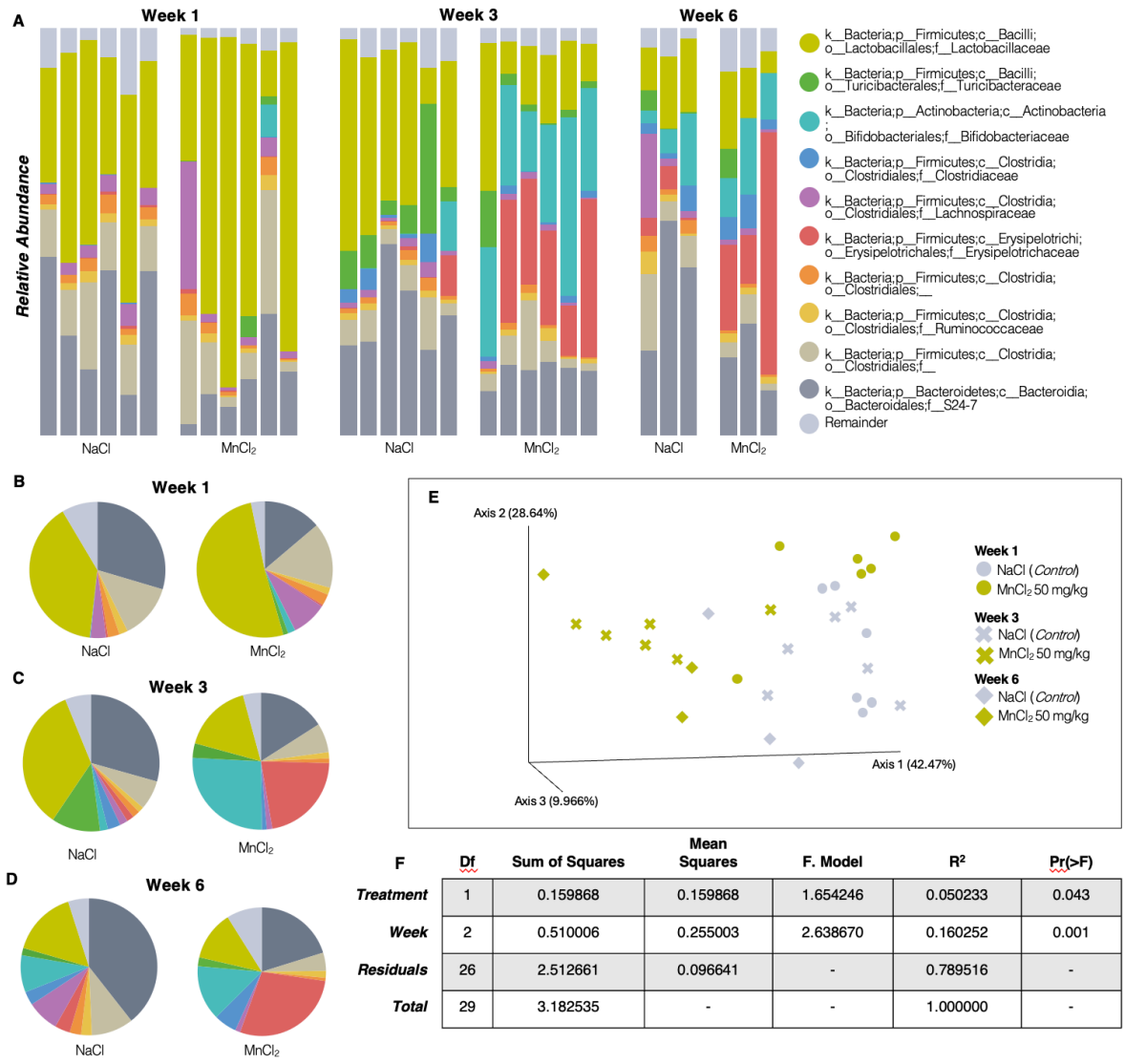


| F | Df | Sum of Squares | Mean Squares | F. Model | $R^2$ | Pr(>F) |
|---|---|---|---|---|---|---|
| ***Treatment*** | 1 | 0.159868 | 0.159868 | 1.654246 | 0.050233 | 0.043 |
| ***Week*** | 2 | 0.510006 | 0.255003 | 2.638670 | 0.160252 | 0.001 |
| ***Residuals*** | 26 | 2.512661 | 0.096641 | - | 0.789516 | - |
| ***Total*** | 29 | 3.182535 | - | - | 1.000000 | - |

**Figure 4.3. Juvenile mice exposed to 50 mg/kg MnCl via drinking water display significant changes to gut microbiome abundance.** (A) Taxonomic bar plots showing relative microbial abundance at Week 1, Week 3, and Week 6 in NaCl (control) and $MnCl_2$-exposed juvenile mice. By Week 6, $MnCl_2$ exposure led to a distinct microbial profile characterized by a depletion of *Lactobacillaceae* and an enrichment of *Clostridia*-associated taxa and *Erysipelotrichaceae*, indicative of dysbiosis. (B–D) Pie charts depicting taxonomic distributions at each time point illustrate the progressive divergence in microbial composition between treatment groups. (E) Weighted UniFrac-based Principal Coordinates Analysis (PCoA) showing microbial beta diversity over time. At Week 1, NaCl and $MnCl_2$ microbiomes largely overlapped, but by Week 6, $MnCl_2$-exposed microbiomes clustered distinctly from controls, indicating progressive microbiome divergence. (F) PERMANOVA (Adonis) statistical analysis quantifying microbiome variance explained by treatment and time. Manganese exposure significantly altered microbial composition ($R^2$ = 5.02%, p = 0.043), with temporal changes accounting for a larger proportion of variance ($R^2$ = 16.03%, p = 0.001).

Minor compositional differences were present, but $MnCl_2$ exposure had not yet elicited a distinct microbial divergence from NaCl controls. However, by Week 3 (Figure 4.3C), $MnCl_2$-exposed microbiomes demonstrated a marked depletion of *Lactobacillaceae*, concomitant with an expansion of *Clostridiaceae* and *Lachnospiraceae*, bacterial families frequently implicated in dysbiosis, inflammatory conditions, and metabolic dysfunction. In contrast, NaCl controls exhibited relative taxonomic stability, maintaining *Lactobacillaceae* and *S24-7* as dominant taxa. By Week 6 (Figure 4.3D), $MnCl_2$ exposure induced a substantial shift in the gut microbiome, marked by a significant expansion of *Erysipelotrichaceae*, a bacterial family associated with inflammatory responses, metabolic dysfunction, and neurodevelopmental disorders[182] In tandem, $MnCl_2$-exposed microbiomes exhibited a sustained proliferation of *Clostridiaceae*, *Lachnospiraceae*, and *Ruminococcaceae*, while *Lactobacillaceae*—a taxon integral to gut homeostasis, metabolic regulation, and neuroactive compound synthesis—remained markedly depleted[183]. Notably, NaCl controls exhibited only subtle taxonomic fluctuations over time, underscoring that the microbial shifts observed in $MnCl_2$-exposed samples were not attributable to natural temporal variation but rather a direct consequence of manganese exposure.

To evaluate microbial community restructuring, we performed Principal Coordinates Analysis (PCoA) using weighted UniFrac distances, a metric that accounts for phylogenetic relationships and relative taxon abundance (Figure 4.3E). The PCoA plot visualizes the similarities and differences between microbial communities, with each point representing a single sample and the distance between points reflecting the degree of similarity. At Week 1, microbial communities exhibited substantial overlap between $MnCl_2$-exposed and NaCl control cohorts, suggesting that manganese had not yet exerted a significant influence on microbiome composition. However, by Week 3, $MnCl_2$-exposed microbiomes began to separate from controls, with the most pronounced divergence emerging by Week 6, particularly along the first two principal coordinate axes (PC1 and PC2), which together explained 71.11% of the total

variation. This trajectory indicates that manganese exposure induces progressive, rather than immediate, microbial restructuring, reinforcing the taxonomic findings (Figures 4.3A–D) that demonstrated a gradual decline in commensal taxa (*Lactobacillaceae*) and an enrichment of inflammatory-associated bacteria (*Clostridiaceae*, *Erysipelotrichaceae*).

Finally, to statistically assess the impact of manganese exposure on microbial community composition, a PERMANOVA (Adonis) test was conducted to quantify the proportion of variance attributable to experimental factors (Figure 4.3F). The analysis revealed that manganese exposure significantly influenced gut microbiome composition, with treatment explaining 5.02% of the variance ($R^2 = 0.0502$, $p = 0.043$). Although statistically significant, the modest effect size suggests that manganese exposure alone is not the primary determinant of microbial community composition but instead exerts an influence that accumulates progressively over time. In contrast, temporal progression (Week 1, 3, 6) accounted for a substantially larger proportion of microbiome variation ($R^2 = 0.1603$, $p = 0.001$), indicating that the gut microbiome undergoes natural shifts over time. Notably, 78.95% of the variance remained unexplained, likely reflecting host-specific variability, dietary influences, and other environmental determinants. Collectively, these findings suggest that manganese exposure induces a gradual yet cumulative microbiome perturbation, culminating in a compositional profile enriched in pro-inflammatory taxa, neurodevelopmentally relevant microbial shifts, and markers of gut dysbiosis.

The Mn-induced disruptions to gut microbial composition provide a potential mechanistic link between Mn exposure and neurodevelopmental outcomes. The progressive depletion of beneficial *Lactobacillaceae* and the expansion of *Erysipelotrichaceae* and *Clostridia*-associated taxa suggest that Mn exposure shifts the gut microbiome toward a pro-inflammatory state[184]. The marked increase in *Erysipelotrichaceae* by Week 6 is particularly concerning, as this bacterial family has been linked to inflammatory bowel disease, metabolic dysfunction, and

neurodevelopmental conditions such as autism spectrum disorder (ASD) and attention-deficit hyperactivity disorder (ADHD)[185]. The depletion of *Lactobacillaceae*, which plays a critical role in gut homeostasis and neurotransmitter biosynthesis, suggests that Mn exposure may reduce microbial contributions to serotonin and dopamine synthesis, further exacerbating neurodevelopmental consequences[186].

*Manganese Exposure Induces Enteric Gliosis and Persistent Inflammatory Lesions in the Small Intestine of Juvenile Mice*

To investigate the impact of manganese ($MnCl_2$) exposure on enteric neuroinflammation and gut immune activation, immunohistochemical staining for glial fibrillary acidic protein (GFAP), a marker of enteric glial cell activation, and ionized calcium-binding adapter molecule 1 (Iba1), a marker of macrophage and microglial infiltration, was performed on intestinal tissue collected at 2-, 3-, 4-, and 13-weeks post-exposure.

Representative images from male (Figure 4.4A–C) and female (Figure 4.4D–F) juvenile mice at 3 and 13 weeks illustrate a dose-dependent increase in GFAP+ enteric glial cells, particularly in the 50 mg/kg $MnCl_2$-exposed groups, relative to NaCl controls. Quantification of GFAP+ cells (Figure 4.4M) confirmed a statistically significant increase in gliosis in male mice at weeks 2, 3, and 4 ($p < 0.0001$), as well as in female mice at weeks 2, 4, and 13 ($p < 0.005$ to $p < 0.0001$).

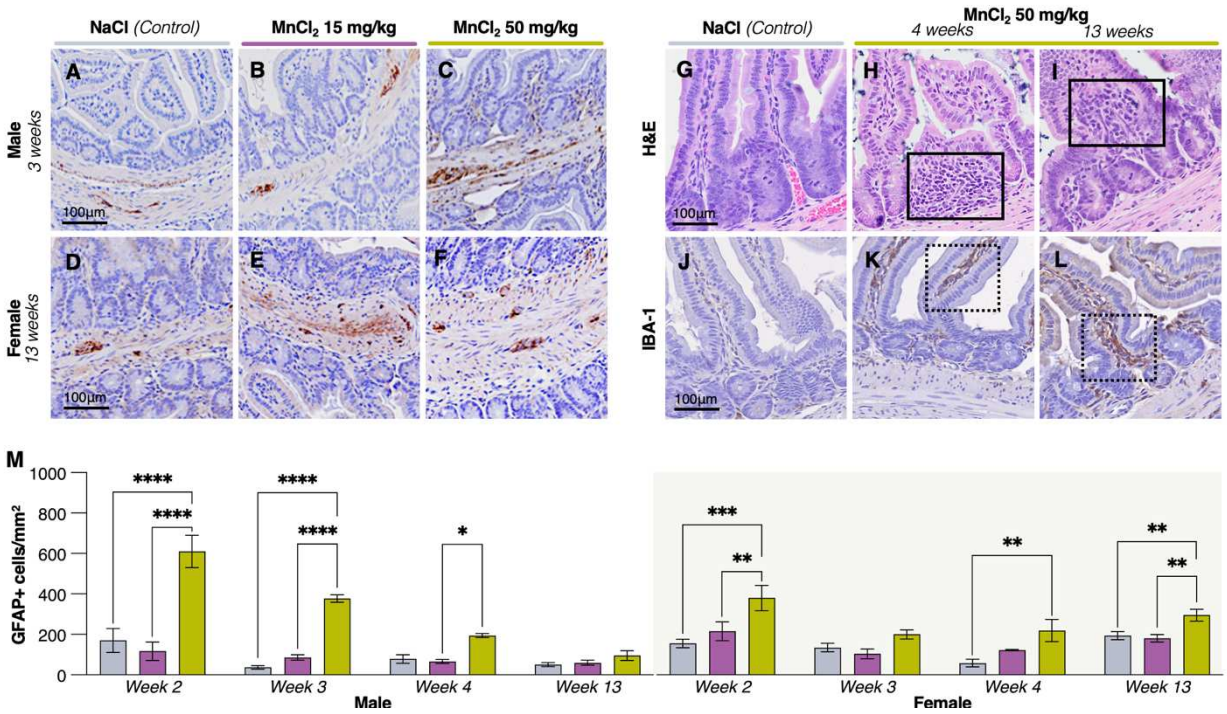


**Figure 4.4. Developmental exposure to Mn induces enteric gliosis and immunopathological lesions in small intestine of juvenile mice.** Intestinal tissue collected at 2-, 3-, 4-, and 13-weeks of Mn exposure was immunohistochemically stained for against activated enteric glial cell marker GFAP. Representative images at 20x are displayed for control, 15 mg/kg, and 50 mg/kg male (A-C) and female (D-F) mice at 3-, and 13-weeks of exposure, respectively. Scale bar = 100µm. Inflammatory lesions present at both 4- and 13-weeks of 50 mg/kg Mn (H and I, respectively), compared to control (G). Solid boxes identify areas of inflammation. Iba1+ cells (brown) are present throughout lamina of small intestine villi at 4- and 13-weeks of 50 mg/kg Mn exposure (K and L, respectively) compared to control (J). Dotted boxes identify cluster of Iba1+ cells. Scale bar = 100µm. Quantification of GFAP+ cells was completed using Olympus CellSens Software and is presented as cells/mm$^2$. GFAP+ enteric glial cells are significantly increased at weeks 2-4 in male mice exposed to 50 mg/kg Mn and 2-, 4-, and 13-weeks of 50 mg/kg Mn exposure in female mice. No significant increase in GFAP+ in any group at all timepoints with 15 mg/kg Mn. One-way ANOVA with post-hoc Tukey test, error bars = SEM ($n$ = 3-6 for all groups; outlier analysis performed using ROUT analysis at Q = 1%). * = $p < 0.05$, ** = $p < 0.005$, *** $p < 0.0005$, **** $p < 0.0001$.

These findings indicate a robust activation of enteric glia following manganese exposure, suggestive of neuroinflammatory stress within the intestinal nervous system. Notably, no significant GFAP+ upregulation was observed in the low 15 mg/kg Mn group, implying that a higher Mn burden is required to elicit a pronounced enteric glia response.

Histopathological examination further revealed pronounced inflammatory lesions in the small intestine of mice exposed to 50 mg/kg $MnCl_2$ for 4 and 13 weeks (Figure 4.4H, I), compared to NaCl controls (Figure 4.4G). The presence of Iba1+ immune cells (macrophages) was markedly increased in the $MnCl_2$-exposed groups, with clustering observed throughout the lamina propria and submucosal layers (Figures 4.4K, L), relative to NaCl-exposed controls (Figure 4.4J). Solid-boxed regions highlight areas of overt inflammation, whereas dotted-boxed regions denote dense immune cell aggregates, suggesting a persistent inflammatory response at both early (4-week) and late (13-week) time points. This sustained immune activation raises concerns about potential gut barrier dysfunction, as chronic macrophage infiltration is commonly associated with intestinal permeability defects, microbial translocation, and systemic inflammation[187].

The concurrent activation of enteric glial cells and macrophages in the gut further supports the notion that Mn exposure induces a chronic inflammatory state that spans multiple organ systems[64, 188]. The parallel emergence of enteric gliosis and immune cell infiltration reinforces the hypothesis that Mn exposure induces gut inflammation, potentially disrupting gut barrier integrity and promoting systemic inflammatory signaling that influences brain function. Given the well-established role of the gut-brain axis in shaping neurodevelopment, these findings raise concerns about whether Mn-induced gut dysbiosis and inflammation could contribute to behavioral deficits through inflammatory cytokine signaling and altered microbial metabolite production[189, 190].

*Manganese Exposure Alters Intestinal Tryptophan Metabolism and Increases the Kynurenine-to-Serotonin Ratio*

Given the gut dysbiosis and neuroimmune activation observed in $MnCl_2$-exposed mice, we investigated whether manganese exposure affects intestinal tryptophan metabolism, a key biochemical pathway involved in neurotransmitter production, immune regulation, and oxidative

stress responses. Tryptophan (TRP) serves as a precursor for two major metabolic fates: the serotonin (5-HT) biosynthetic pathway, mediated by tryptophan hydroxylase (TPH), and the kynurenine (KYN) pathway, catalyzed by indoleamine 2,3-dioxygenase (IDO) (Figure 4.5A). An increased KYN/5-HT ratio reflects a metabolic shift favoring kynurenine production, often associated with neuroinflammation, excitotoxicity, and cognitive impairments.

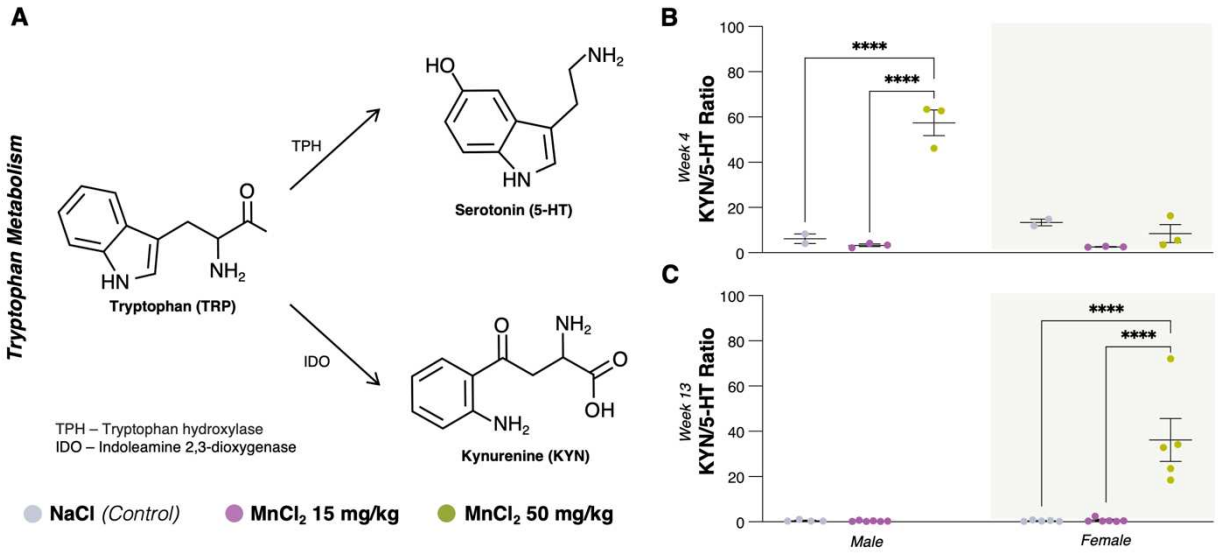


**Figure 4.5. Manganese exposure modulates intestinal tryptophan metabolism by significantly increasing KYN/5-HT ratio.** Enteric kynurenine (KYN)/5-HT ratio is significantly higher in males at 4-weeks (B) and females at 12-weeks of 50 mg/kg Mn exposure[2] (C). Statistical analysis for each dataset was performed using a Two-way ANOVA with post-hoc Tukey test, error bars = SEM (at 4-week time point $n = 2$ for female NaCl, and $n = 3$ for all other groups; at 13-week timepoint $n = 4$ for male NaCl, $n = 5$ for male $MnCl_2$ 15 mg/kg, $n = 0$ for male $MnCl_2$ 50 mg/kg[2], $n = 5$ for female NaCl, $n = 6$ for female $MnCl_2$ 15 mg/kg, and $n = 5$ for female $MnCl_2$ 50 mg/kg; outliers removed using ROUT analysis at Q = 1%). * = $p < 0.05$, ** = $p < 0.005$, *** $p < 0.0005$, **** $p < 0.0001$.

At Week 4, $MnCl_2$ exposure at 50 mg/Kg significantly elevated the KYN/5-HT ratio in male mice compared to NaCl controls and the 15 mg/Kg $MnCl_2$ group ($p < 0.0001$, Figure 5B). However, no significant metabolic shift was observed in females at this time point, suggesting a sex-dependent delay in manganese-induced neurotransmitter disruptions. By Week 13, a marked increase in the KYN/5-HT ratio was observed in $MnCl_2$-exposed females ($p < 0.0001$, Figure 4.5C). These findings indicate that manganese exposure disrupts tryptophan metabolism in a dose-dependent manner in females, with males exhibiting earlier neurotransmitter metabolic disturbances, while females experience delayed but pronounced alterations over time.

The progressive increase in the KYN/5-HT ratio in $MnCl_2$-exposed mice parallels the chronic gut inflammation, microbial dysbiosis, and neuroimmune activation observed in previous analyses (Figures 4.2–4). Notably, kynurenine pathway activation is commonly linked to chronic inflammation, as IDO expression is upregulated in response to pro-inflammatory cytokines, including interferon-gamma (IFN-γ) and tumor necrosis factor-alpha (TNF-α). Given that $MnCl_2$ exposure induced persistent enteric gliosis (Figure 4.4), increased inflammatory macrophage infiltration (Iba1+ cells), and a shift toward pro-inflammatory microbial taxa (Figures 4.2–3), the observed metabolic dysregulation may be a downstream consequence of manganese-induced gut inflammation driving a systemic neuroimmune response.

The metabolic disruptions observed in tryptophan metabolism further reinforce the role of gut-derived neurotoxicity in Mn exposure. The increased kynurenine-to-serotonin (KYN/5-HT) ratio in Mn-exposed mice suggests a shift in tryptophan metabolism toward kynurenine production, a pathway that is often upregulated in response to inflammation[191]. This shift was sex-dependent, with males exhibiting earlier metabolic disruptions at Week 4, whereas females showed a delayed but more pronounced alteration at Week 13. Given that kynurenine metabolites such as quinolinic acid are neurotoxic and have been implicated in excitotoxicity,

oxidative stress, and neuroinflammation, the Mn-induced activation of this metabolic pathway could serve as a critical mechanism linking gut dysbiosis to altered neurotransmitter signaling and behavioral changes[192]. Serotonin depletion resulting from this metabolic shift may further exacerbate gut-brain axis dysfunction, impacting both intestinal motility and central serotonergic neurotransmission[193]. These findings suggest that Mn exposure alters systemic metabolic regulation in a manner that extends beyond the gut and may influence broader neurodevelopmental processes.

*Manganese Exposure Induces Widespread Astrogliosis in the CNS of Juvenile Mice*

To assess the impact of manganese ($MnCl_2$) exposure on neuroinflammatory activation in the central nervous system (CNS), we quantified GFAP+ astrocytes, as a rise in the number of these cells is a hallmark of reactive gliosis, in three key brain regions associated with motor control, dopamine regulation, and neurotoxicity susceptibility during Mn exposure: the striatum (ST), globus pallidus (GP), and substantia nigra (SN). Representative immunohistochemical images illustrate a dose-dependent increase in GFAP+ astrocytes in both male (Figure 4.6A–L) and female (Figure 4.6M–X) mice following $MnCl_2$ exposure for 13 weeks.

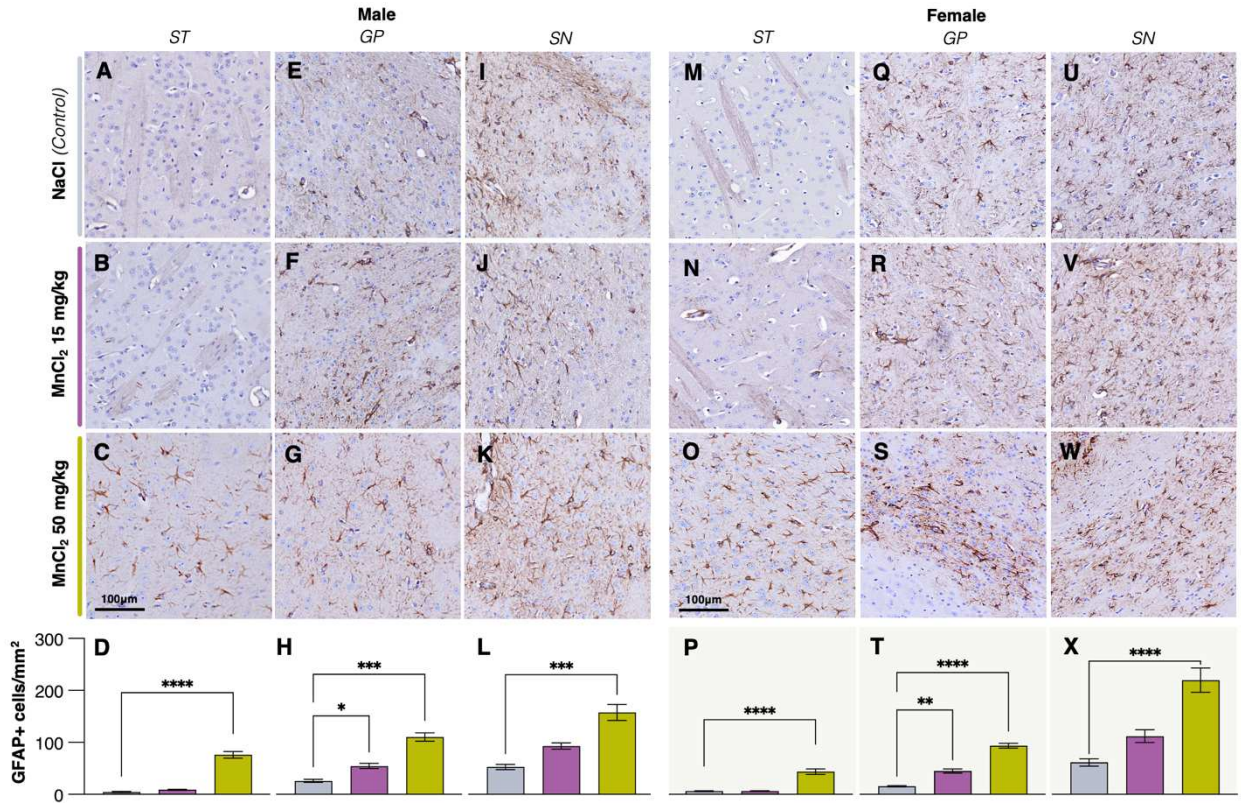


**Figure 4.6. Mn exposure induces astrogliosis in CNS of juvenile mice.** 13-weeks of developmental exposure to Mn increases GFAP+ astrocytes in male (A-L) and female (M-X) mice in the striatum (ST), globus pallidus (GP), and substantia nigra (SN). Representative images at 20x are shown for each brain region in male and female mice. Quantification of GFAP+ cells was completed using QuPath Software and is presented as cells/mm$^2$ within in corresponding brain region; ST, GP, and SN in both male (D, H, L) and female (P, T, X) groups, respectively. Developmental exposure to 15 mg/kg Mn increases GFAP+ astrocytes in the globus pallidus of both male and female mice. 50 mg/kg Mn results in increased GFAP+ astrocytes in all indicated brain regions for both male and female mice. Statistical analysis for each dataset was performed using a One-way ANOVA with post-hoc Tukey test, error bars = SEM (n = 3-6 for all groups; outlier analysis performed using ROUT analysis at Q = 1%). * = $p < 0.05$, ** = $p < 0.005$, *** $p < 0.0005$, **** $p < 0.0001$. Scale bar = 100µm.

In male mice, significant astrogliosis was detected across all three brain regions, with quantification revealing a robust increase in GFAP+ cells/mm² in the striatum ($p < 0.0001$, Figure 4.6D), globus pallidus ($p < 0.05$, Figure 6H), and substantia nigra ($p < 0.0005$, Figure 4.6L) in the 50 mg/kg $MnCl_2$ exposure group compared to NaCl controls. Notably, even at the lower $MnCl_2$ dose (15 mg/kg), a significant increase in GFAP+ astrocytes was observed in the globus pallidus ($p < 0.05$, Figure 6H), suggesting that this brain region may exhibit heightened susceptibility to manganese-induced neuroinflammatory stress.

A similar trend was observed in female mice, with significant $MnCl_2$-induced astrogliosis in the striatum ($p < 0.0001$, Figure 4.6P), globus pallidus ($p < 0.005$, Figure 4.6T), and substantia nigra ($p < 0.0001$, Figure 6X) following exposure to 50 mg/kg $MnCl_2$. Importantly, while the globus pallidus exhibited increased GFAP+ cells in response to 15 mg/kg $MnCl_2$ in both sexes, the striatum and substantia nigra only showed significant astrogliosis at the higher manganese dose (50 mg/kg), suggesting that the extent of neuroinflammatory activation is both region- and dose-dependent.

These findings indicate that developmental manganese exposure induces widespread gliotic activation in basal ganglia-associated brain regions, with the globus pallidus appearing particularly vulnerable to Mn-induced astrocytosis. Given the role of these structures in dopaminergic signaling and motor function, persistent astrogliosis in these regions may have implications for Mn-related movement disorders and neurodevelopmental impairments.

The widespread neuroinflammatory response observed in both the CNS and ENS underscores the systemic impact of Mn exposure on neuroimmune interactions. The significant increase in GFAP+ astrocytes in motor-associated brain regions, including the striatum, globus pallidus, and substantia nigra, indicates that Mn exposure triggers chronic neuroinflammation in key dopaminergic circuits[194]. The heightened gliotic response in the globus pallidus, even at lower Mn doses, suggests that this region is particularly susceptible to Mn-induced oxidative

stress[195]. Given that astrocytes play a central role in synaptic homeostasis, glutamate regulation, and neuroimmune signaling, persistent gliosis in these regions could contribute to long-term motor impairments and behavioral dysregulation[196]. These findings highlight the need to consider neurodevelopmental toxicants such as Mn within the broader framework of systemic inflammation and immune activation, rather than as isolated neurotoxic agents.

*Manganese Exposure Disrupts Striatal Dopamine and Serotonin Turnover in Juvenile Mice*

To determine whether manganese ($MnCl_2$) exposure alters neurotransmitter homeostasis in the striatum, we quantified levels of dopamine (DA) and serotonin (5-HT), along with their respective turnover ratios, in $MnCl_2$-exposed and control mice at 4 and 13 weeks of exposure. Given the established role of these neurotransmitters in motor function, reward processing, and neurodevelopment, disruptions in their transmitter metabolism may provide mechanistic insights into Mn-associated neurotoxicity (Figures 4.7A, 4.7D).

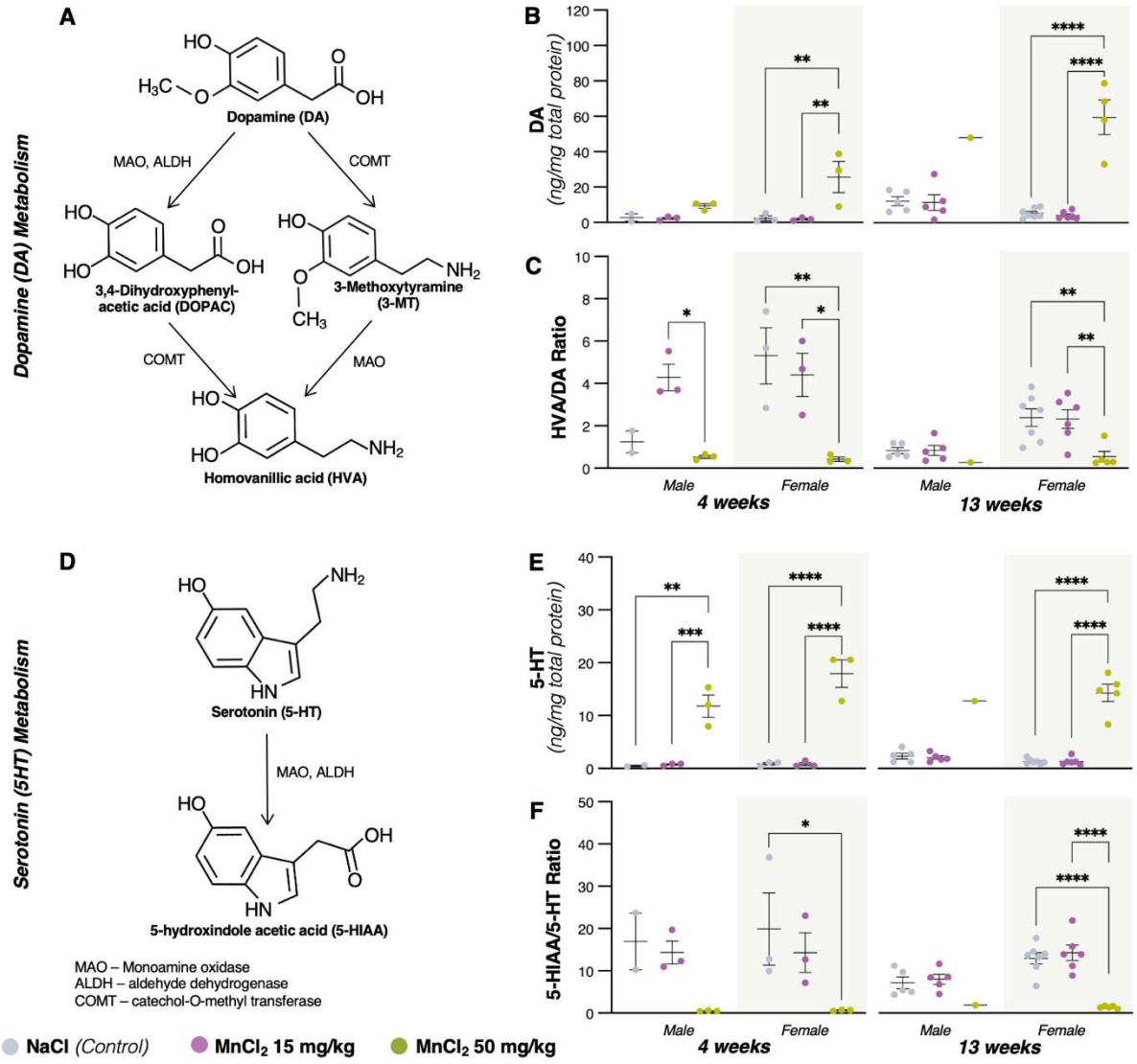


**Figure 4.7. Developmental exposure to Mn significantly decreases striatal dopamine and serotonin turnover in juvenile mice.** Dopamine (DA) metabolism pathway (A). Exposure to 50 mg/kg Mn significantly increases striatal DA levels in female juvenile mice at 4- and 13-weeks (B). DA turnover (HVA/DA) is significantly decreased in female mice at 4- and 13-weeks of exposure to 50 mg/kg Mn (C). Serotonin (5-HT) metabolism pathway (D). Exposure to 50 mg/kg Mn significantly increases striatal 5-HT levels in female and male juvenile mice at 4-weeks of exposure and female mice at 12-weeks of exposure (E). 5-HT turnover (5-HIAA/5-HT)) is significantly decreased in female mice at 4- and 12-weeks of exposure to 50 mg/kg Mn (F). Statistical analysis for each dataset was performed using a One-way ANOVA with post-hoc Tukey test, error bars = SEM (At 4-week time point $n$ = 2 male for NaCl, and $n$ = 3 for all other groups; at 13-week timepoint $n$ = 5 for male NaCl and $MnCl_2$ 15 mg/kg, $n$ = 1 male for $MnCl_2$ 50 mg/kg[1], $n$ = 7 for female NaCl, $n$ = 6 for female $MnCl_2$ 15 mg/kg, and $n$ = 5 for female $MnCl_2$ 50 mg/kg; Outliers removed using ROUT analysis at Q = 1%). * = $p < 0.05$, ** = $p < 0.005$, *** $p < 0.0005$, **** $p < 0.0001$.

At Week 4, exposure to 50 mg/kg $MnCl_2$ significantly increased DA levels in male mice compared to controls ($p < 0.005$, Figure 4.7B). However, by Week 13, female mice exhibited a striking elevation in striatal DA levels following 50 mg/kg $MnCl_2$ exposure ($p < 0.0001$, Figure 9B), while male samples were unavailable due to sample degradation. Notably, DA turnover (HVA/DA ratio) was significantly reduced in female $MnCl_2$-exposed mice at both 4 and 13 weeks ($p < 0.05$ to $p < 0.005$, Figure 4.7C), indicating impaired dopamine metabolism despite increased DA accumulation.

Similarly, $MnCl_2$ exposure significantly increased striatal serotonin (5-HT) levels in both male and female mice at multiple time points. By Week 4, $MnCl_2$-exposed female and male mice exhibited a significant increase in 5-HT levels compared to controls ($p < 0.005$ to $p < 0.0001$, Figure 9E). However, by Week 13, only female $MnCl_2$-exposed mice retained significantly elevated 5-HT levels ($p < 0.0001$, Figure 4.7E), suggesting a progressive and sex-dependent disruption in serotoninergic regulation over time.

To assess serotonin turnover, we calculated the 5-HIAA/5-HT ratio, which reflects serotonin metabolism and clearance. At Week 4, male $MnCl_2$-exposed mice exhibited a significant reduction in 5-HT turnover ($p < 0.05$, Figure 4.7F), while at Week 13, $MnCl_2$-exposed females showed a pronounced reduction in serotonin turnover ($p < 0.0001$, Figure 9F). These findings suggest that while 5-HT levels increase following manganese exposure, serotonin metabolism is impaired, potentially leading to an accumulation of serotonin in the striatum.

Taken together, these results indicate that manganese exposure disrupts both dopamine and serotonin homeostasis in a dose-dependent and sex-specific manner. The early disruption of DA metabolism in males, followed by delayed but pronounced DA and 5-HT dysregulation in females, suggests a cumulative neurotoxic effect of manganese that becomes more pronounced over time.

The findings of this study underscore the need for future research aimed at elucidating the mechanisms underlying Mn-induced neurotoxicity and its broader implications for neurodevelopmental health. One important area for investigation is the role of the gut microbiome in mediating Mn toxicity. Longitudinal studies assessing whether microbial shifts precede, coincide with, or follow behavioral alterations will help clarify the causal relationship between gut dysbiosis and neurodevelopmental impairment[53, 70]. Further characterization of microbial-derived metabolites, particularly those related to tryptophan metabolism, short-chain fatty acids, and neurotransmitter precursors, could provide valuable insights into how gut microbiota influence Mn-induced changes in neurotransmission and behavior.

Given the observed sex differences in behavioral, metabolic, and neuroimmune responses, future research should also explore the role of sex hormones in modulating Mn susceptibility[197]. Studies investigating estrogen and androgen signaling in relation to Mn bioaccumulation, gut microbial composition, and neuroinflammatory pathways could help explain why males exhibit earlier motor impairments and stereotypic behaviors, while females show delayed but more pronounced metabolic and inflammatory changes. Additionally, investigating whether sex-dependent differences in Mn metabolism influence Mn transport across the blood-brain barrier may provide further insight into sex-specific vulnerability to Mn neurotoxicity.

Another critical avenue for future research is the exploration of therapeutic interventions aimed at mitigating Mn-induced neurodevelopmental deficits. Probiotic supplementation, particularly with *Lactobacillaceae* strains known to promote neurotransmitter synthesis and gut homeostasis, could be evaluated as a potential strategy for restoring microbial balance and mitigating Mn-induced dysbiosis[198]. Given the observed disruption of tryptophan metabolism, interventions targeting kynurenine pathway enzymes, such as IDO inhibitors, could be explored for their potential to reduce neurotoxic metabolite production[199]. Anti-inflammatory compounds

capable of modulating astrocyte activation and mitigating neuroinflammation, such as omega-3 fatty acids or gut-targeted immune modulators, may also hold promise as protective strategies against Mn-induced CNS and ENS neuroinflammation[200].

Finally, further studies are needed to determine whether early-life Mn exposure leads to persistent, long-term neurodevelopmental impairments. Behavioral assessments beyond the juvenile period, coupled with neuroimaging and transcriptomic analyses, could help determine whether Mn-induced alterations in neurodevelopment stabilize, worsen, or recover over time. Given the increasing awareness of environmental factors in neurodevelopmental disorders, these findings highlight the importance of assessing dietary and environmental sources of Mn exposure, particularly in infants and young children[201]. Refining regulatory guidelines for Mn intake, developing biomarkers for early Mn toxicity, and identifying individuals at heightened risk for Mn neurotoxicity should be prioritized in future public health research.

By integrating behavioral, microbiome, metabolic, and neuroinflammatory analyses, this study provides a comprehensive foundation for understanding Mn toxicity as a multi-systemic process. The findings emphasize the necessity of interdisciplinary approaches in environmental neurotoxicology, bringing together microbiology, neuroimmunology, and behavioral neuroscience to unravel the complex interactions between environmental toxins and neurodevelopment.

## Methods

*Animal Model Exposure*

C57/Bl6 mice (Jackson Laboratories) were housed in microisolator cages (4 to 5 animals per cage) and kept on 12-hr light/dark cycles with access to laboratory chow and water. Bi-weekly, mice were weighed to determine a 50 mg/Kg MnCl2 dose needed per cage to be administered in the mouse water bottles. Mn delivered into water bottles were adjusted

accordingly, using similar methods in previous studies in (Moreno et al. 2009, 2011, Streifel et al. 2012). An equivalent of 0.9% NaCl was used as the control. All procedures were carried out under the supervision of the institutional animal care at Colorado State University under the care of veterinary staff at the laboratory animal resources facility.

*Open Field Behavioral Assay*

Open-field activity parameters were determined using Versamax behavior chambers with an infrared beam grid detection array to assess animals' movements in x-, y-, and z-planes. Activity was measured in the juvenile exposure group every other day for 2 weeks and for the adult exposure group once a week for 2 months during the period of oral gavage. Activity parameters were binned every minute for a total of 10 min and then analyzed using Versadat software (v. 4.00-127E; Accuscan Instruments, Inc., Columbus, OH). Analysis of juvenile animals compared 11–18 animals within each female and male treatment group, whereas 8–10 animals were assessed in adult treatment groups.

*Novel Object Recognition Assay*

Mice were tested on the same day in randomized order. Mice were given a 10-minute familiarization session and recordings with two similar objects were made from small building blocks. Mice were then isolated in a clean cage for 60 minutes. The arena and object were cleaned with 70% ethanol and let to air-dry prior to adding in an additional animal. One clean familiar object and one clean novel object in the original positions of the two identical objects during familiarization. After a 60 minutes delay, mice were given 5 minutes to interact with the familiar and novel object and recorded for future analysis. Mice were then weighed after this behavioral assay. Analysis was performed using GoPro camera for recordings and a timer was used to distinguish the amount of time the mice spent on both objects. Minutes were converted into seconds by multiplying the time value by 60. Data was then analyzed using Graph Pad Prism v9 was used to make graphs and statistical analysis.

*Immunohistochemistry*

Immunohistochemical stains were performed on whole brain sagittal sections. To deparaffinize the tissue sections, slides were heated for 20 minutes at 60°C followed by a series of incubations in xylene and graded ethanol (xylene, 1 part xylene to 1 part 100% EtOH, 100% EtOH, 95% EtOH, 70% EtOH, 1.0 M TBS) for 5 minutes each. Heat and chemical-induced antigen retrieval was performed on the tissue by incubating in 0.01 M sodium citrate (pH = 6.0) for 20 minutes at 95°C. Removal of endoperoxides was performed through incubation in 0.3% hydrogen peroxide for 30 minutes at room temperature. Wash steps and tissue permeabilization were performed using 2% bovine serum albumin [25] and 2% Triton-X in 0.05 M TBS respectively. Tissue was blocked in 10% goat or donkey serum diluted in 1.0 M TBS for 1 hour at room temperature. After being diluted to their optimized concentrations, primary antibodies were incubated on the tissue at 4°C overnight. Iba-1 antibody (1:400; Abcam, ab5076) was used for microglial counts. Nonspecific binding was blocked before primary antibodies with 10% Horse Serum (Sigma Aldrich). A biotinylated secondary antibody (Vector Labs) was used, and stain was visualized with diaminobenzidine reagent. All images were taken with CellSens Dimension Desktop 3.1 and counted with CellSens (Iba-1 and GFAP).

*Metal Analysis*

Neurochemistry Analysis of brain tissue and small intestinal tissue

Small molecule neurotransmitters were measured in the Vanderbilt University Neurochemistry Core. Stock solutions of each analyte of interest (5ng/uL each) were made in DI water and stored at -80oC. To prepare internal standards, stock solutions were derivatized in a similar manner to samples using isotopically labeled benzoyl chloride (13C6-BZC) as follows: 200uL of the stock solution was mixed with 400uL each of 500mM NaCO3 (aq) and 2% 13C6-BZC in acetonitrile was added to the solution. After two minutes, the reaction was stopped by the addition of 400uL 20% acetonitrile in water containing 3% sulfuric acid. The solution was mixed

well and stored in 10uL aliquots at -80oC. One aliquot was diluted 100x with 20% acetonitrile in water containing 3% sulfuric acid to make the working internal standard solution used in the sample analysis. Tissues were homogenized, using a tissue homogenizer, in 100-750 ul of 0.1M TCA, which contained 10-2 M sodium acetate, 10-4 M EDTA, and 10.5 % methanol (pH 3.8). Ten microliters of homogenate was used for protein quantification. Samples were spun in a microcentrifuge at 10,000 g for 20 minutes at 4oC. The supernatant was removed for LC/MS analysis. Analytes in tissue extract supernatant were quantified using liquid chromatography/mass spectrometry (LC/MS) following derivatization with benzoyl chloride (BZC). 5uL of supernatant was then mixed with 10uL each of 500mM NaCO3 (aq) and 2% BZC in acetonitrile in an LC/MS vial. After two minutes, the reaction was stopped by the addition of 10uL internal standard solution. LC was performed on a 2.1 x 100 mm, 1.6mm particle CORTECS Phenyl column (Waters Corporation, Milford, MA, USA) using a Waters Acquity UPLC. Mobile phase A was 0.1% aqueous formic acid and mobile phase B was acetonitrile with 0.1% formic acid. MS analysis was performed using a Waters Xevo TQ-XS triple quadrupole tandem mass spectrometer. The source temperature was 150oC, and the desolvation temperature was 400oC. Protein concentration was determined using the BCA Protein Assay Kit (Thermo Scientific, Waltham, MA USA) in a 96-well plate format. 10uL of tissue homogenate was mixed with 200 ml of mixed BCA reagent per manufacturer instructions. The plate was incubated at 23oC for two hours before absorbance was measured by the plate reader (POLARstar Omega), purchased from BMG LABTECH Company.

*Microbiome Analysis*

Fecal samples were collected weekly from juvenile mice exposed to either 50 mg/kg $MnCl_2$ or NaCl (control) via drinking water for 6 weeks. Samples were collected immediately after defecation and stored at -80°C until processing. Genomic DNA was extracted from fecal pellets using the DNeasy PowerSoil Pro DNA isolation kit (Qiagen) according to the

manufacturer's instructions. Bacterial communities were characterized using 16S rRNA sequencing using 515F/806R primers targeting the V4 region of the 16S rRNA gene. These primers were barcoded for multiplexing. V4 amplicons were generated following the Earth Microbiome Project protocols (https://earthmicrobiome.org/protocols-and-standards/16s/). PCR amplification was performed in triplicate for each sample, and amplicons were pooled and normalized by concentration. Pooled amplicons were sequenced using the Illumina MiSeq platform with paired-end 250 bp reads. Blank DNA extraction and PCR negative controls were included to assess contamination. Raw sequencing data were processed using QIIME2 (v2023.5). Paired-end reads were demultiplexed, quality filtered, and denoised using DADA2 to generate amplicon sequence variants (ASVs). Sequences were rarefied to even depth for diversity analyses. ASVs were filtered to remove contaminants identified in negative controls and low-abundance taxa (present in fewer than 5% of samples). Taxonomic composition at the family level was analyzed across treatment groups and time points. Alpha diversity metrics (Shannon diversity) and beta diversity (weighted UniFrac distances) were calculated. Principal Coordinates Analysis (PCoA) was performed to visualize differences in microbial community structure between groups. PERMANOVA (Adonis) was used to assess the significance of treatment and time effects on microbiome composition. Statistical analyses were performed in R (v4.2.0). Significant differences were determined at $p < 0.05$

# CHAPTER 5 – NEUROINFLAMMTION AT THE CROSSROADS OF NEURODEVELOPMENT & NEURODEGERNATION: MECHANIMS, IMPLICATIONS, AND FUTURE DIRECTIONS

## Neuroinflammation as a Fundamental Mechanism of Neural Dysfunction

Neuroinflammation represents a complex and multifaceted pathological mechanism that fundamentally influences neurological disease progression across diverse conditions. This dissertation provides comprehensive insights into the molecular and environmental determinants of neuroinflammatory processes through two primary investigative approaches: targeted molecular inhibition of inflammatory pathways in a prion disease model and systematic examination of manganese-induced neurotoxicity. The prion disease investigation utilizing the novel therapeutic SB_NI_112 demonstrates the potential of targeted molecular intervention in modulating neuroinflammatory cascades. By selectively inhibiting NF-κB and NLRP3 inflammatory pathways, the intervention significantly attenuated microglial and astrocytic activation, revealing a nuanced approach to interrupting chronic neuroinflammatory processes[50]. The observed reduction in pro-inflammatory cytokine levels and preservation of synaptic integrity provides compelling evidence for the therapeutic potential of targeted inflammatory pathway modulation.

The intervention unveiled complex sex-dependent variations in neuroinflammatory responses, highlighting the intricate nature of inflammatory mechanisms[50]. These observations underscore the necessity of considering physiological heterogeneity in neuroinflammatory research, challenging traditional uniform conceptualizations of disease progression. The differential responses to NF-κB and NLRP3 inhibition suggest that inflammatory processes are dynamically regulated by multifaceted biological mechanisms that extend beyond simplistic linear models of neuroinflammation.

Complementary insights emerged from the manganese exposure studies, which provided a comprehensive exploration of environmental modulation of neuroinflammatory processes. Chronic manganese exposure triggered extensive inflammatory responses that transcended traditional boundaries between central and enteric nervous systems. The research elucidated complex interactions between environmental exposures, gut microbiome composition, and neuroinflammatory signaling cascades, demonstrating the profound impact of environmental factors on neural homeostasis.

**The Gut-Brain Axis as a Lifelong Mediator of Neurological Disease**

Emerging research highlights the gut-brain axis as a key regulator of both neurodevelopmental disorders, such as Attention-Deficit/Hyperactivity Disorder (ADHD) and Autism Spectrum Disorder (ASD), and neurodegenerative protein misfolding disorders (NPMDs). The gut microbiome influences neuroinflammation through systemic immune activation, cytokine signaling, and microbial metabolite production, all of which contribute to disease pathology[186]. Disruptions in gut microbiota have been linked to the accumulation of misfolded proteins, with evidence suggesting that pathogenic proteins may spread from the gut to the brain via the vagus nerve, exacerbating neurodegenerative processes[106, 176]. Chronic gut inflammation is thought to compromise the integrity of the blood-brain barrier through systemic inflammation that allows for the facilitation of the entry of peripheral inflammatory mediators into the central nervous system amplifying the neuroimmune responses[22]. Additionally, prolonged gut dysbiosis and enteric gliosis have been associated with increased neuroinflammation and a heightened risk of neurodegeneration in adulthood[175]. These findings suggest that gut dysfunction may act as both a trigger and amplifier of neurodegenerative pathology, providing a

potential therapeutic avenue for targeting early inflammatory and microbial imbalances to slow disease progression.

Beyond neurodegeneration, early-life exposure to environmental toxicants has been associated with persistent gut inflammation, which may predispose individuals to long-term neurological consequences. Experimental models demonstrate that toxicant-induced disruptions in gut microbiota composition coincide with increased enteric gliosis and neuroimmune priming, altering inflammatory responses as the patients ages[185]. Prenatal and early postnatal exposure to environmental stressors has been linked to sustained pro-inflammatory states, reinforcing the notion that gut health during early life is critical for long-term neuroprotection. The gut microbiota plays a crucial role in neurodevelopment, regulating synaptogenesis, neurotransmitter availability, and microglial maturation during early brain formation[71]. Therefore, alterations in microbial composition during sensitive developmental windows may have profound effects on later-life cognitive and neuroimmune function. Longitudinal studies in both human and animal models suggest that disturbances in early gut microbiota balance can lead to persistent alterations in brain connectivity and immune homeostasis, creating a long-term vulnerability to neurological disorders[201].

Additionally, individuals with neurodevelopmental disorders such as ASD and ADHD frequently exhibit significant gut microbiome alterations and chronic gastrointestinal inflammation. Some studies suggest that these microbiome disturbances contribute to increased neuroinflammatory susceptibility, which may elevate the risk of developing neurodegenerative conditions later in life. For instance, a study found that adults diagnosed with ADHD had a 2.77-fold increased risk of developing dementia compared to those without ADHD[202]. Regarding ASD, evidence indicates that neurodegeneration may underlie the loss of neurological function in children who have experienced regression, suggesting a potential link between ASD and neurodegenerative processes[203]. While further longitudinal studies are needed to establish

direct causal relationships, these findings highlight the necessity of considering gut health as an important factor in both neurodevelopmental and neurodegenerative disease risk.

**Bridging Neurodevelopmental and Neurodegenerative Disorders**

The research presented in this dissertation challenges traditional boundaries between neurodevelopmental and neurodegenerative disorders by demonstrating shared inflammatory mechanisms. The molecular pathways explored through targeted NF-κB and NLRP3 inhibition reveal remarkable parallels in inflammatory responses across different neurological conditions, suggesting that these pathways may represent common therapeutic targets. Manganese exposure studies further support this integrated perspective by demonstrating how early-life environmental factors can trigger inflammatory cascades with potential long-term consequences. The observed alterations in gut microbiome composition and systemic inflammatory responses suggest that environmental exposures may set the stage for later neurological dysfunction through persistent modulation of inflammatory pathways.

Sex-dependent variations in inflammatory responses, observed in both the prion disease and manganese exposure models, underscore the complex interplay between biological factors and environmental influences in shaping neuroinflammatory vulnerability. These findings challenge uniform approaches to neurological disorders and suggest the need for more personalized strategies that account for individual variability in inflammatory susceptibility. The gut-brain axis emerges as a critical mediator of neuroinflammatory processes, bridging environmental exposures and central nervous system outcomes. The observed interactions between gut microbiome alterations, peripheral inflammation, and neuroinflammatory signaling suggest that targeting the gut-brain axis may offer novel therapeutic approaches for a range of neurological conditions.

Collectively, these insights reinforce the emerging recognition of the gut-brain axis as a central regulator of neurological function across the lifespan. By integrating perspectives from

microbiome research, neuroimmunology, and environmental health, a more comprehensive understanding of how gut health influences both early neurodevelopment and late-stage neurodegeneration can be achieved. Future research should explore gut-targeted interventions, such as probiotics, dietary modifications, and environmental toxin mitigation strategies, as potential approaches to reduce the long-term neurological burden associated with gut dysbiosis and chronic inflammation.

**Advancing Therapeutic Strategies for Neuroinflammatory Disorders**

The findings from this dissertation have significant implications for the development of novel therapeutic strategies targeting neuroinflammation. The efficacy of SB_NI_112 in modulating NF-κB and NLRP3 pathways demonstrates the potential for targeted molecular interventions to interrupt chronic inflammatory cascades in neurological disorders. This approach could be extended to other neurodegenerative and neurodevelopmental conditions, potentially offering new treatment options for a broad spectrum of patients.

The observed sex-dependent variations in inflammatory responses warrant extensive further investigation. Future studies should employ comprehensive approaches to elucidate the molecular mechanisms underlying these differential responses, including detailed investigations of hormonal influences, genetic predispositions, and physiological variations that contribute to sex-specific neuroinflammatory vulnerabilities.

Environmental exposure research represents a critical frontier for future neuroinflammatory investigations. The manganese exposure studies highlight the profound impact of environmental factors on neural inflammatory processes. Future research should develop more comprehensive models for understanding how various environmental toxicants interact with biological systems to trigger inflammatory responses. Longitudinal studies tracking

the long-term consequences of early-life environmental exposures could provide crucial insights into the mechanisms of neurological disease initiation and progression.

Furthermore, the gut-brain axis emerges as a particularly promising area for future research. The observed interactions between gut microbiome composition, inflammatory responses, and neural function suggest complex communication pathways that remain incompletely understood. Future investigations should focus on developing more sophisticated models to elucidate the molecular mechanisms of gut-brain communication, potentially identifying novel therapeutic targets for neuroinflammatory disorders.

**Research and Clinical Innovation in Neuroinflammation in Neuroinflammation Pipeline**

The research presented in this dissertation provides a foundation for developing more sophisticated approaches to diagnosing, monitoring, and treating neuroinflammatory disorders. The identification of specific molecular pathways involved in neuroinflammation, such as NF-κB and NLRP3, offers potential targets for biomarker development. Future studies should focus on validating these pathways as reliable indicators of neuroinflammatory status, potentially enabling earlier detection and more precise monitoring of disease progression.

The observed interactions between environmental exposures, gut microbiome alterations, and neuroinflammation suggest the potential for developing novel preventive strategies. Prospective research could explore interventions targeting the gut-brain axis, such as dietary modifications or probiotic treatments, as potential approaches to mitigate neuroinflammatory risk.

The complex, multifaceted nature of neuroinflammation displayed by this research underscores the need for integrated, systems-level approaches to studying and treating neurological disorders. Continued research should aim to bridge disciplinary boundaries, combining insights from molecular biology, immunology, microbiology, and environmental science to develop more comprehensive models of neuroinflammatory processes.

**A New Perspective on Neuroinflammation and Neurological Disease**

The research presented in this dissertation provides a comprehensive exploration of neuroinflammation as a critical mechanism underlying neurological dysfunction across diverse conditions. By integrating molecular, environmental, and systemic approaches, this work builds upon recent advances in the field that increasingly recognize neuroinflammation as a key driver of disease rather than a secondary consequence. While traditional perspectives have often framed inflammation as merely a byproduct of neural dysfunction, emerging research supports its active role in disease initiation and progression. This work showcased here contributes to and further reinforces this shift by demonstrating how neuroinflammatory processes transcend traditional boundaries between neurodevelopmental and neurodegenerative disorders, highlighting their potential as therapeutic targets.

The targeted molecular intervention studies, utilizing the novel therapeutic SB_NI_112, demonstrated the potential for precisely modulating inflammatory pathways. By selectively inhibiting NF-κB and NLRP3 inflammatory mechanisms, the investigation revealed the possibility of interrupting destructive inflammatory cascades, challenging deterministic models of neurological disease progression. In parallel, environmental exposure investigations, particularly the manganese study, underscored the profound impact of external factors on neuroinflammatory processes. These studies illuminated the complex interactions between environmental exposures, gut microbiome composition, and systemic inflammatory responses,

demonstrating how external factors can compromise neural health through persistent neuroimmune activation. Together, these findings reinforce the importance of considering both intrinsic and extrinsic factors in shaping neuroinflammatory vulnerability.

The observed sex-dependent variations in inflammatory responses represent another significant contribution of this research. By revealing the nuanced physiological mechanisms underlying differential inflammatory responses, these findings challenge uniform conceptualizations of neuroinflammation and provide a more sophisticated understanding of biological complexity. Sex differences in immune function, hormonal regulation, and inflammatory reactivity may contribute to varying susceptibilities to neurological disorders, emphasizing the need for sex-specific therapeutic strategies. These insights, combined with the molecular and environmental findings, support a more personalized and integrative approach to understanding neuroinflammatory dynamics.

Methodologically, this dissertation demonstrates the value of interdisciplinary research approaches. By integrating molecular, environmental, behavioral, and systems-level analyses, these studies provide a comprehensive framework for investigating complex neuroinflammatory mechanisms. This approach offers a more nuanced understanding of neural dysfunction, emphasizing the interconnected nature of biological processes and the necessity of multi-dimensional research strategies. The ability to bridge mechanistic insights with broader environmental and systemic factors provides a more holistic perspective on neuroinflammation and strengthening the foundation for translational applications.

Ultimately, this research contributes to an emerging paradigm shift in understanding neurological disorders. By demonstrating the fundamental role of inflammatory processes across diverse conditions, it challenges traditional diagnostic boundaries and promotes a more integrated perspective on neural health. These findings highlight the potential for developing more sophisticated, mechanism-informed approaches to preventing, diagnosing, and treating

neurological conditions at all stages of life. As scientific understanding continues to evolve, the insights presented in this dissertation offer a promising path forward. By emphasizing that neuroinflammation is not merely a consequence of disease but a critical modifiable mechanism, this work underscores the need for comprehensive, interdisciplinary approaches to preserve neural function across the lifespan.

REFERENCES

(1) Feigin, V. L.; Vos, T.; Nichols, E.; Owolabi, M. O.; Carroll, W. M.; Dichgans, M.; Deuschl, G.; Parmar, P.; Brainin, M.; Murray, C. The global burden of neurological disorders: translating evidence into policy. *Lancet Neurol* **2020**, *19* (3), 255-265. DOI: 10.1016/S1474-4422(19)30411-9.

(2) Soto, C.; Pritzkow, S. Protein misfolding, aggregation, and conformational strains in neurodegenerative diseases. *Nat Neurosci* **2018**, *21* (10), 1332-1340. DOI: 10.1038/s41593-018-0235-9.

(3) Hyman, S. L.; Levy, S. E.; Myers, S. M.; COUNCIL ON CHILDREN WITH DISABILITIES, S. E. C. T. O. D. A. B. P. Identification, Evaluation, and Management of Children With Autism Spectrum Disorder. *Pediatrics* **2020**, *145* (1). DOI: 10.1542/peds.2019-3447.

(4) Hammond, T. R.; Marsh, S. E.; Stevens, B. Immune Signaling in Neurodegeneration. *Immunity* **2019**, *50* (4), 955-974. DOI: 10.1016/j.immuni.2019.03.016.

(5) Hughes, H. K.; R J Moreno; Ashwood, P. Innate immune dysfunction and neuroinflammation in autism spectrum disorder (ASD). *Brain Behav Immun* **2023**, *108*, 245-254. DOI: 10.1016/j.bbi.2022.12.001.

(6) Jha, M. K.; Jo, M.; Kim, J. H.; Suk, K. Microglia-Astrocyte Crosstalk: An Intimate Molecular Conversation. *Neuroscientist* **2019**, *25* (3), 227-240. DOI: 10.1177/1073858418783959.

(7) Kono, R.; Ikegaya, Y.; Koyama, R. Phagocytic Glial Cells in Brain Homeostasis. *Cells* **2021**, *10* (6). DOI: 10.3390/cells10061348.

(8) Prinz, M.; Jung, S.; Priller, J. Microglia Biology: One Century of Evolving Concepts. *Cell* **2019**, *179* (2), 292-311. DOI: 10.1016/j.cell.2019.08.053.

(9) Heneka, M. T.; Carson, M. J.; El Khoury, J.; Landreth, G. E.; Brosseron, F.; Feinstein, D. L.; Jacobs, A. H.; Wyss-Coray, T.; Vitorica, J.; Ransohoff, R. M.; et al. Neuroinflammation in Alzheimer's disease. *Lancet Neurol* **2015**, *14* (4), 388-405. DOI: 10.1016/S1474-4422(15)70016-5.

(10) Phatnani, H.; Maniatis, T. Astrocytes in neurodegenerative disease. *Cold Spring Harb Perspect Biol* **2015**, *7* (6). DOI: 10.1101/cshperspect.a020628.

(11) Schafer, D. P.; Stevens, B. Microglia Function in Central Nervous System Development and Plasticity. *Cold Spring Harb Perspect Biol* **2015**, *7* (10), a020545. DOI: 10.1101/cshperspect.a020545.

(12) Stogsdill, J. A.; Eroglu, C. The interplay between neurons and glia in synapse development and plasticity. *Curr Opin Neurobiol* **2017**, *42*, 1-8. DOI: 10.1016/j.conb.2016.09.016.

(13) Chitnis, T.; Weiner, H. L. CNS inflammation and neurodegeneration. *J Clin Invest* **2017**, *127* (10), 3577-3587. DOI: 10.1172/JCI90609.

(14) McCauley, M. E.; Baloh, R. H. Inflammation in ALS/FTD pathogenesis. *Acta Neuropathol* **2019**, *137* (5), 715-730. DOI: 10.1007/s00401-018-1933-9.

(15) Moreno, J. A.; Yeomans, E. C.; Streifel, K. M.; Brattin, B. L.; Taylor, R. J.; Tjalkens, R. B. Age-dependent susceptibility to manganese-induced neurological dysfunction. *Toxicol Sci* **2009**, *112* (2), 394-404. DOI: 10.1093/toxsci/kfp220.

(16) McManus, R. M.; Heneka, M. T. Role of neuroinflammation in neurodegeneration: new insights. *Alzheimers Res Ther* **2017**, *9* (1), 14. DOI: 10.1186/s13195-017-0241-2.

(17) LaRocca, T. J.; Cavalier, A. N.; Roberts, C. M.; Lemieux, M. R.; Ramesh, P.; Garcia, M. A.; Link, C. D. Amyloid beta acts synergistically as a pro-inflammatory cytokine. *Neurobiol Dis* **2021**, *159*, 105493. DOI: 10.1016/j.nbd.2021.105493.

(18) Linnerbauer, M.; Rothhammer, V. Protective Functions of Reactive Astrocytes Following Central Nervous System Insult. *Front Immunol* **2020**, *11*, 573256. DOI: 10.3389/fimmu.2020.573256.

(19) Ransohoff, R. M. How neuroinflammation contributes to neurodegeneration. *Science* **2016**, *353* (6301), 777-783. DOI: 10.1126/science.aag2590.

(20) Labzin, L. I.; Heneka, M. T.; Latz, E. Innate Immunity and Neurodegeneration. *Annu Rev Med* **2018**, *69*, 437-449. DOI: 10.1146/annurev-med-050715-104343.

(21) Paouri, E.; Georgopoulos, S. Systemic and CNS Inflammation Crosstalk: Implications for Alzheimer's Disease. *Curr Alzheimer Res* **2019**, *16* (6), 559-574. DOI: 10.2174/1567205016666190321154618.

(22) Mou, Y.; Du, Y.; Zhou, L.; Yue, J.; Hu, X.; Liu, Y.; Chen, S.; Lin, X.; Zhang, G.; Xiao, H.; et al. Gut Microbiota Interact With the Brain Through Systemic Chronic Inflammation: Implications on Neuroinflammation, Neurodegeneration, and Aging. *Front Immunol* **2022**, *13*, 796288. DOI: 10.3389/fimmu.2022.796288.

(23) Latham, A. S.; Moreno, J. A.; Geer, C. E. Biological agents and the aging brain: glial inflammation and neurotoxic signaling. *Front Aging* **2023**, *4*, 1244149. DOI: 10.3389/fragi.2023.1244149.

(24) Paolicelli, R. C.; Ferretti, M. T. Function and Dysfunction of Microglia during Brain Development: Consequences for Synapses and Neural Circuits. *Front Synaptic Neurosci* **2017**, *9*, 9. DOI: 10.3389/fnsyn.2017.00009.

(25) Wang, C.; Zong, S.; Cui, X.; Wang, X.; Wu, S.; Wang, L.; Liu, Y.; Lu, Z. The effects of microglia-associated neuroinflammation on Alzheimer's disease. *Front Immunol* **2023**, *14*, 1117172. DOI: 10.3389/fimmu.2023.1117172.

(26) Patani, R.; Hardingham, G. E.; Liddelow, S. A. Functional roles of reactive astrocytes in neuroinflammation and neurodegeneration. *Nat Rev Neurol* **2023**, *19* (7), 395-409. DOI: 10.1038/s41582-023-00822-1.

(27) Allen, N. J.; Lyons, D. A. Glia as architects of central nervous system formation and function. *Science* **2018**, *362* (6411), 181-185. DOI: 10.1126/science.aat0473.

(28) Knoop, M.; Possovre, M. L.; Jacquens, A.; Charlet, A.; Baud, O.; Darbon, P. The Role of Oxytocin in Abnormal Brain Development: Effect on Glial Cells and Neuroinflammation. *Cells* **2022**, *11* (23). DOI: 10.3390/cells11233899.

(29) Zhang, Z.; Yang, X.; Song, Y. Q.; Tu, J. Autophagy in Alzheimer's disease pathogenesis: Therapeutic potential and future perspectives. *Ageing Res Rev* **2021**, *72*, 101464. DOI: 10.1016/j.arr.2021.101464.

(30) Picca, A.; Guerra, F.; Calvani, R.; Romano, R.; Coelho-Júnior, H. J.; Bucci, C.; Marzetti, E. Mitochondrial Dysfunction, Protein Misfolding and Neuroinflammation in Parkinson's Disease: Roads to Biomarker Discovery. *Biomolecules* **2021**, *11* (10). DOI: 10.3390/biom11101508.

(31) Govindarajulu, M.; Ramesh, S.; Beasley, M.; Lynn, G.; Wallace, C.; Labeau, S.; Pathak, S.; Nadar, R.; Moore, T.; Dhanasekaran, M. Role of cGAS-Sting Signaling in Alzheimer's Disease. *Int J Mol Sci* **2023**, *24* (9). DOI: 10.3390/ijms24098151.

(32) Pinheiro, L.; Faustino, C. Therapeutic Strategies Targeting Amyloid-β in Alzheimer's Disease. *Curr Alzheimer Res* **2019**, *16* (5), 418-452. DOI: 10.2174/1567205016666190321163438.

(33) Long, J. M.; Holtzman, D. M. Alzheimer Disease: An Update on Pathobiology and Treatment Strategies. *Cell* **2019**, *179* (2), 312-339. DOI: 10.1016/j.cell.2019.09.001.

(34) Colonna, M.; Butovsky, O. Microglia Function in the Central Nervous System During Health and Neurodegeneration. *Annu Rev Immunol* **2017**, *35*, 441-468. DOI: 10.1146/annurev-immunol-051116-052358.

(35) Liddelow, S. A.; Barres, B. A. Reactive Astrocytes: Production, Function, and Therapeutic Potential. *Immunity* **2017**, *46* (6), 957-967. DOI: 10.1016/j.immuni.2017.06.006.

(36) Sun, E.; Motolani, A.; Campos, L.; Lu, T. The Pivotal Role of NF-kB in the Pathogenesis and Therapeutics of Alzheimer's Disease. *Int J Mol Sci* **2022**, *23* (16). DOI: 10.3390/ijms23168972.

(37) Fu, J.; Wu, H. Structural Mechanisms of NLRP3 Inflammasome Assembly and Activation. *Annu Rev Immunol* **2023**, *41*, 301-316. DOI: 10.1146/annurev-immunol-081022-021207.

(38) Ising, C.; Venegas, C.; Zhang, S.; Scheiblich, H.; Schmidt, S. V.; Vieira-Saecker, A.; Schwartz, S.; Albasset, S.; McManus, R. M.; Tejera, D.; et al. NLRP3 inflammasome activation drives tau pathology. *Nature* **2019**, *575* (7784), 669-673. DOI: 10.1038/s41586-019-1769-z.

(39) Sita, G.; Graziosi, A.; Hrelia, P.; Morroni, F. NLRP3 and Infections: β-Amyloid in Inflammasome beyond Neurodegeneration. *Int J Mol Sci* **2021**, *22* (13). DOI: 10.3390/ijms22136984.

(40) Hashemiaghdam, A.; Mroczek, M. Microglia heterogeneity and neurodegeneration: The emerging paradigm of the role of immunity in Alzheimer's disease. *J Neuroimmunol* **2020**, *341*, 577185. DOI: 10.1016/j.jneuroim.2020.577185.

(41) Marogianni, C.; Sokratous, M.; Dardiotis, E.; Hadjigeorgiou, G. M.; Bogdanos, D.; Xiromerisiou, G. Neurodegeneration and Inflammation-An Interesting Interplay in Parkinson's Disease. *Int J Mol Sci* **2020**, *21* (22). DOI: 10.3390/ijms21228421.

(42) Savage, J. C.; Carrier, M.; Tremblay, M. Morphology of Microglia Across Contexts of Health and Disease. *Methods Mol Biol* **2019**, *2034*, 13-26. DOI: 10.1007/978-1-4939-9658-2_2.

(43) Liu, C. C.; Hu, J.; Zhao, N.; Wang, J.; Wang, N.; Cirrito, J. R.; Kanekiyo, T.; Holtzman, D. M.; Bu, G. Astrocytic LRP1 Mediates Brain Aβ Clearance and Impacts Amyloid Deposition. *J Neurosci* **2017**, *37* (15), 4023-4031. DOI: 10.1523/JNEUROSCI.3442-16.2017.

(44) Perea, J. R.; Llorens-Martín, M.; Ávila, J.; Bolós, M. The Role of Microglia in the Spread of Tau: Relevance for Tauopathies. *Front Cell Neurosci* **2018**, *12*, 172. DOI: 10.3389/fncel.2018.00172.

(45) Hegdekar, N.; Sarkar, C.; Bustos, S.; Ritzel, R. M.; Hanscom, M.; Ravishankar, P.; Philkana, D.; Wu, J.; Loane, D. J.; Lipinski, M. M. Inhibition of autophagy in microglia and macrophages exacerbates innate immune responses and worsens brain injury outcomes. *Autophagy* **2023**, *19* (7), 2026-2044. DOI: 10.1080/15548627.2023.2167689.

(46) Matejuk, A.; Ransohoff, R. M. Crosstalk Between Astrocytes and Microglia: An Overview. *Front Immunol* **2020**, *11*, 1416. DOI: 10.3389/fimmu.2020.01416.

(47) Yang, J.; Wise, L.; Fukuchi, K. I. TLR4 Cross-Talk With NLRP3 Inflammasome and Complement Signaling Pathways in Alzheimer's Disease. *Front Immunol* **2020**, *11*, 724. DOI: 10.3389/fimmu.2020.00724.

(48) Wahl, D.; Risen, S. J.; Osburn, S. C.; Emge, T.; Sharma, S.; Gilberto, V. S.; Chatterjee, A.; Nagpal, P.; Moreno, J. A.; LaRocca, T. J. Nanoligomers targeting NF-κB and NLRP3 reduce neuroinflammation and improve cognitive function with aging and tauopathy. *J Neuroinflammation* **2024**, *21* (1), 182. DOI: 10.1186/s12974-024-03182-9.

(49) Sharma, S.; Risen, S.; Gilberto, V. S.; Boland, S.; Chatterjee, A.; Moreno, J. A.; Nagpal, P. Targeted-Neuroinflammation Mitigation Using Inflammasome-Inhibiting Nanoligomers is Therapeutic in an Experimental Autoimmune Encephalomyelitis Mouse Model. *ACS Chem Neurosci* **2024**, *15* (7), 1596-1608. DOI: 10.1021/acschemneuro.4c00024.

(50) Risen, S. J.; Boland, S. W.; Sharma, S.; Weisman, G. M.; Shirley, P. M.; Latham, A. S.; Hay, A. J. D.; Gilberto, V. S.; Hines, A. D.; Brindley, S.; et al. Targeting Neuroinflammation by Pharmacologic Downregulation of Inflammatory Pathways Is Neuroprotective in Protein Misfolding Disorders. *ACS Chem Neurosci* **2024**, *15* (7), 1533-1547. DOI: 10.1021/acschemneuro.3c00846.

(51) Carroll, J. A.; Chesebro, B. Neuroinflammation, Microglia, and Cell-Association during Prion Disease. *Viruses* **2019**, *11* (1). DOI: 10.3390/v11010065.

(52) Watts, J. C.; Prusiner, S. B. β-Amyloid Prions and the Pathobiology of Alzheimer's Disease. *Cold Spring Harb Perspect Med* **2018**, *8* (5). DOI: 10.1101/cshperspect.a023507.

(53) Heng, Y. Y.; Asad, I.; Coleman, B.; Menard, L.; Benki-Nugent, S.; Hussein Were, F.; Karr, C. J.; McHenry, M. S. Heavy metals and neurodevelopment of children in low and middle-income countries: A systematic review. *PLoS One* **2022**, *17* (3), e0265536. DOI: 10.1371/journal.pone.0265536.

(54) Kwon, H. K.; Choi, G. B.; Huh, J. R. Maternal inflammation and its ramifications on fetal neurodevelopment. *Trends Immunol* **2022**, *43* (3), 230-244. DOI: 10.1016/j.it.2022.01.007.

(55) Galler, J. R.; Koethe, J. R.; Yolken, R. H. Neurodevelopment: The Impact of Nutrition and Inflammation During Adolescence in Low-Resource Settings. *Pediatrics* **2017**, *139* (Suppl 1), S72-S84. DOI: 10.1542/peds.2016-2828I.

(56) Bolton, J. L.; Bilbo, S. D. Developmental programming of brain and behavior by perinatal diet: focus on inflammatory mechanisms. *Dialogues Clin Neurosci* **2014**, *16* (3), 307-320. DOI: 10.31887/DCNS.2014.16.3/jbolton.

(57) Lehrman, E. K.; Wilton, D. K.; Litvina, E. Y.; Welsh, C. A.; Chang, S. T.; Frouin, A.; Walker, A. J.; Heller, M. D.; Umemori, H.; Chen, C.; et al. CD47 Protects Synapses from Excess Microglia-Mediated Pruning during Development. *Neuron* **2018**, *100* (1), 120-134.e126. DOI: 10.1016/j.neuron.2018.09.017.

(58) Takeda, K.; Watanabe, T.; Oyabu, K.; Tsukamoto, S.; Oba, Y.; Nakano, T.; Kubota, K.; Katsurabayashi, S.; Iwasaki, K. Valproic acid-exposed astrocytes impair inhibitory synapse formation and function. *Sci Rep* **2021**, *11* (1), 23. DOI: 10.1038/s41598-020-79520-7.

(59) Buss, C. Maternal oxidative stress during pregnancy and offspring neurodevelopment. *Brain Behav Immun* **2021**, *93*, 6-7. DOI: 10.1016/j.bbi.2021.01.007.

(60) Peres, T. V.; Eyng, H.; Lopes, S. C.; Colle, D.; Gonçalves, F. M.; Venske, D. K.; Lopes, M. W.; Ben, J.; Bornhorst, J.; Schwerdtle, T.; et al. Developmental exposure to manganese induces lasting motor and cognitive impairment in rats. *Neurotoxicology* **2015**, *50*, 28-37. DOI: 10.1016/j.neuro.2015.07.005.

(61) Bantle, C. M.; French, C. T.; Cummings, J. E.; Sadasivan, S.; Tran, K.; Slayden, R. A.; Smeyne, R. J.; Tjalkens, R. B. Manganese exposure in juvenile C57BL/6 mice increases glial inflammatory responses in the substantia nigra following infection with H1N1 influenza virus. *PLoS One* **2021**, *16* (1), e0245171. DOI: 10.1371/journal.pone.0245171.

(62) Schmidt, C. W. Manganese Intake in Babies: Drinking Water plus Formula Can Cause High Exposures. *Environ Health Perspect* **2021**, *129* (7), 74002. DOI: 10.1289/EHP9786.

(63) Huynh, U.; Zastrow, M. L. Metallobiology of Lactobacillaceae in the gut microbiome. *J Inorg Biochem* **2023**, *238*, 112023. DOI: 10.1016/j.jinorgbio.2022.112023.

(64) Ghaisas, S.; Harischandra, D. S.; Palanisamy, B.; Proctor, A.; Jin, H.; Dutta, S.; Sarkar, S.; Langley, M.; Zenitsky, G.; Anantharam, V.; et al. Chronic Manganese Exposure and the Enteric Nervous System: An. *Environ Health Perspect* **2021**, *129* (8), 87005. DOI: 10.1289/EHP7877.

(65) Skogheim, T. S.; Weyde, K. V. F.; Engel, S. M.; Aase, H.; Surén, P.; Øie, M. G.; Biele, G.; Reichborn-Kjennerud, T.; Caspersen, I. H.; Hornig, M.; et al. Metal and essential element concentrations during pregnancy and associations with autism spectrum disorder and attention-deficit/hyperactivity disorder in children. *Environ Int* **2021**, *152*, 106468. DOI: 10.1016/j.envint.2021.106468.

(66) Lucchini, R.; Placidi, D.; Cagna, G.; Fedrighi, C.; Oppini, M.; Peli, M.; Zoni, S. Manganese and Developmental Neurotoxicity. *Adv Neurobiol* **2017**, *18*, 13-34. DOI: 10.1007/978-3-319-60189-2_2.

(67) Schullehner, J.; Thygesen, M.; Kristiansen, S. M.; Hansen, B.; Pedersen, C. B.; Dalsgaard, S. Exposure to Manganese in Drinking Water during Childhood and Association with Attention-Deficit Hyperactivity Disorder: A Nationwide Cohort Study. *Environ Health Perspect* **2020**, *128* (9), 97004. DOI: 10.1289/EHP6391.

(68) Mawe, G. M.; Sanders, K. M.; Camilleri, M. Overview of the Enteric Nervous System. *Semin Neurol* **2023**, *43* (4), 495-505. DOI: 10.1055/s-0043-1771466.

(69) Nakhal, M. M.; Yassin, L. K.; Alyaqoubi, R.; Saeed, S.; Alderei, A.; Alhammadi, A.; Alshehhi, M.; Almehairbi, A.; Al Houqani, S.; BaniYas, S.; et al. The Microbiota-Gut-Brain Axis and Neurological Disorders: A Comprehensive Review. *Life (Basel)* **2024**, *14* (10). DOI: 10.3390/life14101234.

(70) Friedman, A.; Boselli, E.; Ogneva-Himmelberger, Y.; Heiger-Bernays, W.; Brochu, P.; Burgess, M.; Schildroth, S.; Denehy, A.; Downs, T.; Papautsky, I.; et al. Manganese in residential drinking water from a community-initiated case study in Massachusetts. *J Expo Sci Environ Epidemiol* **2024**, *34* (1), 58-67. DOI: 10.1038/s41370-023-00563-9.

(71) Claus Henn, B.; Austin, C.; Coull, B. A.; Schnaas, L.; Gennings, C.; Horton, M. K.; Hernández-Ávila, M.; Hu, H.; Téllez-Rojo, M. M.; Wright, R. O.; et al. Uncovering neurodevelopmental windows of susceptibility to manganese exposure using dentine microspatial analyses. *Environ Res* **2018**, *161*, 588-598. DOI: 10.1016/j.envres.2017.12.003.

(72) Ouellette, J.; Lacoste, B. From Neurodevelopmental to Neurodegenerative Disorders: The Vascular Continuum. *Front Aging Neurosci* **2021**, *13*, 749026. DOI: 10.3389/fnagi.2021.749026.

(73) Pellegrini, C.; Fornai, M.; D'Antongiovanni, V.; Antonioli, L.; Bernardini, N.; Derkinderen, P. The intestinal barrier in disorders of the central nervous system. *Lancet Gastroenterol Hepatol* **2023**, *8* (1), 66-80. DOI: 10.1016/S2468-1253(22)00241-2.

(74) Tartaglione, A. M.; Venerosi, A.; Calamandrei, G. Early-Life Toxic Insults and Onset of Sporadic Neurodegenerative Diseases-an Overview of Experimental Studies. *Curr Top Behav Neurosci* **2016**, *29*, 231-264. DOI: 10.1007/7854_2015_416.

(75) Marzola, P.; Melzer, T.; Pavesi, E.; Gil-Mohapel, J.; Brocardo, P. S. Exploring the Role of Neuroplasticity in Development, Aging, and Neurodegeneration. *Brain Sci* **2023**, *13* (12). DOI: 10.3390/brainsci13121610.

(76) Fonken, L. K.; Frank, M. G.; Gaudet, A. D.; Maier, S. F. Stress and aging act through common mechanisms to elicit neuroinflammatory priming. *Brain Behav Immun* **2018**, *73*, 133-148. DOI: 10.1016/j.bbi.2018.07.012.

(77) Cooper, G. S.; Bynum, M. L.; Somers, E. C. Recent insights in the epidemiology of autoimmune diseases: improved prevalence estimates and understanding of clustering of diseases. *J Autoimmun* **2009**, *33* (3-4), 197-207. DOI: 10.1016/j.jaut.2009.09.008.

(78) Fairweather, D.; Rose, N. R. Women and autoimmune diseases. *Emerg Infect Dis* **2004**, *10* (11), 2005-2011. DOI: 10.3201/eid1011.040367.

(79) Heneka, M. T. Inflammasome activation and innate immunity in Alzheimer's disease. *Brain Pathol* **2017**, *27* (2), 220-222. DOI: 10.1111/bpa.12483.

(80) Ní Chasaide, C.; Lynch, M. A. The role of the immune system in driving neuroinflammation. *Brain Neurosci Adv* **2020**, *4*, 2398212819901082. DOI: 10.1177/2398212819901082.

(81) Wes, P. D.; Easton, A.; Corradi, J.; Barten, D. M.; Devidze, N.; DeCarr, L. B.; Truong, A.; He, A.; Barrezueta, N. X.; Polson, C.; et al. Tau overexpression impacts a neuroinflammation gene expression network perturbed in Alzheimer's disease. *PLoS One* **2014**, *9* (8), e106050. DOI: 10.1371/journal.pone.0106050.

(82) Yasir, M.; Goyal, A.; Sonthalia, S. Corticosteroid Adverse Effects. NIH: StatPearls, 2022.

(83) Jung, S. M.; Kim, W. U. Targeted Immunotherapy for Autoimmune Disease. *Immune Netw* **2022**, *22* (1), e9. DOI: 10.4110/in.2022.22.e9.

(84) Villoslada, P.; Moreno, B.; Melero, I.; Pablos, J. L.; Martino, G.; Uccelli, A.; Montalban, X.; Avila, J.; Rivest, S.; Acarin, L.; et al. Immunotherapy for neurological diseases. *Clin Immunol* **2008**, *128* (3), 294-305. DOI: 10.1016/j.clim.2008.04.003.

(85) Chimalakonda, A.; Burke, J.; Cheng, L.; Catlett, I.; Tagen, M.; Zhao, Q.; Patel, A.; Shen, J.; Girgis, I. G.; Banerjee, S.; et al. Selectivity Profile of the Tyrosine Kinase 2 Inhibitor Deucravacitinib Compared with Janus Kinase 1/2/3 Inhibitors. *Dermatol Ther (Heidelb)* **2021**, *11* (5), 1763-1776. DOI: 10.1007/s13555-021-00596-8.

(86) Rinaldi, C.; Wood, M. J. A. Antisense oligonucleotides: the next frontier for treatment of neurological disorders. *Nat Rev Neurol* **2018**, *14* (1), 9-21. DOI: 10.1038/nrneurol.2017.148.

(87) Mazur, C.; Powers, B.; Zasadny, K.; Sullivan, J. M.; Dimant, H.; Kamme, F.; Hesterman, J.; Matson, J.; Oestergaard, M.; Seaman, M.; et al. Brain pharmacology of intrathecal antisense oligonucleotides revealed through multimodal imaging. *JCI Insight* **2019**, *4* (20). DOI: 10.1172/jci.insight.129240.

(88) Goto, A.; Yamamoto, S.; Iwasaki, S. Biodistribution and delivery of oligonucleotide therapeutics to the central nervous system: Advances, challenges, and future perspectives. *Biopharm Drug Dispos* **2023**, *44* (1), 26-47. DOI: 10.1002/bdd.2338.

(89) Geary, R. S.; Yu, R. Z.; Siwkowski, A.; Levin, A. A. Pharmacokinetic/Pharmacodynamic Properties of Phosphorothioate 2′-O-(2-Methoxyethyl)-Modified Antisense Oligonucleotides in Animals and Man . Taylor & Francis: Antisense Drug Technology: Principles, Strategies, and Applications , 2 nd ed., 2007.

(90) Gagliardi, M.; Ashizawa, A. T. The Challenges and Strategies of Antisense Oligonucleotide Drug Delivery. *Biomedicines* **2021**, *9* (4). DOI: 10.3390/biomedicines9040433.

(91) Courtney, C. M.; Sharma, S.; Fallgren, C.; Weil, M. M.; Chatterjee, A.; Nagpal, P. Reversing radiation-induced immunosuppression using a new therapeutic modality. *Life Sci Space Res (Amst)* **2022**, *35*, 127-139. DOI: 10.1016/j.lssr.2022.05.002.

(92) McCollum, C. R.; Courtney, C. M.; O'Connor, N. J.; Aunins, T. R.; Ding, Y.; Jordan, T. X.; Rogers, K. L.; Brindley, S.; Brown, J. M.; Nagpal, P.; et al. Nanoligomers Targeting Human miRNA for the Treatment of Severe COVID-19 Are Safe and Nontoxic in Mice. *ACS Biomater Sci Eng* **2022**, *8* (7), 3087-3106. DOI: 10.1021/acsbiomaterials.2c00510.

(93) Sharma, S.; Borski, C.; Hanson, J.; Garcia, M. A.; Link, C. D.; Hoeffer, C.; Chatterjee, A.; Nagpal, P. Identifying an Optimal Neuroinflammation Treatment Using a Nanoligomer Discovery Engine. *ACS Chem Neurosci* **2022**, *13* (23), 3247-3256. DOI: 10.1021/acschemneuro.2c00365.

(94) McDonald, J. T.; Enguita, F. J.; Taylor, D.; Griffin, R. J.; Priebe, W.; Emmett, M. R.; Sajadi, M. M.; Harris, A. D.; Clement, J.; Dybas, J. M.; et al. Role of miR-2392 in driving SARS-CoV-2 infection. *Cell Rep* **2021**, *37* (3), 109839. DOI: 10.1016/j.celrep.2021.109839.

(95) McCollum, C. R.; Courtney, C. M.; O'Connor, N. J.; Aunins, T. R.; Jordan, T. X.; Rogers, K. L.; Brindley, S.; Brown, J. M.; Nagpal, P.; Chatterjee, A. Safety and Biodistribution of Nanoligomers Targeting the SARS-CoV-2 Genome for the Treatment of COVID-19. *ACS Biomater Sci Eng* **2023**, *9* (3), 1656-1671. DOI: 10.1021/acsbiomaterials.2c00669.

(96) Gagliardi, C.; Bunnell, B. A. Large animal models of neurological disorders for gene therapy. *ILAR J* **2009**, *50* (2), 128-143. DOI: 10.1093/ilar.50.2.128.

(97) Jensen, K. K.; Orum, H.; Nielsen, P. E.; Nordén, B. Kinetics for hybridization of peptide nucleic acids (PNA) with DNA and RNA studied with the BIAcore technique. *Biochemistry* **1997**, *36* (16), 5072-5077. DOI: 10.1021/bi9627525.

(98) Reagan-Shaw, S.; Nihal, M.; Ahmad, N. Dose translation from animal to human studies revisited. *FASEB J* **2008**, *22* (3), 659-661. DOI: 10.1096/fj.07-9574LSF.

(99) Zhang, Y.; Huo, M.; Zhou, J.; Xie, S. PKSolver: An add-in program for pharmacokinetic and pharmacodynamic data analysis in Microsoft Excel. *Comput Methods Programs Biomed* **2010**, *99* (3), 306-314. DOI: 10.1016/j.cmpb.2010.01.007.

(100) Larsen, H. J.; Bentin, T.; Nielsen, P. E. Antisense properties of peptide nucleic acid. *Biochim Biophys Acta* **1999**, *1489* (1), 159-166. DOI: 10.1016/s0167-4781(99)00145-1.

(101) Gavilán, M. P.; Revilla, E.; Pintado, C.; Castaño, A.; Vizuete, M. L.; Moreno-González, I.; Baglietto-Vargas, D.; Sánchez-Varo, R.; Vitorica, J.; Gutiérrez, A.; et al. Molecular and cellular characterization of the age-related neuroinflammatory processes occurring in normal rat hippocampus: potential relation with the loss of somatostatin GABAergic neurons. *J Neurochem* **2007**, *103* (3), 984-996. DOI: 10.1111/j.1471-4159.2007.04787.x.

(102) Jimenez, S.; Baglietto-Vargas, D.; Caballero, C.; Moreno-Gonzalez, I.; Torres, M.; Sanchez-Varo, R.; Ruano, D.; Vizuete, M.; Gutierrez, A.; Vitorica, J. Inflammatory response in the hippocampus of PS1M146L/APP751SL mouse model of Alzheimer's disease: age-

dependent switch in the microglial phenotype from alternative to classic. *J Neurosci* **2008**, *28* (45), 11650-11661. DOI: 10.1523/JNEUROSCI.3024-08.2008.

(103) Zhao, J.; Bi, W.; Xiao, S.; Lan, X.; Cheng, X.; Zhang, J.; Lu, D.; Wei, W.; Wang, Y.; Li, H.; et al. Neuroinflammation induced by lipopolysaccharide causes cognitive impairment in mice. *Sci Rep* **2019**, *9* (1), 5790. DOI: 10.1038/s41598-019-42286-8.

(104) Guan, Y.; Han, F. Key Mechanisms and Potential Targets of the NLRP3 Inflammasome in Neurodegenerative Diseases. *Front Integr Neurosci* **2020**, *14*, 37. DOI: 10.3389/fnint.2020.00037.

(105) Holbrook, J. A.; Jarosz-Griffiths, H. H.; Caseley, E.; Lara-Reyna, S.; Poulter, J. A.; Williams-Gray, C. H.; Peckham, D.; McDermott, M. F. Neurodegenerative Disease and the NLRP3 Inflammasome. *Front Pharmacol* **2021**, *12*, 643254. DOI: 10.3389/fphar.2021.643254.

(106) González-Sanmiguel, J.; Schuh, C. M. A. P.; Muñoz-Montesino, C.; Contreras-Kallens, P.; Aguayo, L. G.; Aguayo, S. Complex Interaction between Resident Microbiota and Misfolded Proteins: Role in Neuroinflammation and Neurodegeneration. *Cells* **2020**, *9* (11). DOI: 10.3390/cells9112476.

(107) Yiannopoulou, K. G.; Anastasiou, A. I.; Zachariou, V.; Pelidou, S. H. Reasons for Failed Trials of Disease-Modifying Treatments for Alzheimer Disease and Their Contribution in Recent Research. *Biomedicines* **2019**, *7* (4). DOI: 10.3390/biomedicines7040097.

(108) Amirian, R.; Badrbani, M. A.; Derakhshankhah, H.; Izadi, Z.; Shahbazi, M. A. Targeted protein degradation for the treatment of Parkinson's disease: Advances and future perspective. *Biomed Pharmacother* **2023**, *166*, 115408. DOI: 10.1016/j.biopha.2023.115408.

(109) Relaño-Ginés, A.; Lehmann, S.; Crozet, C. Cell-based therapy against prion diseases. *Curr Opin Pharmacol* **2019**, *44*, 8-14. DOI: 10.1016/j.coph.2018.11.001.

(110) Kannarkat, G. T.; Boss, J. M.; Tansey, M. G. The role of innate and adaptive immunity in Parkinson's disease. *J Parkinsons Dis* **2013**, *3* (4), 493-514. DOI: 10.3233/JPD-130250.

(111) Guzman-Martinez, L.; Maccioni, R. B.; Andrade, V.; Navarrete, L. P.; Pastor, M. G.; Ramos-Escobar, N. Neuroinflammation as a Common Feature of Neurodegenerative Disorders. *Front Pharmacol* **2019**, *10*, 1008. DOI: 10.3389/fphar.2019.01008.

(112) Mabbott, N. A.; Bradford, B. M.; Pal, R.; Young, R.; Donaldson, D. S. The Effects of Immune System Modulation on Prion Disease Susceptibility and Pathogenesis. *Int J Mol Sci* **2020**, *21* (19). DOI: 10.3390/ijms21197299.

(113) Gustot, A.; Gallea, J. I.; Sarroukh, R.; Celej, M. S.; Ruysschaert, J. M.; Raussens, V. Amyloid fibrils are the molecular trigger of inflammation in Parkinson's disease. *Biochem J* **2015**, *471* (3), 323-333. DOI: 10.1042/BJ20150617.

(114) Stancu, I. C.; Cremers, N.; Vanrusselt, H.; Couturier, J.; Vanoosthuyse, A.; Kessels, S.; Lodder, C.; Brône, B.; Huaux, F.; Octave, J. N.; et al. Aggregated Tau activates NLRP3-ASC inflammasome exacerbating exogenously seeded and non-exogenously seeded Tau pathology in vivo. *Acta Neuropathol* **2019**, *137* (4), 599-617. DOI: 10.1007/s00401-018-01957-y.

(115) Akwa, Y. Steroids and Alzheimer's Disease: Changes Associated with Pathology and Therapeutic Potential. *Int J Mol Sci* **2020**, *21* (13). DOI: 10.3390/ijms21134812.

(116) Wang, J. M.; Irwin, R. W.; Liu, L.; Chen, S.; Brinton, R. D. Regeneration in a degenerating brain: potential of allopregnanolone as a neuroregenerative agent. *Curr Alzheimer Res* **2007**, *4* (5), 510-517. DOI: 10.2174/156720507783018262.

(117) Hanslik, K. L.; Ulland, T. K. The Role of Microglia and the Nlrp3 Inflammasome in Alzheimer's Disease. *Front Neurol* **2020**, *11*, 570711. DOI: 10.3389/fneur.2020.570711.

(118) Cheng, J.; Liao, Y.; Dong, Y.; Hu, H.; Yang, N.; Kong, X.; Li, S.; Li, X.; Guo, J.; Qin, L.; et al. Microglial autophagy defect causes parkinson disease-like symptoms by accelerating inflammasome activation in mice. *Autophagy* **2020**, *16* (12), 2193-2205. DOI: 10.1080/15548627.2020.1719723.

(119) Kim, T. K.; Lee, I.; Cho, J. H.; Canine, B.; Keller, A.; Price, N. D.; Hwang, D.; Carlson, G.; Hood, L. Core transcriptional regulatory circuits in prion diseases. *Mol Brain* **2020**, *13* (1), 10. DOI: 10.1186/s13041-020-0551-3.

(120) Liu, T.; Zhang, L.; Joo, D.; Sun, S. C. NF-κB signaling in inflammation. *Signal Transduct Target Ther* **2017**, *2*, 17023-. DOI: 10.1038/sigtrans.2017.23.

(121) Kushwaha, R.; Sinha, A.; Makarava, N.; Molesworth, K.; Baskakov, I. V. Non-cell autonomous astrocyte-mediated neuronal toxicity in prion diseases. *Acta Neuropathol Commun* **2021**, *9* (1), 22. DOI: 10.1186/s40478-021-01123-8.

(122) Kushwaha, R.; Li, Y.; Makarava, N.; Pandit, N. P.; Molesworth, K.; Birukov, K. G.; Baskakov, I. V. Reactive astrocytes associated with prion disease impair the blood brain barrier. *Neurobiol Dis* **2023**, *185*, 106264. DOI: 10.1016/j.nbd.2023.106264.

(123) Venegas, C.; Kumar, S.; Franklin, B. S.; Dierkes, T.; Brinkschulte, R.; Tejera, D.; Vieira-Saecker, A.; Schwartz, S.; Santarelli, F.; Kummer, M. P.; et al. Microglia-derived ASC specks cross-seed amyloid-β in Alzheimer's disease. *Nature* **2017**, *552* (7685), 355-361. DOI: 10.1038/nature25158.

(124) Hafner-Bratkovič, I.; Benčina, M.; Fitzgerald, K. A.; Golenbock, D.; Jerala, R. NLRP3 inflammasome activation in macrophage cell lines by prion protein fibrils as the source of IL-1β and neuronal toxicity. *Cell Mol Life Sci* **2012**, *69* (24), 4215-4228. DOI: 10.1007/s00018-012-1140-0.

(125) Shi, F.; Yang, L.; Kouadir, M.; Yang, Y.; Wang, J.; Zhou, X.; Yin, X.; Zhao, D. The NALP3 inflammasome is involved in neurotoxic prion peptide-induced microglial activation. *J Neuroinflammation* **2012**, *9*, 73. DOI: 10.1186/1742-2094-9-73.

(126) Scheiblich, H.; Bousset, L.; Schwartz, S.; Griep, A.; Latz, E.; Melki, R.; Heneka, M. T. Microglial NLRP3 Inflammasome Activation upon TLR2 and TLR5 Ligation by Distinct α-Synuclein Assemblies. *J Immunol* **2021**, *207* (8), 2143-2154. DOI: 10.4049/jimmunol.2100035.

(127) Kim, T. K.; Bae, E. J.; Jung, B. C.; Choi, M.; Shin, S. J.; Park, S. J.; Kim, J. T.; Jung, M. K.; Ulusoy, A.; Song, M. Y.; et al. Inflammation promotes synucleinopathy propagation. *Exp Mol Med* **2022**, *54* (12), 2148-2161. DOI: 10.1038/s12276-022-00895-w.

(128) Kelley, N.; Jeltema, D.; Duan, Y.; He, Y. The NLRP3 Inflammasome: An Overview of Mechanisms of Activation and Regulation. *Int J Mol Sci* **2019**, *20* (13). DOI: 10.3390/ijms20133328.

(129) Shi, J.; Zhao, Y.; Wang, K.; Shi, X.; Wang, Y.; Huang, H.; Zhuang, Y.; Cai, T.; Wang, F.; Shao, F. Cleavage of GSDMD by inflammatory caspases determines pyroptotic cell death. *Nature* **2015**, *526* (7575), 660-665. DOI: 10.1038/nature15514.

(130) Martinon, F.; Burns, K.; Tschopp, J. The inflammasome: a molecular platform triggering activation of inflammatory caspases and processing of proIL-beta. *Mol Cell* **2002**, *10* (2), 417-426. DOI: 10.1016/s1097-2765(02)00599-3.

(131) Bacot, S. M.; Lenz, P.; Frazier-Jessen, M. R.; Feldman, G. M. Activation by prion peptide PrP106-126 induces a NF-kappaB-driven proinflammatory response in human monocyte-derived dendritic cells. *J Leukoc Biol* **2003**, *74* (1), 118-125. DOI: 10.1189/jlb.1102521.

(132) Prasad, K. N.; Bondy, S. C. Oxidative and Inflammatory Events in Prion Diseases: Can They Be Therapeutic Targets? *Curr Aging Sci* **2019**, *11* (4), 216-225. DOI: 10.2174/1874609812666190111100205.

(133) Wu, G. R.; Mu, T. C.; Gao, Z. X.; Wang, J.; Sy, M. S.; Li, C. Y. Prion protein is required for tumor necrosis factor α (TNFα)-triggered nuclear factor κB (NF-κB) signaling and cytokine production. *J Biol Chem* **2017**, *292* (46), 18747-18759. DOI: 10.1074/jbc.M117.787283.

(134) Bourgognon, J. M.; Spiers, J. G.; Robinson, S. W.; Scheiblich, H.; Glynn, P.; Ortori, C.; Bradley, S. J.; Tobin, A. B.; Steinert, J. R. Inhibition of neuroinflammatory nitric oxide signaling suppresses glycation and prevents neuronal dysfunction in mouse prion disease. *Proc Natl Acad Sci U S A* **2021**, *118* (10). DOI: 10.1073/pnas.2009579118.

(135) Choi, I.; Wang, M.; Yoo, S.; Xu, P.; Seegobin, S. P.; Li, X.; Han, X.; Wang, Q.; Peng, J.; Zhang, B.; et al. Autophagy enables microglia to engage amyloid plaques and prevents microglial senescence. *Nat Cell Biol* **2023**, *25* (7), 963-974. DOI: 10.1038/s41556-023-01158-0.

(136) Lv, Q. K.; Tao, K. X.; Wang, X. B.; Yao, X. Y.; Pang, M. Z.; Liu, J. Y.; Wang, F.; Liu, C. F. Role of α-synuclein in microglia: autophagy and phagocytosis balance neuroinflammation in Parkinson's disease. *Inflamm Res* **2023**, *72* (3), 443-462. DOI: 10.1007/s00011-022-01676-x.

(137) Lai, M.; Yao, H.; Shah, S. Z. A.; Wu, W.; Wang, D.; Zhao, Y.; Wang, L.; Zhou, X.; Zhao, D.; Yang, L. The NLRP3-Caspase 1 Inflammasome Negatively Regulates Autophagy via TLR4-TRIF in Prion Peptide-Infected Microglia. *Front Aging Neurosci* **2018**, *10*, 116. DOI: 10.3389/fnagi.2018.00116.

(138) Kovacs, G. G.; Budka, H. Molecular pathology of human prion diseases. *Int J Mol Sci* **2009**, *10* (3), 976-999. DOI: 10.3390/ijms10030976.

(139) Prusiner, S. B. Prions. *Proc Natl Acad Sci U S A* **1998**, *95* (23), 13363-13383. DOI: 10.1073/pnas.95.23.13363.

(140) Mari, Z.; Mestre, T. A. The Disease Modification Conundrum in Parkinson's Disease: Failures and Hopes. *Front Aging Neurosci* **2022**, *14*, 810860. DOI: 10.3389/fnagi.2022.810860.

(141) Geschwind, M. D.; Kuo, A. L.; Wong, K. S.; Haman, A.; Devereux, G.; Raudabaugh, B. J.; Johnson, D. Y.; Torres-Chae, C. C.; Finley, R.; Garcia, P.; et al. Quinacrine treatment trial for sporadic Creutzfeldt-Jakob disease. *Neurology* **2013**, *81* (23), 2015-2023. DOI: 10.1212/WNL.0b013e3182a9f3b4.

(142) Moreno, J. A.; Radford, H.; Peretti, D.; Steinert, J. R.; Verity, N.; Martin, M. G.; Halliday, M.; Morgan, J.; Dinsdale, D.; Ortori, C. A.; et al. Sustained translational repression by eIF2α-P mediates prion neurodegeneration. *Nature* **2012**, *485* (7399), 507-511. DOI: 10.1038/nature11058.

(143) Moreno, J. A.; Halliday, M.; Molloy, C.; Radford, H.; Verity, N.; Axten, J. M.; Ortori, C. A.; Willis, A. E.; Fischer, P. M.; Barrett, D. A.; et al. Oral treatment targeting the unfolded protein response prevents neurodegeneration and clinical disease in prion-infected mice. *Sci Transl Med* **2013**, *5* (206), 206ra138. DOI: 10.1126/scitranslmed.3006767.

(144) Deacon, R. M.; Raley, J. M.; Perry, V. H.; Rawlins, J. N. Burrowing into prion disease. *Neuroreport* **2001**, *12* (9), 2053-2057. DOI: 10.1097/00001756-200107030-00052.

(145) Mallucci, G. R.; White, M. D.; Farmer, M.; Dickinson, A.; Khatun, H.; Powell, A. D.; Brandner, S.; Jefferys, J. G.; Collinge, J. Targeting cellular prion protein reverses early cognitive deficits and neurophysiological dysfunction in prion-infected mice. *Neuron* **2007**, *53* (3), 325-335. DOI: 10.1016/j.neuron.2007.01.005.

(146) Hay, A. J. D.; Latham, A. S.; Mumford, G.; Hines, A. D.; Risen, S.; Gordon, E.; Siebenaler, C.; Gilberto, V. S.; Zabel, M. D.; Moreno, J. A. Intranasally delivered mesenchymal stromal cells decrease glial inflammation early in prion disease. *Front Neurosci* **2023**, *17*, 1158408. DOI: 10.3389/fnins.2023.1158408.

(147) de Melo, A. S. L. F.; Lima, J. L. D.; Malta, M. C. S.; Marroquim, N. F.; Moreira, Á.; de Almeida Ladeia, I.; Dos Santos Cardoso, F.; Gonçalves, D. B.; Dutra, B. G.; Dos Santos, J. C. C. The role of microglia in prion diseases and possible therapeutic targets: a literature review. *Prion* **2021**, *15* (1), 191-206. DOI: 10.1080/19336896.2021.1991771.

(148) Aguzzi, A.; Zhu, C. Microglia in prion diseases. *J Clin Invest* **2017**, *127* (9), 3230-3239. DOI: 10.1172/JCI90605.

(149) Alibhai, J.; Blanco, R. A.; Barria, M. A.; Piccardo, P.; Caughey, B.; Perry, V. H.; Freeman, T. C.; Manson, J. C. Distribution of Misfolded Prion Protein Seeding Activity Alone Does Not Predict Regions of Neurodegeneration. *PLoS Biol* **2016**, *14* (11), e1002579. DOI: 10.1371/journal.pbio.1002579.

(150) Li, S.; Fang, Y.; Zhang, Y.; Song, M.; Zhang, X.; Ding, X.; Yao, H.; Chen, M.; Sun, Y.; Ding, J.; et al. Microglial NLRP3 inflammasome activates neurotoxic astrocytes in depression-like mice. *Cell Rep* **2022**, *41* (4), 111532. DOI: 10.1016/j.celrep.2022.111532.

(151) Latham, A. S.; Geer, C. E.; Ackart, D. F.; Anderson, I. K.; Vittoria, K. M.; Podell, B. K.; Basaraba, R. J.; Moreno, J. A. Gliosis, misfolded protein aggregation, and neuronal loss in a guinea pig model of pulmonary tuberculosis. *Front Neurosci* **2023**, *17*, 1157652. DOI: 10.3389/fnins.2023.1157652.

(152) Dutta, S.; Sengupta, P. Men and mice: Relating their ages. *Life Sci* **2016**, *152*, 244-248. DOI: 10.1016/j.lfs.2015.10.025.

(153) Agostini, L.; Martinon, F.; Burns, K.; McDermott, M. F.; Hawkins, P. N.; Tschopp, J. NALP3 forms an IL-1beta-processing inflammasome with increased activity in Muckle-Wells autoinflammatory disorder. *Immunity* **2004**, *20* (3), 319-325. DOI: 10.1016/s1074-7613(04)00046-9.

(154) Nuvolone, M.; Sorce, S.; Schwarz, P.; Aguzzi, A. Prion pathogenesis in the absence of NLRP3/ASC inflammasomes. *PLoS One* **2015**, *10* (2), e0117208. DOI: 10.1371/journal.pone.0117208.

(155) Soto, C.; Satani, N. The intricate mechanisms of neurodegeneration in prion diseases. *Trends Mol Med* **2011**, *17* (1), 14-24. DOI: 10.1016/j.molmed.2010.09.001.

(156) Giovannoni, F.; Quintana, F. J. The Role of Astrocytes in CNS Inflammation. *Trends Immunol* **2020**, *41* (9), 805-819. DOI: 10.1016/j.it.2020.07.007.

(157) Salehi, P.; Clark, M.; Pinzon, J.; Patil, A. Sporadic Creutzfeldt-Jakob disease. *Am J Emerg Med* **2022**, *52*, 267.e261-267.e263. DOI: 10.1016/j.ajem.2021.07.038.

(158) Collinge, J.; Gorham, M.; Hudson, F.; Kennedy, A.; Keogh, G.; Pal, S.; Rossor, M.; Rudge, P.; Siddique, D.; Spyer, M.; et al. Safety and efficacy of quinacrine in human prion

disease (PRION-1 study): a patient-preference trial. *Lancet Neurol* **2009**, *8* (4), 334-344. DOI: 10.1016/S1474-4422(09)70049-3.

(159) Minikel, E. V.; Zhao, H. T.; Le, J.; O'Moore, J.; Pitstick, R.; Graffam, S.; Carlson, G. A.; Kavanaugh, M. P.; Kriz, J.; Kim, J. B.; et al. Prion protein lowering is a disease-modifying therapy across prion disease stages, strains and endpoints. *Nucleic Acids Res* **2020**, *48* (19), 10615-10631. DOI: 10.1093/nar/gkaa616.

(160) Rovis, T. L.; Legname, G. Prion protein-specific antibodies-development, modes of action and therapeutics application. *Viruses* **2014**, *6* (10), 3719-3737. DOI: 10.3390/v6103719.

(161) Gayrard, V.; Picard-Hagen, N.; Viguié, C.; Laroute, V.; Andréoletti, O.; Toutain, P. L. A possible pharmacological explanation for quinacrine failure to treat prion diseases: pharmacokinetic investigations in a ovine model of scrapie. *Br J Pharmacol* **2005**, *144* (3), 386-393. DOI: 10.1038/sj.bjp.0706072.

(162) Collins, S. J.; Lewis, V.; Brazier, M.; Hill, A. F.; Fletcher, A.; Masters, C. L. Quinacrine does not prolong survival in a murine Creutzfeldt-Jakob disease model. *Ann Neurol* **2002**, *52* (4), 503-506. DOI: 10.1002/ana.10336.

(163) Ghaemmaghami, S.; Ahn, M.; Lessard, P.; Giles, K.; Legname, G.; DeArmond, S. J.; Prusiner, S. B. Continuous quinacrine treatment results in the formation of drug-resistant prions. *PLoS Pathog* **2009**, *5* (11), e1000673. DOI: 10.1371/journal.ppat.1000673.

(164) Haïk, S.; Brandel, J. P.; Salomon, D.; Sazdovitch, V.; Delasnerie-Lauprêtre, N.; Laplanche, J. L.; Faucheux, B. A.; Soubrié, C.; Boher, E.; Belorgey, C.; et al. Compassionate use of quinacrine in Creutzfeldt-Jakob disease fails to show significant effects. *Neurology* **2004**, *63* (12), 2413-2415. DOI: 10.1212/01.wnl.0000148596.15681.4d.

(165) Mead, S.; Khalili-Shirazi, A.; Potter, C.; Mok, T.; Nihat, A.; Hyare, H.; Canning, S.; Schmidt, C.; Campbell, T.; Darwent, L.; et al. Prion protein monoclonal antibody (PRN100) therapy for Creutzfeldt-Jakob disease: evaluation of a first-in-human treatment programme. *Lancet Neurol* **2022**, *21* (4), 342-354. DOI: 10.1016/S1474-4422(22)00082-5.

(166) Nazor Friberg, K.; Hung, G.; Wancewicz, E.; Giles, K.; Black, C.; Freier, S.; Bennett, F.; Dearmond, S. J.; Freyman, Y.; Lessard, P.; et al. Intracerebral Infusion of Antisense Oligonucleotides Into Prion-infected Mice. *Mol Ther Nucleic Acids* **2012**, *1* (2), e9. DOI: 10.1038/mtna.2011.6.

(167) Aunins, T. R.; Erickson, K. E.; Chatterjee, A. Transcriptome-based design of antisense inhibitors potentiates carbapenem efficacy in CRE. *Proc Natl Acad Sci U S A* **2020**, *117* (48), 30699-30709. DOI: 10.1073/pnas.1922187117.

(168) Hay, A. J. D.; Murphy, T. J.; Popichak, K. A.; Zabel, M. D.; Moreno, J. A. Adipose-derived mesenchymal stromal cells decrease prion-induced glial inflammation in vitro. *Sci Rep* **2022**, *12* (1), 22567. DOI: 10.1038/s41598-022-26628-7.

(169) Oulhote, Y.; Mergler, D.; Barbeau, B.; Bellinger, D. C.; Bouffard, T.; Brodeur, M.; Saint-Amour, D.; Legrand, M.; Sauvé, S.; Bouchard, M. F. Neurobehavioral function in school-age children exposed to manganese in drinking water. *Environ Health Perspect* **2014**, *122* (12), 1343-1350. DOI: 10.1289/ehp.1307918.

(170) Pajarillo, E.; Nyarko-Danquah, I.; Adinew, G.; Rizor, A.; Aschner, M.; Lee, E. Neurotoxicity mechanisms of manganese in the central nervous system. *Adv Neurotoxicol* **2021**, *5*, 215-238. DOI: 10.1016/bs.ant.2020.11.003.

(171) Bouchard, M. F.; Sauvé, S.; Barbeau, B.; Legrand, M.; Brodeur, M.; Bouffard, T.; Limoges, E.; Bellinger, D. C.; Mergler, D. Intellectual impairment in school-age children exposed to manganese from drinking water. *Environ Health Perspect* **2011**, *119* (1), 138-143. DOI: 10.1289/ehp.1002321.

(172) Conley, T. E.; Beaudin, S. A.; Lasley, S. M.; Fornal, C. A.; Hartman, J.; Uribe, W.; Khan, T.; Strupp, B. J.; Smith, D. R. Early postnatal manganese exposure causes arousal dysregulation and lasting hypofunctioning of the prefrontal cortex catecholaminergic systems. *J Neurochem* **2020**, *153* (5), 631-649. DOI: 10.1111/jnc.14934.

(173) Sidoryk-Wegrzynowicz, M. Impairment of glutamine/glutamate-γ-aminobutyric acid cycle in manganese toxicity in the central nervous system. *Folia Neuropathol* **2014**, *52* (4), 377-382. DOI: 10.5114/fn.2014.47838.

(174) Farías, P.; Hernández-Bonilla, D.; Moreno-Macías, H.; Montes-López, S.; Schnaas, L.; Texcalac-Sangrador, J. L.; Ríos, C.; Riojas-Rodríguez, H. Prenatal Co-Exposure to Manganese, Mercury, and Lead, and Neurodevelopment in Children during the First Year of Life. *Int J Environ Res Public Health* **2022**, *19* (20). DOI: 10.3390/ijerph192013020.

(175) Chen, C.; Zhou, Y.; Wang, H.; Alam, A.; Kang, S. S.; Ahn, E. H.; Liu, X.; Jia, J.; Ye, K. Gut inflammation triggers C/EBPβ/δ-secretase-dependent gut-to-brain propagation of Aβ and Tau fibrils in Alzheimer's disease. *EMBO J* **2021**, *40* (17), e106320. DOI: 10.15252/embj.2020106320.

(176) Gao, V.; Crawford, C. V.; Burré, J. The Gut-Brain Axis in Parkinson's Disease. *Cold Spring Harb Perspect Med* **2025**, *15* (1). DOI: 10.1101/cshperspect.a041618.

(177) Porru, S.; Esplugues, A.; Llop, S.; Delgado-Saborit, J. M. The effects of heavy metal exposure on brain and gut microbiota: A systematic review of animal studies. *Environ Pollut* **2024**, *348*, 123732. DOI: 10.1016/j.envpol.2024.123732.

(178) Stanwood, G. D.; Leitch, D. B.; Savchenko, V.; Wu, J.; Fitsanakis, V. A.; Anderson, D. J.; Stankowski, J. N.; Aschner, M.; McLaughlin, B. Manganese exposure is cytotoxic and alters dopaminergic and GABAergic neurons within the basal ganglia. *J Neurochem* **2009**, *110* (1), 378-389. DOI: 10.1111/j.1471-4159.2009.06145.x.

(179) Bouabid, S.; Tinakoua, A.; Lakhdar-Ghazal, N.; Benazzouz, A. Manganese neurotoxicity: behavioral disorders associated with dysfunctions in the basal ganglia and neurochemical transmission. *J Neurochem* **2016**, *136* (4), 677-691. DOI: 10.1111/jnc.13442.

(180) Cordova, F. M.; Aguiar, A. S.; Peres, T. V.; Lopes, M. W.; Gonçalves, F. M.; Remor, A. P.; Lopes, S. C.; Pilati, C.; Latini, A. S.; Prediger, R. D.; et al. In vivo manganese exposure modulates Erk, Akt and Darpp-32 in the striatum of developing rats, and impairs their motor function. *PLoS One* **2012**, *7* (3), e33057. DOI: 10.1371/journal.pone.0033057.

(181) Ivleva, I.; Pestereva, N.; Zubov, A.; Karpenko, M. Intranasal exposure of manganese induces neuroinflammation and disrupts dopamine metabolism in the striatum and hippocampus. *Neurosci Lett* **2020**, *738*, 135344. DOI: 10.1016/j.neulet.2020.135344.

(182) Passos, M. D. C. F.; Moraes-Filho, J. P. INTESTINAL MICROBIOTA IN DIGESTIVE DISEASES. *Arq Gastroenterol* **2017**, *54* (3), 255-262. DOI: 10.1590/S0004-2803.201700000-31.

(183) O'Callaghan, J.; O'Toole, P. W. Lactobacillus: host-microbe relationships. *Curr Top Microbiol Immunol* **2013**, *358*, 119-154. DOI: 10.1007/82_2011_187.

(184) Qiu, P.; Ishimoto, T.; Fu, L.; Zhang, J.; Zhang, Z.; Liu, Y. The Gut Microbiota in Inflammatory Bowel Disease. *Front Cell Infect Microbiol* **2022**, *12*, 733992. DOI: 10.3389/fcimb.2022.733992.

(185) Felice, V. D.; O'Mahony, S. M. The microbiome and disorders of the central nervous system. *Pharmacol Biochem Behav* **2017**, *160*, 1-13. DOI: 10.1016/j.pbb.2017.06.016.

(186) Doney, E.; Cadoret, A.; Dion-Albert, L.; Lebel, M.; Menard, C. Inflammation-driven brain and gut barrier dysfunction in stress and mood disorders. *Eur J Neurosci* **2022**, *55* (9-10), 2851-2894. DOI: 10.1111/ejn.15239.

(187) Di Tommaso, N.; Gasbarrini, A.; Ponziani, F. R. Intestinal Barrier in Human Health and Disease. *Int J Environ Res Public Health* **2021**, *18* (23). DOI: 10.3390/ijerph182312836.

(188) Harischandra, D. S.; Ghaisas, S.; Zenitsky, G.; Jin, H.; Kanthasamy, A.; Anantharam, V.; Kanthasamy, A. G. Manganese-Induced Neurotoxicity: New Insights Into the Triad of Protein Misfolding, Mitochondrial Impairment, and Neuroinflammation. *Front Neurosci* **2019**, *13*, 654. DOI: 10.3389/fnins.2019.00654.

(189) Park, J. C.; Im, S. H. The gut-immune-brain axis in neurodevelopment and neurological disorders. *Microbiome Res Rep* **2022**, *1* (4), 23. DOI: 10.20517/mrr.2022.11.

(190) Wang, Q.; Yang, Q.; Liu, X. The microbiota-gut-brain axis and neurodevelopmental disorders. *Protein Cell* **2023**, *14* (10), 762-775. DOI: 10.1093/procel/pwad026.

(191) Kearns, R. The Kynurenine Pathway in Gut Permeability and Inflammation. *Inflammation* **2024**. DOI: 10.1007/s10753-024-02135-x.

(192) Guillemin, G. J. Quinolinic acid, the inescapable neurotoxin. *FEBS J* **2012**, *279* (8), 1356-1365. DOI: 10.1111/j.1742-4658.2012.08485.x.

(193) Margolis, K. G.; Cryan, J. F.; Mayer, E. A. The Microbiota-Gut-Brain Axis: From Motility to Mood. *Gastroenterology* **2021**, *160* (5), 1486-1501. DOI: 10.1053/j.gastro.2020.10.066.

(194) Nyarko-Danquah, I.; Pajarillo, E.; Digman, A.; Soliman, K. F. A.; Aschner, M.; Lee, E. Manganese Accumulation in the Brain via Various Transporters and Its Neurotoxicity Mechanisms. *Molecules* **2020**, *25* (24). DOI: 10.3390/molecules25245880.

(195) Zhang, K.; He, K.; Xu, J.; Nie, L.; Li, S.; Liu, J.; Long, D.; Dai, Z.; Yang, X. Manganese exposure causes movement deficit and changes in the protein profile of the external globus pallidus in Sprague Dawley rats. *Toxicol Ind Health* **2021**, *37* (12), 715-726. DOI: 10.1177/07482337211022223.

(196) Blackburn, D.; Sargsyan, S.; Monk, P. N.; Shaw, P. J. Astrocyte function and role in motor neuron disease: a future therapeutic target? *Glia* **2009**, *57* (12), 1251-1264. DOI: 10.1002/glia.20848.

(197) Chiu, Y. M.; Claus Henn, B.; Hsu, H. L.; Pendo, M. P.; Coull, B. A.; Austin, C.; Cagna, G.; Fedrighi, C.; Placidi, D.; Smith, D. R.; et al. Sex differences in sensitivity to prenatal and early childhood manganese exposure on neuromotor function in adolescents. *Environ Res* **2017**, *159*, 458-465. DOI: 10.1016/j.envres.2017.08.035.

(198) Samsel, A.; Seneff, S. Glyphosate, pathways to modern diseases III: Manganese, neurological diseases, and associated pathologies. *Surg Neurol Int* **2015**, *6*, 45. DOI: 10.4103/2152-7806.153876.

(199) Chen, X.; Xu, D.; Yu, J.; Song, X. J.; Li, X.; Cui, Y. L. Tryptophan Metabolism Disorder-Triggered Diseases, Mechanisms, and Therapeutic Strategies: A Scientometric Review. *Nutrients* **2024**, *16* (19). DOI: 10.3390/nu16193380.

(200) Danese, S.; Colombel, J. F.; Lukas, M.; Gisbert, J. P.; D'Haens, G.; Hayee, B.; Panaccione, R.; Kim, H. S.; Reinisch, W.; Tyrrell, H.; et al. Etrolizumab versus infliximab for the treatment of moderately to severely active ulcerative colitis (GARDENIA): a randomised,

double-blind, double-dummy, phase 3 study. *Lancet Gastroenterol Hepatol* **2022**, *7* (2), 118-127. DOI: 10.1016/S2468-1253(21)00294-6.

(201) Erikson, K. M.; Aschner, M. Manganese: Its Role in Disease and Health. *Met Ions Life Sci* **2019**, *19*. DOI: 10.1515/9783110527872-016.

(202) Tzeng, N. S.; Chung, C. H.; Lin, F. H.; Yeh, C. B.; Huang, S. Y.; Lu, R. B.; Chang, H. A.; Kao, Y. C.; Yeh, H. W.; Chiang, W. S.; et al. Risk of Dementia in Adults With ADHD: A Nationwide, Population-Based Cohort Study in Taiwan. *J Atten Disord* **2019**, *23* (9), 995-1006. DOI: 10.1177/1087054717714057.

(203) Bicknell, B.; Liebert, A.; Borody, T.; Herkes, G.; McLachlan, C.; Kiat, H. Neurodegenerative and Neurodevelopmental Diseases and the Gut-Brain Axis: The Potential of Therapeutic Targeting of the Microbiome. *Int J Mol Sci* **2023**, *24* (11). DOI: 10.3390/ijms24119577.